Final Technical Report

Project Title: Development of Bulk Nanocrystalline Cemented Tungsten Carbide for Industrial Applications

DOE Award Number: DE-FC36-04GO14041

Project Period: April 2004 – September 2008

Principle Investigator: Professor Z. Zak Fang
Tel. (801)581-8128
Email: zak.fang@utah.edu

Co-PI: Prof. H. Y. Sohn,
Tel. (801)581-5491
Email: h.y.sohn@utah.edu

Recipient organization: University of Utah
Salt Lake City, UT 84102

Other project team member organizations:

Idaho National Laboratory,
P. O. Box 1625
Idaho Falls, ID 83415-2210
Dr. Peter Kong

Kennametal, Inc.
205 N. 13th St.
Rogers, AR 72756
Dr. Shivanand Majagi

Smith International, Inc.
16740 Hardy Street
Houston, TX 77205
Dr. Anthony Griffo

Date of Report: January 31, 2009

Acknowledgment:

This report is based upon work supported by the U. S. Department of Energy under Award No. DE-FC36-04GO14041

Disclaimer:

Any findings, opinions, and conclusions or recommendations expressed in this report are those of the author(s) and do not necessarily reflect the views of the Department of Energy.

Proprietary Data Notice:

None.

Table of Contents

Lists of Figures

List of Tables

Lists of Acronyms

APT – Ammonium Paratungstate
ASTM – American Society of Testing and Materials
CVS – Chemical Vapor Synthesis
EDS – Energy Dispersive Spectroscopy
FGM – Functionally Graded Material
HFIHS – High Frequency Induction-Heated Sintering
HIPing – Hot Isostatic Pressing
HTHP – High Temperature High Pressure
LPS – liquid Phase Sintering
MFP – Mean Free Path
MS – Microwave Sintering
PCB – Printed Circuit Board
PPS – Pulse Plasma Sintering
ROC – Rapid Omni Compaction
SEM – Scanning Electron Microscopy
SENB – Single-Edge Notched Bending
SPS – Spark Plasma Sintering
TEM – Transmission Electron Microscopy
UPRC – Ultrahigh Pressure Rapid Hot Consolidation
XRD – X-ray Diffraction

Executive Summary

Cemented tungsten carbide is an indispensable industrial material. They are used in metalworking, oil and gas drilling, mining, construction, wear components for steel, aluminum, and chemical industries. It is the largest sector within metal powder industries. Nanocrystalline WC/Co powder was discovered over a decade ago. It was among the first group of materials that demonstrated the potential of nanocrystalline materials. The advances in **nanoscale** powder producing technologies raised hopes for dramatically improving mechanical properties.

Assuming successful development and implementation of the nano WC-Co technologies developed during this program, energy savings from applying the process technology and using nanocrystalline cemented tungsten carbide materials are expected from multiple industrial sectors including industrial materials, manufacturing, mining, chemical, and oil and gas exploration industries. These energy savings will be realized from four different perspectives.

- The **powder synthesis process is more energy efficient** than the conventional commercial production processes for manufacturing tungsten carbide powders.
- The **consolidation technology** also reduces energy consumption by dramatically shortening the sintering cycle time at high temperatures.
- It is expected that the productivity of **mining operations** can be increased by 15% by using the nanocrystalline cemented tungsten carbide materials that **increases tool life and reduces down time**.
- The nanocrystalline cemented tungsten can also be used for **metalworking cutting tools** to **increase productivity**.

However, in 2003 when this project was proposed, the development of nanocrystalline WC-Co materials were stalled because of the lack of sintering technologies that could produce *bulk* WC-Co materials with true nanometer grain sizes (<100nm). The lack of success with the sintered materials also affects adversely the further development of powder synthesis processes. Consequently, the cost/benefit ratios of nanocrystalline WC-Co powders produced by the technologies at the time were unacceptable to the industry.

This project investigated and developed processes for the synthesis of nanocrystalline tungsten carbide and cobalt composite powder and the consolidation of nanocrystalline WC/Co powders into bulk nanocrystalline materials. The original goal of developing processes that can produce bulk materials with true nanoscale grain sizes (<100 nm) and demonstrating potentially superior mechanical properties of cermet materials with a microstructure scale that has never been achieved before at a consolidated bulk state were achieved.

The synthesis of nanosized WC, Co, and WC/Co composite powders employs the basic methodology of “chemical vapor synthesis” (CVS) process. Two versions of the CVS processes were developed for making nanosized WC and WC/Co composite powders. The first one uses an electrically heated tubular reactor. The reduction and carburization of volatilized tungsten hexachloride together with cobalt chloride by a hydrogen-methane mixture produced nanosized WC-Co composite powder. The second one is based on a plasma powder synthesis process. The

products obtained from the plasma reactor with tungsten hexachloride or ammonium paratungstate (APT) as the W precursor were nanosized WC_{1-x}, which sometimes contained small amounts of W_2C and/or WC phase. When cobalt oxide (Co_3O_4) was fed together with APT, WC_{1-x}-Co composite powder was synthesized. The particle sizes of the product obtained from the tubular reactor and the plasma reactor were less than 30 nm and 20 nm, respectively. Since excess methane was used in the reaction, free carbon was always present in the produced powders. Therefore, a post-treatment using H_2 is necessary for removing excess carbon and producing product powders with correct chemistry. We also determined certain synthesis conditions in which the product WC-Co composite powder did not require post-treatment. Especially, the plasma reactor system is suitable for the industrial application because it is readily scaled up to a larger scale The most significant result of this research is the development of a process in which nanosized and very uniformly mixed WC-Co composite powders can be produced.

For consolidation of nanocrystalline WC-Co powders, a new ultrahigh pressure rapid hot consolidation (UPRC) process was developed. The UPRC process is capable of a heating rate of 100 to 300 ^oC/min and consolidating powder compacts under 800 MPa pressure within minutes. Consolidated cemented tungsten carbide using the nanocrystalline WC-Co composite powders has unique properties. When vacuum sintering process is used, the use of grain growth inhibitor is necessary to minimize grain growth. When the UPRC process is used for consolidation, WC-10wt%Co specimens with very high hardness (greater than 1800 Kg/mm^2) were achieved without using grain growth inhibitor. Because grain growth inhibitors are known to have adverse effects on the toughness of WC-Co materials, the material produced using UPRC in this program has unique potential for commercial applications.

The enhanced sinterability of nanosized WC-Co powders was also exploited for making binder-less tungsten carbide, i.e. pure WC without cobalt binder. Pure fully densified (>99% relative density) WC materials were produced using standard vacuum sintering process. The hardness of the sintered material was approximately 2300 Kg/mm^2. This material also has good commercial potential.

This research program also explored the use of nano WC-Co powders for making functionally graded WC-Co. Research has established the quantitative dependence of cobalt migration on WC particle sizes, by which WC-Co composites with graded cobalt compositions can be manufactured.

As a general strategy and plan for going forward, we will seek partners from both the government and private industries to undertake “development” projects based on the “research” results of this program. It is expected that relatively large scale pilot production trials will establish a necessary data base for launching any future commercial productions based on the technologies developed in this program.

I. Introduction

Cemented tungsten carbide (WC-Co) is an indispensable industrial material. They are used in metalworking, oil and gas drilling, mining, construction, wear components for steel, aluminum, and chemical industries. It is the largest sector within metal powder industries. Nanocrystalline WC/Co powder was discovered near the end of 1980s and perfected in the 1990s. It was among the first group of industrial materials that demonstrated the potential of nanocrystalline materials. The advances in nanoscale powder producing technologies raised hopes for dramatically improving mechanical properties.

To benefit from the technologies for producing nanosized WC powders, the powders must be consolidated. A critical challenge for sintering nanosized powders is to minimize grain growth while achieving full densification. Although significant progress had been made at the time this project was proposed in 2003, further development of the technology was stalled and slowed because of the lack of sintering technologies for producing *bulk* WC-Co with grain size <100 nm. The potential for dramatically stronger and tougher cermets was not demonstrated.

A comprehensive R&D program was then proposed and conducted in the past four years to develop ***bulk*** nanocrystalline cemented tungsten carbide materials. Specific technology innovations involves the consolidation of nanocrystalline WC/Co powder using an ultrahigh pressure rapid heating and consolidation process to produce *bulk* materials with true nanometer grain sizes (<100 nm) and a new powder synthesis process based on chemical vapor phase reactions. Nanocrystalline WC/Co composite powder can be produced directly from volatile chemical precursors by vapor phase reactions. Full characterizations of the mechanical properties of sintered WC-Co samples using nanosized powders were also performed.

Specific technical targets of the projects were:

- Produce uniformly mixed nano-sized WC and cobalt powders as well as cobalt-coated WC powder by the vapor-phase co-reduction of chloride vapor mixtures with controlled grain sizes, cobalt contents, and yields that are economically viable,
- Develop a rapid heating technique and ultimately a semi-continuous process for consolidation of nanostructure WC/Co powders,
- Achieve <100 nm grain size in fully consolidated bulk WC-Co cermets, and
- Evaluate and analyze the mechanical properties of consolidated WC-Co with grain sizes <100 nm.

By developing and implementing the technology, economic benefits will be realized in many different ways including: direct savings from reduced energy consumptions, increased tool life for end-users, and indirect savings through increased productivity for end users. As an example, it is expected that the proposed technology will increase productivity of mining by increasing durability and reliability of tools, which will in turn drastically reduce maintenance-related labor time. It is estimated that by using more durable tools it is possible to reduce the need for maintenance labor by 25-30% for a typical mine, which amounts to 12-15% of total labor cost.

In terms of dollar values, assuming that the average increased productivity will be 15% per employee, and that will affect 10% of all employees in the mining industry (10% of 355,000 people is 33,500 people). That is equivalent to 1.5% increased productivity for the whole industry. Since the total value of fuel and non-fuel mining in the U.S. is around $60 billion, the potential savings can be estimated to be around $900 million per year.

As another example of potential economic benefits through productivity gains, based on a public presentation by Kennametal of Latrobe, Pennsylvania, a world leader in the industry, It was estimated that 3% of productivity gain can be achieved by using better tool materials. Since 4% of total cost of machining is on tooling, it would save $3.75 billion per year in the US alone [1].

By employing the technology, there will also be significant energy savings. The energy savings from applying the proposed process technology and using nanocrystalline cemented tungsten carbide materials are expected from multiple industrial sectors including Industrial Materials, manufacturing, mining, chemical, and oil and gas exploration industries. These energy savings will be realized from four different perspectives.

- The **powder synthesis process is more energy efficient** than the conventional commercial production processes for manufacturing tungsten carbide powders,
- The **consolidation technology** also reduces energy consumption by dramatically shortening the sintering cycle time at high temperatures.
- It is expected that the productivity of **mining operations** can be increased by 15% by using the nanocrystalline cemented tungsten carbide materials that **increases tool life and reduces down time**.
- The nanocrystalline cemented tungsten can also be used for **metalworking cutting tools** to **increase productivity**.

II. Background

Nanocrystalline WC-Co was among the first group of industrial materials that demonstrated the potential of nanocrystalline materials. McCandlish and Kear reported successful synthesis of nanocrystalline WC/Co powder using a spray conversion process in late 1980s [2]. Since then, nanocrystalline WC/Co powders have been produced using various processes by different companies and labs [3]. These advances in nanoscale powder producing technologies raised hopes for dramatically improving mechanical properties. However, further development of nanocrystalline WC-Co materials were stalled since 1990s because of the lack of sintering technologies that could produce *bulk* WC-Co materials with true nanometer grain sizes (<100 nm). Consequently, cost/benefit ratios of nanocrystalline WC-Co powders produced by existing technologies at the time were unacceptable to the industry.

Cemented tungsten carbide consists of large volume fractions of WC particles in a cobalt metal matrix. The hardness of WC-Co is inversely proportional to its grain size and that the fracture toughness is inversely proportional to the hardness. For nanocrystalline materials, however, it has been noted that the mechanisms of strengthening are different because of the large volume fractions of grain boundaries. Deformation depends on grain boundary sliding and diffusion-controlled processes [4, 5]. Grain boundaries in polycrystalline metals also impede the motion of cracks, which contribute to better fracture toughness. Therefore, it is hypothesized that the fracture toughness of WC-Co will improve when its grains size reaches nanoscale. However, few experimental evidence of the hypothesis was available.

All the data analyzed and reported prior to 2003 showed that due to rapid grain growth at high temperature sintering conditions, no bulk WC-Co material with grain sizes truly in the nanometer scale (<100 nm) had ever been produced. Therefore, the true mechanical behavior of nanocrystalline WC-Co remains unexplored.

Indeed, the development of nanocrystalline WC-Co was at a critical juncture. On the one hand, initial exploratory research had been completed, and there were many indications of promising unique and superior properties when the grain size becomes finer and finer. On the other hand, the lack of effective sintering technologies hindered researchers from being able to produce nanocrystalline WC-Co in the *bulk* form and study their properties. In-depth research and breakthroughs were needed.

With regard to powder production method, emerging technologies included several processes based on conversion of chemical precursors in solid state [2, 3]. The most notable one is the spray conversion process that was first reported by B. Kear and L. McCandlish in late 1980's. In this process, APT and cobalt nitrate precursors are first spray dried. The spray dried granules are then reduced and carburized in a fluidized bed in a single run cycle. The process is used to produce nanocrystalline WC/Co powder.

These processes that first form, from an aqueous solution, ammonium salts containing tungsten and cobalt at the desired ratio require numerous aqueous process steps of purification and crystallization and difficult control of process conditions. Furthermore, production of fine

powders from these aqueous processes requires spray drying, which is highly energy-intensive, and also generates large amounts of waste liquids.

It would be advantageous if WC-Co mixtures can directly be produced in a powder form using less energy and fewer chemical steps. The process described in this report uses precursors that are the raw materials for WC and Co, and it consumes considerably less energy because it will take a full advantage of the substantial heat as well as free energy of reaction.

Given the technology background as described above, the project was proposed in 2003 and initiated in 2004. The basic approaches that were proposed and planned are two: 1) Synthesis of nano composite WC-Co powders using the "chemical vapor synthesis" techniques, and 2). Consolidation of the nano powders using an ultrahigh pressure rapid heating and consolidation technology. The goal was to develop a parcel of process technologies that can be used in combination to produce bulk nanocrystalline WC-Co materials for industrial applications.

The project team consisted of the University of Utah, Idaho National Lab, Kennametal Inc., and Smith International Inc. The University of Utah was responsible for planning and execution of the program. Idaho National Lab was responsible for developing rapid heating techniques for the rapid hot consolidation process. Kennametal and Smith Internationals are industrial partners that contributed considerable cash as well as in-kind resources to the project.

The details of the research activities and results, and the accomplishments that were achieved during the program are reported as follows.

III. Critical Review of Literature

Engineering materials with nanocrystalline microstructure are of interest to the science and engineering communities owing to their potential superior mechanical properties. With respect to cemented tungsten carbide, improving fracture toughness without sacrificing wear resistance or vice versa is the Holy Grail. By using nanocrystalline microstructure, the properties of WC-Co could be improved because the large grain boundary areas that may enable local plastic deformation by grain boundary sliding and rotation, which ultimately improves the toughness of the material. The challenge is, however, how to produce such nanocrystalline bulk materials.

There are many methods for producing nanocrystalline materials. In principle, those methods can be divided into two categories: "bottom-up" methods and "top-down" methods. The "top-down" methods involve breakdown of bulk form or coarse particulate material down to nanosize scale. The "bottom-up" methods involve synthesis of nanosized powders and consolidation of the nanosized powders.

Given the scope and objectives of this work, the following review will cover both the synthesis of nanosized powders and the sintering or consolidation of nano powders into bulk form. However, as a result of the aggressive and wide spread research around globe in the past two decades, there many methods for synthesis of nanosized powders. This report will focus on gas phase synthesis method as relevant to the work of this project.

This review will also cover various consolidation methods, the evolution of microstructure during sintering, and mechanical properties of WC-Co made from nanosized powders.

III.1 Previous Work on Tungsten Carbide Synthesis by Gas Phase Reaction

Gas phase reaction offers the advantages of synthesizing high purity nanopowders with good control over size, shape, and crystal structure as well as easy control of reaction rate. Nanopowders synthesized by this method exhibit improved mechanical properties such as material strength, hardness, and toughness and lower sintering temperatures during the consolidation process.

Gas phase synthesis is conducted by creating a supersaturated vapor of a precursor which is thermodynamically unstable than the formation of the solid material to be prepared in nanopowder form. It involves reaching a state of chemical supersaturation in which it is thermodynamically favorable for the vapor phase molecules to react chemically to form a condensed phase rather than stay in vapor form.

There are several methods for preparing nanopowders by gas phase synthesis as described below [6, 7]. The major differences in such methods lie in the energy source used to achieve a state of supersaturation and the nature of the precursors to be used.

Inert gas condensation involves vaporizing the precursor into a background gas and then mixing the vapor with a cold gas to reduce the temperature. This method is well suited for production of metal nanoparticles, since many metals vaporize at reasonable rates at attainable

temperatures. By including a reactive gas such as oxygen in the cold gas stream, oxides or other compounds of the vaporized materials also can be prepared.

Laser ablation uses a laser to vaporize solid materials in an inert flow reactor. This method is good for precursors that have high volatilization temperatures and low vapor pressures such as refractory oxides. The main drawback to this method is that the amount of nanopowder produced is relatively small.

Spark discharge generation involves using electrodes made of the metal to be vaporized in the presence of an inert background gas until the breakdown voltage is reached. The arc formed across the electrodes vaporizes a small amount of metal. This produces very small amounts of nanoparticle with relatively reproducible results.

Ion sputtering involves the use of high velocity ions of an inert gas to vaporize the solid. The advantage of this method is that the composition of the sputtered material is the same as that of the target. The disadvantage of this method is that low pressures are required, which makes further processing of the nanoparticles in aerosol form difficult.

The flame synthesis method utilizes an open flame for particle synthesis. The temperature of the flame gives the necessary heat for the reactions to occur. This is the most successful method of producing nanoparticles industrially. It is primarily useful for making oxides, since the flame environment is quite oxidizing. The drawback to this method is the high agglomeration of the synthesized particles.

Chemical vapor synthesis involves introducing vapor phase precursors into a hot-wall reactor and allowing vapor phase nucleation to occur in the reactor rather than depositing the product as a thin film. When the powder is deposited, the process is referred to as Chemical Vapor Deposition. The precursors can be solid or liquid in nature but are introduced into the reactor as a gas by sublimation or evaporation. Metal chlorides are generally preferred as the precursors owing to their low volatilizing temperature. Chemical vapor synthesis was developed at the University of Utah and has been applied to the synthesis of metallic and intermetallic powders [8-10].

Thermal plasma synthesis involves the use of a plasma flame as the heat source. Plasma flames can facilitate vapor phase reactions by providing sufficient energy for vaporizing precursors and subsequent chemical reactions. The temperature of plasma flame generated is high enough to decompose the reactants into atoms, which can then react and condense to form nanosized particles when cooled by mixing with cool gas or expansion through a nozzle.

Tungsten carbide nanopowder has been synthesized by vapor phase reaction, more specifically by chemical vapor synthesis using volatile precursors. The following section briefly discusses the systematic methods and the effect of processing parameters previously tested by other research groups.

Several articles have been published on the synthesis of nanosized tungsten carbide powder by gas phase reaction. Tungsten hexachloride (WCl_6) or tungsten hexacarbonyl [$W(CO)_6$] have been favored as precursors due to their relatively low volatilization temperatures as well as the

ease of reduction by hydrogen or thermal decomposition.

Hojo et al. [11] synthesized nanosized tungsten carbide powder in a WCl_6-CH_4-H_2 system. The reactor was an alumina tube of 2.2 cm inner diameter placed in a horizontal furnace consisting of sublimation furnace and reaction furnace. The effective length of the reaction furnace was 20 cm. Tungsten hexachloride powder was placed in a sublimation furnace controlled at 400 ^oC and nitrogen gas was used as a carrier gas. Hydrogen and methane were used as the reducing and carburizing agent, respectively. Two methods for the introduction of WCl_6 vapor into the reaction zone were tested. Method A involved mixing all gas streams in a sublimation zone at 400 ^oC before entering the reaction zone. Method B involved mixing all gas streams at a high temperature zone varying from 1000 ^oC to 1400 ^oC. Experiments were carried out to determine the effects of methods for introducing WCl_6 vapor into the reaction zone and reaction temperatures on the production composition and particle size. The effect of methane concentration on the phase compositions was also investigated. The results indicated that the degree of carburization increased as the reaction temperature and methane concentration were increased. The product was mostly WC in method A at the reaction temperature of 1400 ^oC. However, the yield of W_2C was higher in method B than that of method A under the same conditions. Particle sizes were affected by the gas mixing temperatures, with about 40~50 nm in method A and about 80~110 nm in method B. This paper stated that substantial WC formation from WCl_6 started to occur above 1000~1200 ^oC.

Tang et al. [12] synthesized nanosized tungsten carbide powder in a WCl_6-C_3H_8-H_2 system. The reactor was an alumina tube of 2.8 cm inner diameter and placed in a vertical furnace with an effective length of 15 cm. Tungsten hexachloride powder was placed in a sublimation tube controlled in the temperature range of 150 ^oC to 200 ^oC and a hydrogen-propane mixture flowed through the sublimating tube into the reaction zone where the temperature was varied from 1280 ^oC to 1500 ^oC. The results indicated that the product composition was affected by reaction temperature and the C_3H_8 flow rate. In studying the effect of C_3H_8 flow rate, the temperature was held at 1530^oC, sublimation temperature was 200 ^oC, and H_2 flow rate was fixed at 0.25 L/min. In the range of C_3H_8 flow rate from 0.022 L/min to 0.024 L/min, the product was WC with small amounts of W_2C and W, and carbon contents in the product were close to the stoichiometric amount to form WC phase. This paper presented a post-treatment of synthesized powder by hydrogen, in which excess carbon of 9.2 wt % in the product was fully removed after 1 hour of treatment time at 1000 ^oC.

Won et al. [13] synthesized nanosized tungsten carbide powder in a WCl_6-C_2H_2-H_2 system. The reactor was an alumina tube of 3 cm inner diameter and 60 cm length placed in a horizontal furnace. The precursor was introduced into the reactor from a WCl_6 vaporizer. Hydrogen and acetylene were used as the reducing and carburizing agent, respectively. These reactant gases with Argon flowed through the WCl_6 vaporizer to carry WCl_6 vapor. The effects of reaction temperature, WCl_6 vaporizer temperature, and H_2 flow rate on the grain size and product composition were investigated. The experimental conditions were as follows: Reaction temperature was varied from 1000^oC to 1200 ^oC, vaporizer temperature was varied from 250 ^oC to 350^oC, and H_2 flow rate was varied from 1 L/min to 4 L/min with C_2H_2 flow rate of 0.2 L/min. Under most experimental conditions, a mixture of α-WC and β-W_2C was produced. The particle size increased as the reaction temperature and WCl_6 vaporizer temperature were increased but it

decreased with the increase of H_2 flow rate. Particle sizes obtained from this experiment varied from 100 nm to 1 um depending on experimental parameters.

Kim et al. [14] used tungsten hexacarbonyl [$W(CO)_6$] as the precursor and carbon monoxide (CO) as the carburizing agent. The experiments were conducted in the temperature range of 500°C to 1000 °C and three different reaction atmospheres, 1 atm air, 1 atm argon, and 1×10^{-4} atm vacuum were tested. The solid precursor was kept at 120 °C to vaporize it in the vaporizer and no H_2 was used as a reducing agent in this experiment since tungsten hexacarbonyl is decomposed into W and CO at in a temperature range from 150 °C to 205 °C. This paper also stated that CO undergoes a reaction to form CO_2 and C in the presence of tungsten metallic catalyst decomposed from tungsten hexacarbonyl, which then carburizes the W to form WC_{1-x}. No powder was obtained under 600 °C and the product composition, mainly WC_{1-x}, obtained above 600 °C was almost the same, in which the particle size increased with the increase of the reaction temperature. The synthesized powders in air and Ar atmospheres had the same XRD patterns and the XRD peaks were greatly broadened under vacuum condition compared with those of air and Ar atmospheres. The particle sizes obtained in this experiment were less than 50 nm.

In the previous works described above, the chemical vapor synthesis conducted by other research group confirmed the feasibility of producing nanosized WC or WC_{1-x} powder with particle sizes mostly less than 100 nm. However, these methods still require systematic modification since the feeding method is limited to a batch system, which is not advantageous for industrial application. Furthermore, no report on the simultaneous formation of WC-Co composites by this method is found in literature.

III.2 Consolidation of Nano WC/Co Powders

The consolidation of nanostructured WC/Co powder has been studied using a variety of means including the standard liquid phase sintering (LPS) [15-23], hot isostatic pressing (HIP) [24], and unconventional processes such as Microwave Sintering (MS) [25, 26] and Spark Plasma Sintering (SPS) [27-38], High Frequency Induction-Heated Sintering (HFIHS) [39-41], Rapid Omni Compaction (ROC) [42], Pulse Plasma Sintering (PPS) [43]. Under the high temperature during sintering, grains grow rapidly. The finest grain sizes of sintered WC-Co reported in the literature to date, using nanograined powders, is approximately 100 nm. (*Grain size of 70 nm [44, 45] was also reported by measuring the same group of samples as in reference [18]*).

To achieve the goal of sintering nanocrystalline WC-Co to full density while retaining the nanoscaled grain sizes, considerable efforts of the research community have been devoted to the study of the densification and grain growth during sintering of the nanosized WC-Co powders. In this section, both the understanding of the densification and growth behavior of nanosized WC-Co powders and the techniques for controlling gain growth during sintering are summarized.

III.2.1 Densification

In general, the sintering temperature of a material decreases with the reduction of the particle sizes. This is especially true for nanosized powders including nanosized WC-Co powders. Schubert reported that up to 85% of densification of WC-Co was accomplished below 1280^{o}C when grain sizes were <0.3 μm, while up to 70% of densification is accomplished at the same temperature when the grain size was 0.7 μm, which suggests that the onset of sintering is a function of the grain size [46].

In essence, a powder compact can be viewed as consisting of a bi-level hierarchical structure: the compact is made of agglomerates which are made of nanosized particles. There is, therefore, a bimodal pore size distribution. The pores existing within agglomerates are finer than the pores between agglomerates. The densification of individual agglomerates is relatively easy, while the elimination of the inter-agglomerate pores is more difficult. By tracking the evolution of pore size distributions, Peterson et al studied the sintering of fine grain cemented tungsten carbide and cobalt system (WC-Co) [47]. They showed that during the intermediate stage of sintering, the considerable densification obtained is primarily connected to removal of small pores rather than shrinkage of larger ones.

III.2.2 Grain Growth

Studies of the grain growth behavior have found that grain growth occurs extremely rapidly during the early stages of sintering. Fang documented the densification and grain size versus the LPS time and temperature [18]. It was found that the grain sizes of the samples were already dramatically increased from their initial nanometer sizes in the first 5 min. McCandlish observed that the WC grain size in a WC-10wt%Co alloy obtained by sintering nanosizeded WC/Co powder manufactured by Nanodyne, Inc. was 200 nm after 30 seconds of sintering at 1400^{o}C, and it became 2 μm (2000 nm) after additional 30 seconds [19].

Moreover, experimental evidence of the sintering and grain growth in solid state provided by Goren [48] and Porat [21] indicated that a large amount of grain growth was already widespread at 1200^{o}C while liquid phase was not expected to form until 1280^{o}C. Schubert pointed out that grain growth started during heat up to the temperature, which is attributed to the high degree of "meta-stability" of the powder [46].

Fundamental understanding of the mechanisms of grain growth during sintering of nanoscaled powders are of great interest. It is reasonable to assume that there are new mechanisms that are unique to nanocrystalline particles. There have been numerous suggestions that the rapid grain growth occurs by coalescence of grains. Coalescence describes a unique way of grain growth, which can be accomplished through mass transport mechanisms. Possible mechanisms for coalescence include various diffusion process, or even grain rotations. Direct evidence of coalescence is, however, very difficult to identify.

III.2.3 Sintering Processes and Techniques for Controlling Grain Growth

III.2.3.a Grain Growth Inhibitors

Grain growth inhibitors have been used to mitigate grain growth during sintering. It was found that 100-150 nm grain sizes at full density could be obtained via standard LPS with the addition of 1.5wt% VC [18, 22, 49]. The use of grain growth inhibitors is widely practiced for sintering fine grain and ultra-fine grain WC-Co materials in the industry. Commonly used inhibitors include chromium carbide, tantalum carbide, and vanadium carbide. Their relative effectiveness can be ranked in the order VC>Cr_3C_2>NbC>TaC, although other considerations such as corrosion resistance and hot hardness may affect the choice of grain growth inhibitors.

The mechanisms of growth inhibition are the subject of many research reports [24, 30, 31, 37, 38, 49-58]. Sadangi et al. Carried out an in-depth study on the effects of VC addition on grain growth in WC-Co, which suggested that VC or Cr_3C_2 are more effective in inhibiting grain growth because they have higher solubility and diffusivity in cobalt binder phase [58]. The dissolution of VC and Cr_3C_2 in the binder phase suppresses the solution-reprecipitation of tungsten carbide which is the mechanism of grain growth during sintering of WC-Co materials. Based on this theory, grain growth inhibitors are incorporated in a solid solution of cobalt phase. These solid solution grain growth inhibitors form low melting point ternary liquids(s) at temperatures in the range of 1200-1250 ^{o}C. Since these low melting point solid solutions are saturated with grain growth inhibiting elements, the dissolution of W and C in the binder phase are prevented and grain growth are minimized.

S. Lay et al. investigated the microstructure of VC-doped WC-Co alloy using high resolution transmission electron microscopy [52]. Their results attributed the effectiveness of VC to the formation of a thin VC layer deposited on various WC crystal faces with an epitaxial relationship during early sintering process. The formations of such VC and Cr_3C_2 film on WC/Co interfaces were recently modeled by S. A. E. Johansson and G. Wahnstrom [59].

Almost all presently known grain growth inhibition mechanisms are based on the WC grain growth by solution-reprecipitation coarsening in the presence of liquid phase. However, studies are also needed to understand the roles of VC on grain growth during solid state sintering.

III.2.3.b Pressure Assisted Sintering

Pressure assisted sintering is another approach for controlling grain growth. Published microstructures showed WC grains grew from 50 nm to ~200 to 500 nm after HIPing [15, 24]. In particular, Azcona and his colleagues investigated the sintering of nanograined WC/Co powder by HIPing at solid state [24]. Even when grain growth inhibitors were used in combination with HIPing at solid state, the final sintered grain sizes were reported to be between 200 and 600 nm. It has been demonstrated that nanoscale grain sizes after sintering can be achieved with ultrahigh pressure processes such as hot pressing using ultrahigh pressure cells with >1 GPa pressure [60], explosive compaction [61], or severe plastic deformation methods [62]. However, all current high pressure processes (>1 GPa) are laboratory techniques that are not suitable for mass

productions.

In mid 1990s, Dubensky et al. applied the so-called rapid ominidirectional compaction (ROC) process to the consolidation of nanoscaled WC/Co powders [42]. In the reported study, Nanocarb™ WC-8%Co with an initial average grain size of approximately 50 nm was sintered at 1000 °C for 10 second under 830 MPa pressure. The reported grain size at the sintered state was 150 nm. It should be noted that compared to other pressure-assisted consolidation processes, ROC process can and has been used for commercial mass production of tungsten carbide based products.

A fundamental reason for using external pressure during sintering is to promote densification by adding a driving force. It is a particularly important factor for sintering nanostructured powder because it does not directly contribute to the driving force for grain growth. The effects of pressure are constrained by the pores and any gases in the pores. With conventional pressure assisted sintering techniques, such as hot pressing and HIPing, a longer holding time is required to allow diffusion and creep flow controlled mechanisms to contribute to the final densification. The longer holding time, however, leads to significant grain growth. Higher pressures are capable of collapsing pore structures and inducing plastic flow and rapid bonding in powder compacts at elevated temperatures. This eliminates the need for long holding times at high temperatures and hence prevents grain growth.

III.2.3.c Fast Sintering Techniques

Compared to conventional sintering techniques, fast sintering techniques are characterized by shorter densification time at lower temperature, resulting from external field accompanying pressure applications such as SPS, HFIHS etc,. SPS, for example, by application of electrical fields, can generate rapid and simultaneous heating within samples due to the pulse electrical current through the graphite die and/or samples. There have been other expected activated effects by external fields, like plasma surface cleaning, which are not confirmed yet. Even so those characteristics which combine rapid heating with pressure provide high potential to make nanocrystalline WC-Co.

Taking those advantages, even without the addition of grain growth inhibitors, the final sintered grain sizes by fast sintering techniques were reported to be between 50 nm and 800 nm [43, 63]. Shape changes and faceting of the surface of WC grains were observed at low temperature (about 1000 ^{o}C) even with very fast heating rate 1400 ^{o}C /min during the fast sintering process [35, 43]. This result indicated that the mass transport like dissolution or surface diffusion of the WC grains takes place very fast even at low temperature with smaller grain size. Also it has been speculated that there exists liquid cobalt phase which aids the mass transport process. Table 1 summarizes the results of various sintering techniques with respect to densification and grain sizes.

Table 1. Results of various sintering techniques with respect to densification and grain size.

Consolidation process	*Process Temp.& hold time*	*Heating rate (°C/min)*	*Pressure (MPa)*	*Initial powder & grain size*	*Grain growth inhibitor*	*Relative density (%)*	*Sintered grain size (nm)*	*References*
Hot pressing	1300°C,20 min	N/A	30	WC-10Co-0.6 VC	0.6 VC	100	169	[57]
Hot pressing	1700°C,43 Ks	N/A	1500	WC-14Co & 7 nm	No	100	95	[64]
Hot pressing	1300°C,90 min	N/A	25	WC-11Co & 80 nm	No	100	780	[63]
SPS[a]	1100°C,5 min	N/A	25	WC-11Co & 80 nm	No	100	780	[63]
HIP[b]	1000°C,1 h	N/A	150	WC-10Co	No	100	~400	[24]
HIP	1000°C,1 h	N/A	150	WC-10Co-0.4VC	0.4VC	100	~200	[24]
SPS	1150°C,10 min	N/A	60	WC-10Co	No	98	230	[29]
SPS	1100°C,10 min	150	60	WC-12Co & 40-250 nm	No	99.89	800	[30]
SPS	1100°C,10 min	150	60	WC-12Co & 40-250 nm	1VC	95.94	470	[30]
SPS	1240°C, 2 min	100	60	WC-10Co & 50 nm	No		280	[38]
SPS	1240°C, 2 min	100	60	WC-10Co & 50 nm	0.9 VC		170	[38]
SPS	1150 °C, 5 min	100	10 KN	WC-8Co & 33 nm	No		200	[32]
SPS	1200°C, 5 min	N/A	30	WC-10Co-0.8VC & 11 nm	0.8 VC	95.1	< 100 nm	[65]
SPS	1000°C, 10 min	100	100	WC-10Co & 100 nm	No		~350	[35]
HFIHS[c]	1200°C, 55 sec	1400	60	WC-10Co & 100 nm	No	99.4	323	[41]
PPS[d]	1100°C, 5 min	1000	60	WC-12Co & 60 nm	No	98	50	[43]
ROC[e]	1000°C, 10 Sec	N/A	830	WC-8Co & Nanocarb	No	14.6	150	[42]

a- Spark Plasma Sintering; b- hot isostatic pressing; c-High Frequency Induction-Heated Sintering; d- Pulse Plasma Sintering; e-Rapid Omni Compaction;

Spark plasma sintering (SPS) is a new pressure-assisted sintering process that has quickly gained popularity with researchers looking for ways to consolidate materials with nanoscale or simply very fine grain sizes, or with other non-equilibrium microstructures. SPS, a commercial version of several related consolidation techniques, was developed primarily during 1980's and 1990's. The other variations or terms of the technique include plasma activated sintering, field assisted sintering, and electro-consolidation, all of which share the same basic process elements as conventional hot pressing. The main difference between the SPS process and a hot press is that rather than using an external heating source, a current (either or AC or pulsed) is allowed to pass through the electrically conducting die, and the sample itself if it is conductive. Further, the technique of heating using the graphite die has also been used in conventional hot pressing. Therefore, the real uniqueness of the SPS process may lie in the claimed electric spark and plasma that may be generated between particles as the result of pulsed electric current. A comprehensive and critical review of the SPS process is beyond the scope of this paper, for which the reader is referred to the literature [66, 67].

There have been many reported studies of the sintering of nanosized WC-Co using the SPS process [27-38]. In order to retain small grain sizes, most of the reported studies used sintering temperatures in the range of 1100 to 1200 °C, significantly lower than normal sintering temperature of WC-Co materials (1360 – 1500 °C). As described above, the heating rate of SPS is very high ranging from 100 to 150 °C/min, and the pressure of SPS process is moderate (~60 MPa). The grain sizes of the sintered materials using SPS are, however, not as fine as it had been hoped, as indicated by the data in Table 1. Considering that sintered conventional WC-Co materials must have greater than 99.9% relative density to have any prospects for industrial applications, it is clear that sintering nanocrystalline WC-Co is still difficult even when the SPS process is used.

Table 1 summarizes the results of various sintering techniques with respect to densification and grain size. The published data show that no true nanocrystalline (<100 nm) bulk WC-Co materials have been consistently produced to date. Experimental observations seem to suggest that ~100 nm is the low limit of grain size refinement for WC-Co materials given the currently available knowledge and technologies. The need to fully densify the material and limit grain growth at the same time causes opposing considerations in process design.

Finally, it is noted that sintered grain sizes between 0.1 to 0.8 microns are currently manufactured commercially by using conventional ultra-fine tungsten carbide powders. The initial grain size of commercial ultra-fine WC powder ranges between 0.3 and 0.5 microns. For example, Gille reported a new grade of sintered hardmetal with a 100 nm mean linear intercept length using 1% total of a VC/Cr_3C_2 additive [49].

III.3 Mechanical Properties of WC-Co Sintered from Nanosized Powders

Cemented tungsten carbide, consisting of large volume fractions of WC particles in a cobalt metal matrix, is a cermet composite material. It is well understood that the hardness of cermet materials is inversely proportional to its grain size and that the fracture toughness is inversely proportional to the hardness. Therefore, a finer grain size usually results in lower

fracture toughness. However, for nanostructured metal alloys and ceramics, it has been noted that the mechanisms of strengthening are different because of the large volume fractions of grain boundaries. The deformation mechanisms depend on grain boundary sliding and diffusion-controlled processes [5, 68]. Grain boundaries in polycrystalline metals also impede the motion of cracks, which contributes to better fracture toughness. Therefore, it is hypothesized that the fracture toughness of WC-Co composite will improve when WC grain sizes reach nanoscale.

III.3.1 Hardness and Fracture Toughness

Hardness and fracture toughness are the two most important mechanical properties of cemented tungsten carbide and other cermets. Other mechanical properties, such as flexural strength, wear resistance and impact resistance, are fundamentally dependent on the hardness and fracture toughness.

The mechanical properties of nanostructured WC-Co composites were reported in several studies [15, 18, 24, 25, 39, 43-45, 49, 69, 70]. As expected, very high hardness was achieved with the ultrafine-grained microstructure. Data show that the fracture toughness of the sintered WC-Co using nanostructured powder decreases as the hardness increases. Denseley and Hirth studied the fracture toughness of sintered WC-Co with an average grains size of 70-100 nanometer and 6.7% of cobalt using modified compact tension method [44]. They found that the mode I and mode I/III fracture toughness of nanoscale tungsten carbide grains (70 nm) in cobalt was less than the toughness of mesoscale WC-6.7%Co alloys with similar cobalt volume fractions. Although this is consistent with the general trend for the conventional WC-Co, it was disappointing for many in the field because the toughness improvement is much more highly needed than the increase in hardness.

However, several other reported data in the literature indicate that the mechanical behavior of bulk WC-Co deviates significantly from its coarser grain counterpart when the grain sizes approach 100 nm. Fang and Eason showed that the surface crack resistance of sintered bulk WC-Co using nanostructured powder determined by the Palmquist method is higher than that using conventional fine powder when they are compared at the same hardness level [18].

Jia et al. further showed that the reduction in toughness vs. hardness levels off when grain size reaches nanoscale as shown in Fig. 1 [45]. It was suggested that the toughness decreases with increasing hardness in conventional composites but the increase of hardness in nanostructured composites does not decrease their bulk fracture toughness. The difference between the fracture toughness of WC-Co using nanostructured powder and that using conventional ultra fine powder has also been shown to depend on the cobalt contents [Fang unpublished]. For example, when a sample was sintered using nanostructured WC-10%Co powder, the sintered hardness was Ra = 92.0 and the fracture toughness K_{Ic} was 12.0 MPa·m^{½}, while the fracture toughness of the conventional WC-Co is approximately 9.0 MPa·m^{½} when Ra = 92.0. This indicates over 30% increase in the fracture toughness.

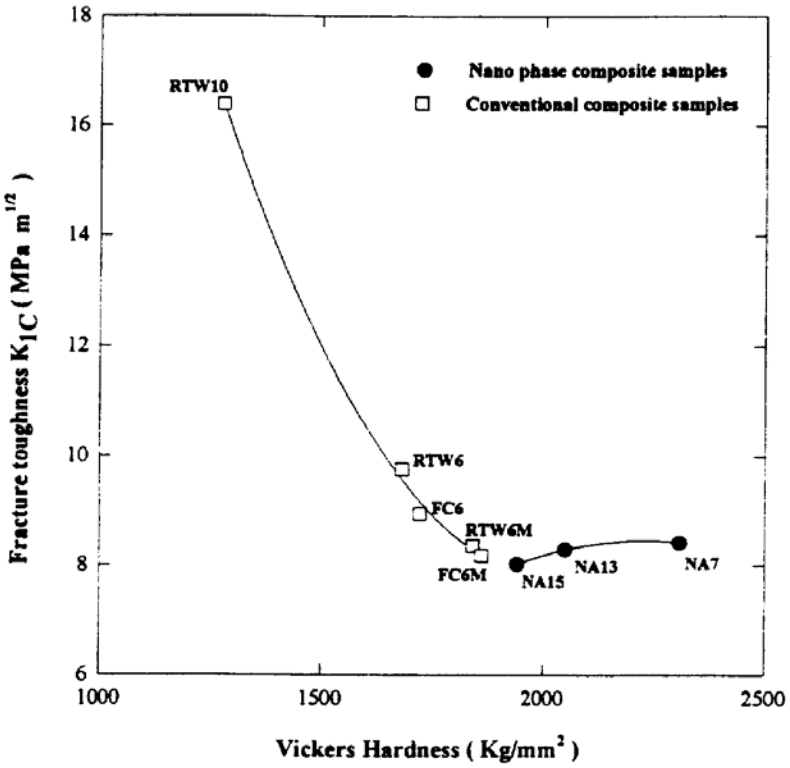

Fig. 1. Fracture toughness versus hardness of WC-Co materials comparing nano phase composite samples to conventional composite samples [45].

A similar result was reported by Barth et al [15]. An isolated case was shown in which the fracture toughness is higher for samples made from nanocrystalline powders than those from conventional powders when compared at a similar hardness level.

Table 2 lists some of the mechanical properties data obtained from the literature. It compares the mechanical properties of WC-Co materials made from nanosized powders using various different consolidation techniques. Based on the data in Table 2, Fig. 2 plots the fracture toughness versus hardness. The dashed line in Fig. 2 represents the relationship of the fracture toughness and hardness of conventional WC-Co materials [71]. It is clear from Table 2 and Figure 2 that some of the reported fracture toughness values are very high. For example, Zhao et al reported that the fracture toughness of a sample was 13.5 MPa.m$^{1/2}$ while hardness is *HRa* 94.5. The specimen was sintered using SPS and has a relatively density value of 98%. Another exceptionally high fracture toughness value was reported by Michalski et al. The sample was sintered via the PPS process. The material had a hardness value of H_V 2250 (kg/mm^2) and the fracture toughness of 15.3 MPa.m$^{1/2}$. However, because almost all of the fracture toughness data listed above were measured indirectly using the Palmquist method and converted to the K_{IC} values, it is not clear if these high fracture toughness values can be reproduced using the standard fracture toughness testing methods such as the shoot-rod method (ASTM-B771) and the SENB method (ASTM-E399). Unfortunately, because there are no information available to date that provides confirmation or further evidence about the reported high fracture toughness values, it still cannot be concluded if the materials made from nanosized powders have better fracture toughness.

Table 2. Hardness and fracture toughness of sintered WC-Co using nanosized powders as reported in the open literature

Consolidation process	*Sintered grain size (nm)*	*Hardness* (H_V)*	*Fracture toughness** ($MPa.m^{1/2}$)*	*References*
Hot pressing	169	2084	8.8	[57]
Hot pressing	95	1100	14	[64]
Hot pressing	780	1575		[63]
SPS	780	1725		[63]
HIP	~400	1740		[24]
HIP	~200	1910		[24]
SPS	230	2030	13.5	[29]
SPS	800	1450	10.9	[30]
SPS	470	1570	11.42	[30]
SPS	280	1569	9.3	[38]
SPS	170	1726	9.5	[38]
SPS	200	2030		[32]
SPS	<100 nm	1887	11.5	[65]
SPS	~350	1800	12	[35]
HFIHS	323	1886	13.5	[41]
PPS	50	2250	15.3	[43]
ROC	0.15	1936	9.8	[42]

**For convenience of comparison, the Original hardness values from papers were converted to Vickers hardness values.*
*** Fracture toughness value was calculated from indentation method.*

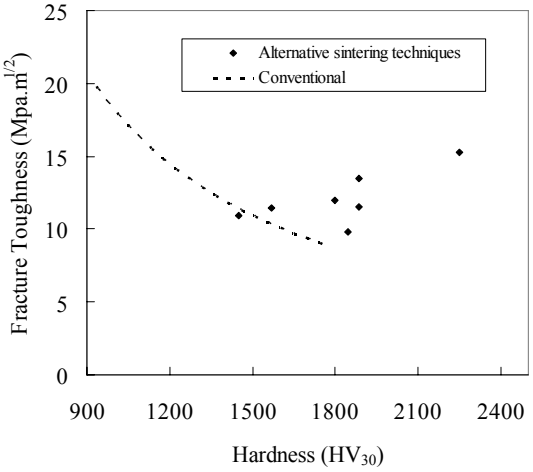

Fig. 2. Fracture toughness vs Hardness relationship of conventional WC-Co materials (dashed line) and the materials made from nanosized WC/Co powders by sintering via alternative techniques as listed in Table 2 (diamond).

However, based on these data, it is clear that the mechanical behavior deviates from the normal trend for hardness vs. toughness for *bulk* WC-Co when grain sizes approach nanoscale. In addition, the trend of deviation is toward the improvement of hardness versus toughness relationship. Because all these data are based on samples that have submicron grain sizes in sintered state, the mechanical behavior of WC-Co with truly nanoscaled grain sizes (<30 nm) remain unexplored. A breakthrough in sintering technologies based on in-depth research is needed to enable one to manufacture *bulk* materials with nanoscaled grain structure before the true mechanical behavior of nanoscale WC-Co can be studied.

There are three categories of possible mechanisms by which the mechanical properties of WC-Co with nanoscale grain sizes may be improved over those of the conventional WC-Co materials. The first is based on the effects of flaws. It is expected, that the flaw sizes, e.g. pore sizes, in the sintered material starting with nanocrystalline WC/Co powder is drastically reduced when compared to that in the conventional bulk WC-Co. If the grain size is preserved at <30 nm, the flaw size will then be a few nanometers or less. This is beneficial for the fracture toughness, independent of the hardness of the material.

The second possibility is based on the effects of interfaces. At nanoscale there is a tremendous increase in the amount of interfaces between the WC grains and the Co binder compared to coarser grained counterparts. The partition of the crack path through binder/carbide (B/C) interfaces as opposed to other interfaces or transgranular cracks will increase dramatically in nanocrystalline WC-Co. It has been shown that the crack does not advance exactly along the interface but proceeds in the binder, forming closely-spaced shallow dimples in conventional WC-Co [72]. There is an appreciable amount of plastic deformation of the binder involved in fracturing through B/C interfaces. The increase in the fractions of crack path through B/C interfaces will contribute a significant amount of fracture energy to the process, which would in turn enhance the overall toughness of the material.

The third possibility is also related to the effects of interfaces involving the deformation mechanisms. As pointed out by Gleiter and Siegel [68, 73], the conventional dislocation generation and migration become increasingly difficult as the scale is reduced into the nanometer range. The more likely mechanisms for deformation will be grain boundary sliding and short range diffusion assisted events such as grain rotation and grain shape accommodation. Both of the above interface dependent mechanisms will be possible particularly at relatively high cobalt content when the nano WC particles are enclosed by the cobalt phase, the grain size of which is also at a nano scale. When the nanocrystalline cobalt becomes the controlling phase, the behavior of the composite will also change.

It should be noted that for conventional bulk WC-Co, the fracture toughness is a function of mean free path (MFP) between the WC grains. It is dependent on the plastic deformation and tearing of cobalt metal binder. A finer grain size results in a smaller MFP at a given constant volume fraction of cobalt and a smaller plastic zone, and therefore, lower fracture toughness. For nanocrystalline WC-Co, the effect of the plastic mechanisms of Co will no doubt be reduced from the viewpoint of MFP. Therefore, all the possible grain boundary mechanisms including sliding and rotation are critical for its toughness. The question is whether the fracture energy through grain boundaries will be enough to compensate for the loss of plastic deformation of

binder phase, and what would be the final relationship between the hardness and the fracture toughness. The answers to these questions will have far reaching scientific and industrial significance not only with respect to WC-Co cermet materials but also many other material systems including other MMC's.

III.3.2 Wear Resistance and Performance

The sliding wear resistance of nanostructured WC-Co materials was studied in detail by Jia and Fisher using a carefully constructed pin-on-disc method without lubricant at room temperature [74]. A series of grades of WC-Co with varying grain sizes and cobalt contents were made into pins with polished hemispherical shape. The radius of the tip was about 3.5 mm. During the tests, the pins slid under a modest load (9.8N) on commercially ground silicon nitride plates. The results showed that the wear resistance of nanostructure WC-Co is higher that that of conventional cermets in proportion to their hardness as shown in Fig. 3. The sliding wear of the conventional and nanostructured WC-Co composites is, in the first approximation, expressed by a Blok-Archard equation with wear coefficient $k=6.9\times10^{-6}$. The Blok-Archard equation is given as follows.

$$V = kPs / H \qquad (1)$$

where k is the wear coefficient, H the hardness, P the load, and s the sliding distance. However, a more detailed analysis found that the wear coefficient k as a function of grain size and cobalt content does not follow the same trend as that of conventional WC-Co composites as shown in Figure 3, which suggests that the general trend of increasing wear with decreasing WC grain size does not extend to nanostructured materials.

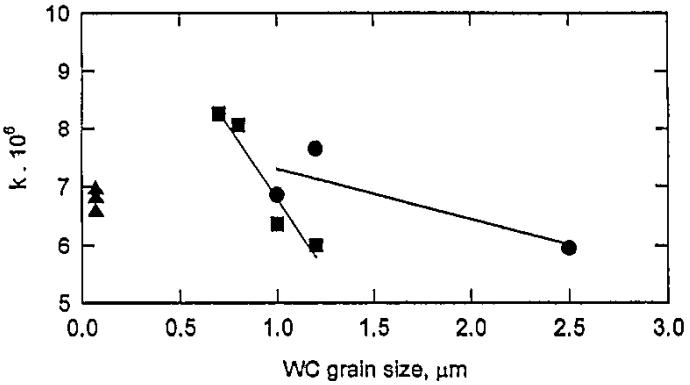

Fig. 3. The variation of wear coefficient k with the carbide grain size in WC-Co composites sliding against silicon nitride at 9.8N applied load and 31.4 mm/s sliding speed. Triangles, nanocomposites; squares, cermets with 6%Co; circles, other commercial grades of WC-Co with 10, 15 and 20%Co respectively.

The wear resistance of WC-Co materials is a functional property that depends on the hardness and fracture toughness of the material, and the wear environment / mechanisms. It is particularly important to note the effects of wear mechanisms. Different wear applications, i.e. wear environment, has different mechanisms of wear. The ranking of the wear resistance of WC-Co materials and the effects of grain size and cobalt content differ depending on specific

applications. Therefore, the results obtained from sliding wear tests may not be directly applicable to sand abrasion or cutting tool applications. There are currently no studies reported in the literature on the wear resistance of nanostrucutred WC-Co materials in machining or sand abrasion applications.

Applications of nanostructured cemented tungsten carbide include all areas where conventional WC-Co materials are used. However, industrial interests have been focused on the manufacturing of printed circuit board (PCB) drills. PCB drills can have drill tip as fine as 40 μm as shown in Fig. 4. The grain size of the material that the drills are made of becomes a significant portion of the tip cross-section. Extremely fine grain sizes are required to achieve long and reliable tool life. Figure 5 compares the tool life of a PCB drill made of nanocrystalline powders with that of conventional powders. The result is consistent with the higher hardness of the nanocrystalline WC-Co composites. But it also demonstrates the effectiveness of using nanocrystalline powder in preventing premature tool failures.

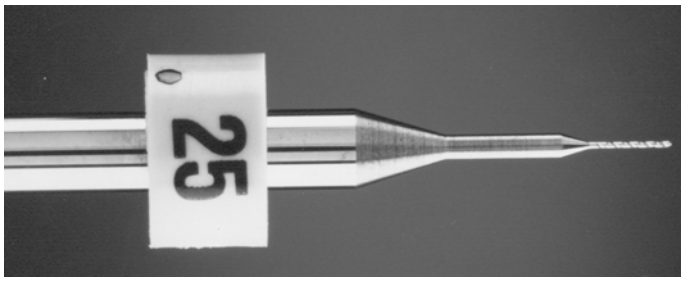

Fig. 4. A printed circuit board drill with a tip diameter of 0.25 mm.

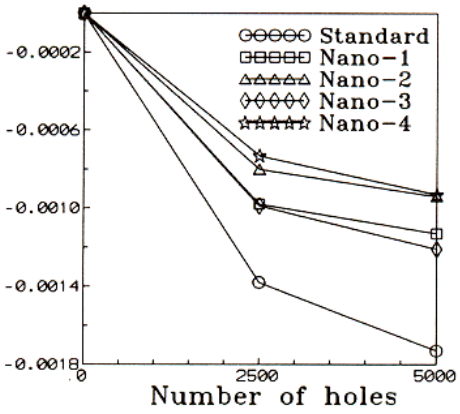

Fig. 5. The primary wear of printed circuit board drills versus the number of holes drilled.

IV. Technical Approach and Hypothesis Guiding This Approach

IV.1 Synthesis of Nanosized WC/Co Powders

Based on literature review, the project team decided to investigate two synthesis methods:

1. Chemical vapor synthesis method with chloride precursors, and

2. Plasma-assisted chemical vapor synthesis using chlorides as well as oxides precursors.

The following section will briefly discuss the aforementioned methods.

It was first decided to synthesize nanosized WC/Co composite powder by a chemical vapor synthesis in a tubular reactor system. The primary concept was to synthesize nanosized WC and then uniformly mixed WC and Co powders from the metal chloride precursors (WCl_6 and $CoCl_2$) rather than the constituent metals as in typical conventional processes. The process involves reducing a vapor phase mixture of precursors and subsequent carburizing by hydrogen/methane mixtures. The reactions for producing the WC/Co mixtures using metal chlorides in the proposed method are as follows:

$$WCl_6\,(g) + xCoCl_2\,(g) + CH_4\,(g) + (x+1)H_2\,(g) = WC\,(s) + xCo\,(s) + (2x+6)HCl\,(g) \quad (2)$$

$$\Delta G^o = -(151+13x)\text{ kcal at } 1200^oC;\ \Delta H^o = -(10.5+20.2x)\text{ kcal}$$

It is seen that the overall reaction is thermodynamically favorable and has a substantial exothermic heat, which indicates that they can be carried out without much external heating. The equilibrium composition diagram for the WCl_6-$CoCl_2$- H_2-CH_4 mixture was obtained by the use of HSC Chemistry software developed by Outokumpu Research Oy [75], as shown in Figure 6(a). The diagram shows it is thermodynamically feasible to synthesize WC and Co from the WCl_6-$CoCl_2$- H_2-CH_4 mixture.

Subsequently, it was decided to use a thermal plasma process in which metal oxide precursors can be used rather than the more volatile but expensive and difficult-to-handle metal chlorides. The temperature generated by plasma flame is high enough to volatilize the metal oxides followed by subsequent reactions in vapor phase to synthesize nanosized WC-Co composite powder. Figure 6(b) shows the equilibrium composition diagram for the WO_3-Co_3O_4-H_2-CH_4 mixture. It also shows feasibility to synthesize WC and Co using metal oxides as the precursors in the plasma reactor system.

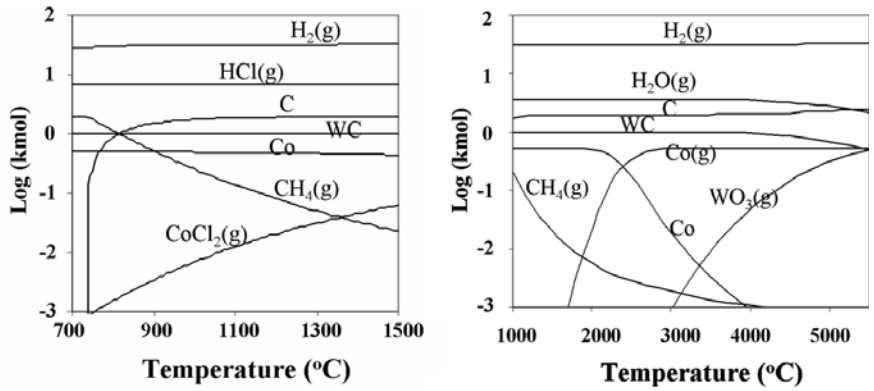

Fig. 6. Calculated equilibrium composition in (a) WCl_6-$CoCl_2$-H_2-CH_4 system with input amounts of WCl_6, $CoCl_2$, H_2 and CH_4 of 1, 0.5, 30, and 3 kmol, respectively and (b) WO_3-Co_3O_4-H_2-CH_4 system with input amounts of WO_3, Co_3O_4, H2, and CH_4 of 1, 0.17, 30, and 3 kmol, respectively.

Again, the advantage of this process is that the vapor phase reactions lead to the formation of nanosized WC particles as well as very uniform WC and Co mixture owing to the simultaneous reactions in gas phase.

IV.2 Consolidations of Nanosized WC/Co Powder by Ultrahigh Pressure Sintering Technologies

Addressing the challenges of achieving nanoscale grain sizes at sintered state with full densification, the main approach used in the program for consolidation is to use ultrahigh pressure rapid hot consolidation. Ultrahigh pressure consolidation processes are defined in this project as those with a higher pressure capacity than the standard hot pressing and HIPing, above 400 Mpa. It is note that the industrially practiced hot pressing or HIPing cannot provide pressures high enough to limit the grain growth in the naoscale during sintering of nanocrystalline WC-Co powders. However, it was hypothesized that the rapid grain growth can be avoided by rapidly heating the material to a high temperature and completing the sintering process within minutes under ultrahigh pressures, thereby minimizing the time duration at the high temperature.

There are two existing high pressure industrial processes as relevant to cermet industries and this project: Rapid Omni-directional Compaction (ROC) and high temperature high pressure (HTHP) processes. The HTHP process is commonly used for synthetic diamond production with pressures up-to 7 GPa. It is not suitable for mass production of cermet materials. The ROC process needs long pre-heating time which is not favorable to prevent the grain growth during heat up. Therefore The UPRC process was developed based on the existing ultrahigh pressure technologies, but incorporating rapid heating, sample / pressure medium interaction control, optimum pressure cell design, and powder processing techniques. The final integrated process had the capability to limit grain growth to <100 nm while achieving full densification at an affordable cost.

The UPRC process offers the following unique advantages:

- Full and rapid densification at much lower temperature or solid state,
- Bonding between solid grains of the phase that has a high melting point, and
- Improved mechanical properties.

V. Experimental Methodology, Test Procedures, Characterization Methods

V.1 Chemical Vapor Synthesis of Nanosized WC/Co Powders

This section describes the apparatuses used to synthesize the Nanosized WC/Co Powders. As indicated earlier, two types of reactors were used: an electrically heated tubular reactor operating in the temperature range of 1000 - 1400°C and a non-transferred thermal plasma reactor. In both units, a continuous feeding system to introduce the precursor into the reactor, describe in detail below, was selected since this is more useful in industrial applications than a batch feed system. Thus, such a feeding system was designed and fabricated. The tubular reactor system consisting of an entrained-flow powder feeder, a vibrator, a carrier-gas line, a precursor container, and a precursor delivery line was specially fabricated to feed the reactant precursors into a volatilizer in the reactor. The plasma reactor system was equipped with a plasma generator with a downward plasma torch, a power supply unit, a cylindrical reactor, a cooling chamber, a cooling system, a precursor feeding system, a powder collector, a gas delivery system, an offgas scrubber, and an offgas exhaust system.

V.1.1 Precursor Feeding System

Metal chlorides are hygroscopic and readily react with oxygen in the air. Thus, it is difficult to handle the metal chloride powder. First, a slurry feeding method was considered as the feeding method. The slurry consisted of metal chloride powder and an organic liquid. This organic medium should not react with metal chloride and should prevent oxidation of the powders. Thus, several organic liquids such as methanol, dichloromethane, benzene, and heptane were considered as the media candidates. In order to choose a suitable organic media, the properties of each candidate were examined and the equilibrium compositions were calculated using HSC software. The comparison of each candidate was performed under the condition of the same volume of the medium for a certain amount of tungsten chloride and cobalt chloride. From the examination, hydrocarbon liquids such as benzene, hexane and heptane were found suitable from the view point of producing WC and Co. However, these organic media also produce too much excess carbon. Thus, it was decided to feed the metal chloride precursors directly as powders and a powder feeding system was designed for this purpose. This system consists of a syringe pump, a vibrator, a carrier gas line, a sample container and a sample delivery line, as shown in Figure 7. The precursors are placed in a glass tube and fed to the volatilizer in the reactor through a stainless steel delivery line. Argon gas is introduced through the powder feeder as the carrier gas as well as an inert gas to keep the atmosphere in the container inert.

V.1.2 Tubular Reactor System

The tubular reactor system consisted of a 1.5 m long and 5.4 cm inner diameter 99.8% Alumina reactor, a vertical furnace with silicon carbide heating elements, powder feeding system using an entrained-low powder feeder, a powder collector using a polyester filter, a gas delivery system, an offgas scrubber containing 5 wt% NaOH solution and Bunsen burner, as shown in Figure 7. The furnace was a resistance heating furnace capable of a maximum temperature of about 1500 ^{o}C. The precursors were tungsten chloride (WCl_6) powder and cobalt chloride ($CoCl_2$) powder. A continuous feeding system for feeding these powders was designed. The

precursors were placed in a glass tube mounted on the powder feeder. A stainless steel tube of 3.2 mm inner diameter was used as the delivery line connected from the powder feeder to the volatilizer in the reactor. The volatilizer was made of an alumina tube of 6.4 mm inner diameter with holes near the closed end to provide an outlet for the vaporized precursors into the reactor. The powders produced were collected using a Teflon-coated polyester filter with a pore size of approximately 1 μm. The gas scrubbing cell was attached to the end of the reactor in order to remove the HCl gas product of the reduction process. Bunsen burner was attached to the very end of the system to burn off excess hydrogen gas fed into the reactor. The mixture of argon, hydrogen, and methane gases were fed into the reactor to reduce and to carburize the precursors. The reactor was purged with Ar gas before and after each experiment.

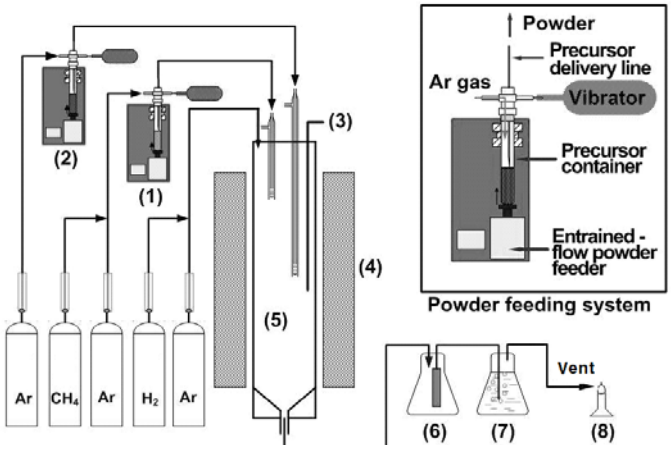

Fig. 7. Schematic diagram of the tubular reactor system: (1) entrained-flow powder feeder for WCl_6, (2) entrained-flow powder feeder for $CoCl_2$, (3) thermocouple, (4) vertical furnace, (5) alumina reactor, (6) powder collector, (7) scrubber, and (8) Bunsen burner.

V.1.3 Plasma Reactor System

The experimental apparatus of the plasma reactor system is shown in Figure 8. The plasma torch consisted of a water-cooled tungsten cathode and a copper anode nozzle operating at atmospheric pressure. The reactor consisted of a vertical water-cooled stainless steel tube of 15 cm inner diameter and 60 cm length and an inner graphite cylinder of 7.6 cm inner diameter and 60 cm length. Graphite felt was placed between the graphite tube and the inner wall of the water-cooled stainless-steel tube for the insulation of the reactor. The cooling chamber connected to the bottom of the reactor was a water-cooled two-layer stainless-steel box to cool the outgoing gas to a temperature lower than 150 ^{o}C. A data acquisition system recorded the temperatures at the reactor exit, the input and output cooling water, and outgoing gas from the cooling chamber. The precursor was fed toward the outside boundary of the visible plasma flame (7 mm diameter) from a distance of 15 mm near the exit of the plasma torch.

Argon and hydrogen were used as the primary and the secondary plasma gas, respectively. Argon, used as the primary plasma gas, was also separately passed through the powder feeder as the carrier gas as well as an inert gas to keep the atmosphere in the container inert. Before delivering the precursor into the plasma flame, the reactor was heated by the plasma flame generated until its temperature reaches a steady level.

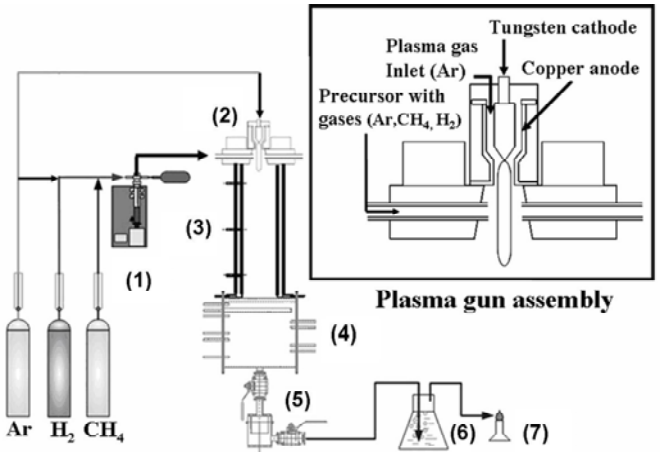

Fig. 8. Schematic diagram of the plasma reactor system: (1) entrained-flow powder feeder of WCl_6, (2) plasma gun, (3) cylindrical reactor, (4) cooling chamber, (5) powder collector, (6) scrubber, and (7) Bunsen burner

V.1.4 Precursor Preparation

For this research, 99.9% tungsten hexachloride (WCl_6) and 97% cobalt dichloride ($CoCl_2$) were used as the precursors. These powders were obtained from Sigma-Aldrich and Alfa Aesar, respectively. The boiling points of these materials are 346°C and 1049°C, respectively. Metal chlorides have been favored as the precursors owing to the ease of the volatilization as well as the ease of reduction by hydrogen followed by subsequent vapor phase reaction in a tubular reactor system. 99.9% Ammonium paratungstate [APT, $(NH_4)_{10}(H_2W_{12}O_{42})\cdot 4H_2O$] and 99% cobalt oxide ($Co_3O_4$) were selected as the precursors for the plasma reactor system. These can be volatilized in the plasma flame generated and subsequent vapor phase reactions occur by the addition of reactant gases of hydrogen and methane for producing tungsten carbide and cobalt. These materials were obtained from An Allegheny Technologies Company and Alfa Aesar, respectively. These are also inexpensive and suitable for industrial application.

The precursors were ground to prevent the tube connecting the powder feeder and the volatilizer from clogging. After grinding, the precursors were placed in the precursor container and weighed to calculate a feeding rate by measuring the weight change before and after experiments. The sample preparation of metal chlorides (WCl_6 and $CoCl_2$) was conducted in a glove box since metal chlorides is readily react with oxygen in the air. The precursor container containing metal chloride was covered with a rubber stopper prior to mounting on the powder feeder. In case of APT and Co_3O_4 the sample preparation followed the same methods as described above except the inert environment needed to prepare the metal chlorides.

V.1.5 Powder Analysis and Characterization

The average particle size, composition, and morphology of the synthesized powder were determined. These included the analyses of the synthesized product by the use of X-ray diffraction, a light scattering tool, SEM, and TEM. The product composition and grain size were

analyzed by X-ray diffraction. The grain size of synthesized WC was calculated from the XRD pattern using the Scherrer equation calibrated by using standard samples. The Scherrer equation relates the XRD peak width and crystallite size, as follows [76]:

$$Crystallite\ Size = \frac{K\lambda}{(B - B_{ex})\cos\theta} \tag{3}$$

where K = Shape factor (0.89 – 1.0 taken as 0.9 in this work)
λ = X-ray wavelength (1.542 Å for Cu-Kα radiation)
B = Full width at half peak height (radians)
θ = Peak position
B_{ex} = Extra broadening due to microstrain and instrumental effects (radians), obtained by the use of a standard sample.

It is noted that because the powders in this study were produced in the vapor phase, no lattice strain effects were considered in this grain size analysis. The molar ratio of different tungsten carbide phases in the product was also estimated from XRD patterns using the internal standard method, combined with the following calibration equation: [76]

$$\frac{I_\alpha}{I_\beta} = \kappa\frac{X_\alpha}{X_\beta} \tag{4}$$

where I_α = integrated intensity of α phase peak
I_β = integrated intensity of β phase peak
X_α = mole fraction of α phase
X_β = mole fraction of β phase, and
κ = constant.

The average particle size and the particle size distribution were analyzed by using a Zeta potential analyzer that determines zeta potential using phase analysis light scattering. The actual particle size and morphology of powders were analyzed by the use of SEM and TEM with energy dispersive X-ray spectrometry (EDS) that also give distribution of the elements.

V.2 Sintering Nanocrystalline WC-Co Powders

This part of research focused on seeking fundamental understandings of the mechanisms and interactions between the grain growth and densification during the early stage of sintering of the nanocrystalline WC-Co powders. Sintering experiments were carried out to study the sintering behaviors as a function of temperature and time. The effects of other influencing factors, such as initial grain size, cobalt content, and grain growth inhibitor, were investigated. Based on the analysis of kinetics of the grain growth and densification and the microstructure evolution during sintering, the possible mechanisms of grain growth and densification were proposed. Meanwhile, an ultrahigh pressure rapid hot consolidation process (UPRC) was developed to consolidate nanocrystalline cemented tungsten carbide powders. The effects of the UPRC process variables (including heating rate, temperature, holding time, and pressure) on grain growth and densification of the nanocrystalline WC-Co powders were studied. The

mechanical properties of nanocrystalline WC-Co materials consolidated by UPRC were also evaluated and compared to those of samples produced by conventional liquid phase sintering and literature values.

For the purpose of studying sintering mechanisms of nanocrystalline WC-Co powders, a high energy milling method was used to prepare the nanocrystalline WC-Co powders. Note that the nano powders produced by the CVS method were not ready at the time when the sintering studies were carried out. A high energy mill, called high energy dual-drive planetary mill (HE-DPM) (see Figure 9) which combines revolution and rotation of the mill canister, can generate an acceleration field that is nearly 60 times the force of gravity [77].

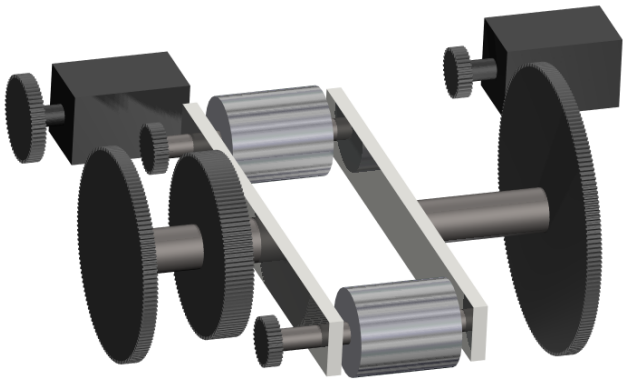

Fig. 9 Photo of high energy dual-drive planetary mill.

The dual-drive planetary mill used in these experiments operates with a single phase 3.73 kW (5 HP) electric motor driving the revolution shaft at a constant rotational velocity of 275 RPM. The rotational gear is driven by a three phase variable speed motor. The internal radius of the milling canister is 31.5 mm. The total volume of each mill canister is approximately 533 mL. Throughout all of the experiments, the milling canisters were filled to 50% with grinding media, while the milled powder was measured to fill 100% of the interstices between media. In order to prevent oxidation and to aid in dispersion, the tungsten carbide particles were immersed in an organic solvent of liquid heptane. Tungsten carbide grinding media was used for its high specific gravity and potential in reducing contamination to the final product. The WC-Co balls (WC-6Co, Diameter 0.5 mm, Glen Mills Inc.) were used as grinding media to minimize the contamination during milling. Oleic Acid was used as a dispersant. Paraffin wax (2 wt %) was added as the lubricant.

The raw materials including WC, Co, and grain growth inhibitors (VC, Cr_3C_2) powders were provided by Kennametal Inc. Initial particle size of the as-received WC, Co, VC and Cr_3C_2 powders were approximately 0.8, 1.0, 1.0 and 1.0 μm, respectively. The mixed powders were milled in the high energy mill for different time to prepare powders with different grain sizes.

V.2.1 Early Stage Sintering

Sintering experiments of nanocrystalline WC-10 wt% Co powders were carried out at temperatures from 800 to 1400 ^{o}C to study the WC grain growth behavior during early stage

sintering, before reaching the normal liquid phase sintering temperature (1400 ^{o}C) as shown in Table 3. The WC-10wt%Co powders were milled for 2, 5, and 12 hours to study the effect of initial grain sizes; the pure WC powder and WC-Co-VC powders were used to manifest the roles of Co and grain growth inhibitor during the grain growth of WC.

Table 3. Sintering matrix for sintering samples in the vacuum furnace.

Time (min)→ Temperature (°C)↓	*0*	*60*	*120*	*180*	*240*	*300*
800	✓					
1000	✓					
1100	✓	✓	✓	✓	✓	✓
1200	✓	✓	✓	✓	✓	✓
1300	✓	✓	✓	✓	✓	✓
1400	✓	✓	✓	✓	✓	✓

To study the grain growth and densification behaviors during heat up, samples were heated to preset temperatures in a vacuum furnace with a heating rate of 10 ^{o}C/min and then furnace cooled immediately. These experiments represent the conditions of the samples during a period of continuous temperature increase to a preset temperature.

To make fully dense samples to evaluate the mechanical properties of WC-Co produced from nanocrystalline WC-Co powders, the sintering temperatures were chosen from 1350 to 1400 ^{o}C with a holding time of 1 hour. After milling, the powders were dried in rotavapor (Buchi Rotavapor R-114) at 80°C before compaction. The powders were pressed uniaxially at 198 MPa in a cylindrical die using a hydraulic laboratory press (Model C-Carver Laboratory press, Fred S. Carver Inc.). A mixture of zinc stearate and ethanol was coated on the inner surface of die wall as a lubricant. The green as pressed samples were dewaxed in the vacuum furnace at 220 °C for 4 hours and 350 °C for 30 min in the presence of H_2/Ar (1:5) gas mixture before subsequent vacuum sintering.

V.2.2 Ultrahigh Pressure Rapid Hot Consolidation

Figure 10 shows the setup for the new process developed in this project which is termed ultrahigh pressure rapid hot consolidation (UPRC). The process was used successfully to produce dense nanocrystalline WC-Co without grain growth inhibitors in a short time with minimum grain growth.

Fig. 10. Photo of UPRC setup.

The compacts were dewaxed and then presintered at 800 ^{o}C for 1 hour in vacuum furnace. The presintered samples were placed in a graphite cell and then introduced into the UPRC system, shown schematically in 11. During the UPRC process, the current goes through the graphite cell, and then heats up the samples by resistance heating. The glass melts and conveys the isostatic pressure. Pyrophyllite is used as thermal and electrical insulation. Temperature was measured by a thermocouple inserted in the graphite cell, very close to the samples.

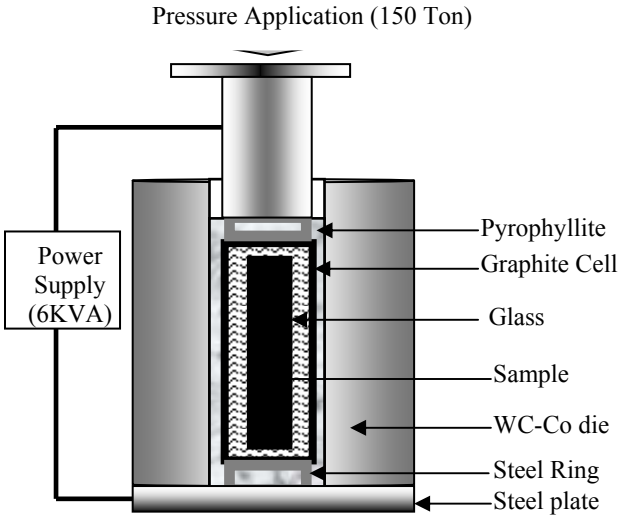

Fig. 11. Schematic diagram of apparatus for Ultrahigh Pressure Rapid Hot Consolidation (UPRC) process.

The UPRC process consists of three steps as shown in Figure 12: preheating, pressing, and cooling. In order to realize the isostatic pressure effect, the glass was melted first by applying 85% output of the total power capability in 2 minutes. Then the pressure was slowly increased to 90 ton. In the meantime, the output power was controlled at a given percent level during a period of time.

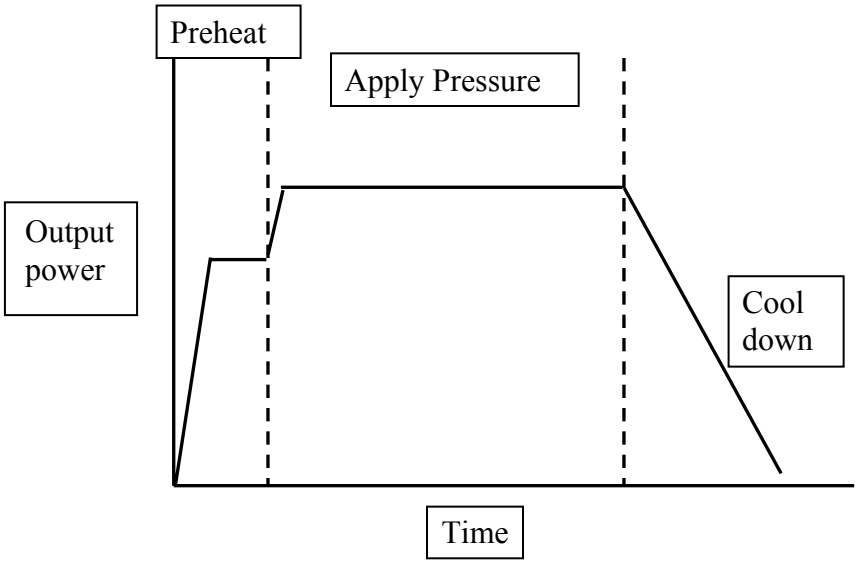

Fig. 12. UPRC procedure.

V.2.3 Sample Characterizations

Microstructure. To determine the grain sizes of as-milled powders as well as the sintered samples, the x-ray diffraction line broadening and the quantitative microscopy techniques were applied. The former is used when grain sizes are smaller than approximately 100 nm, while the latter applies to larger grain sizes. Due to the intense mechanical energy used during milling, there inevitably is strain energy stored within the crystal lattice. In order to quantify the grain size accurately considering the effects of the internal strains, the Stokes and Wilson's formula was used [78].

$$\beta = \beta_d + \beta_\varepsilon = \frac{0.89\lambda}{d\cos\theta} + 4\varepsilon\tan\theta \qquad (5)$$

where β is full width at half maximum (FWHM) of the diffraction peak after instrument correction; β_d and β_ε are FWHM caused by small grain size and internal stress, respectively; and d and ε are, respectively, grain size and internal stress or lattice distortion. The experimentally determined line broadening was corrected for $K\alpha_1$-$K\alpha_2$ separation and instrumental line broadening using coarse WC powders (average grain size about 10μm). To determine both d and ε from equation (5), line broadening data corresponding to multiple 2θ values are used. Grain size and internal strain can be calculated by plotting $\beta\cos\theta$ *vs.* $\sin\theta$. The grain size and lattice strain are derived from the intercept and the slope of the linear plot.

Figure 13 shows the X-ray diffraction patterns of the original WC powder and as-milled WC-10Co powder. It is obvious that the peaks of the WC phase become broader after milling. The Co peaks cannot even be seen because the peaks are too broadened and weak to be distinct from the background.

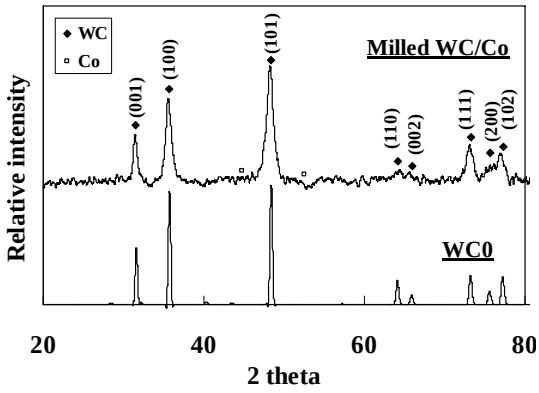

Fig. 13. X-ray diffraction patterns of high energy milled powder and original powder WC0 (0.8 μm).

The calculated grain size and internal strain as a function of milling time are plotted in Figure 14 where the inverse relationship between grain size and internal strain was demonstrated. It was found that the grain size of WC was reduced drastically at the initial stage of the milling process and reached about 50 nm in 2 hours. Then the milling efficiency decreases with increasing milling time. The grain size of WC reached about 10 nm after 12 hours. Further milling did not lead to reduction of the grain size and might result in serious contamination. In this research, most of the powders were milled for 12 hours except the powders for studying the effects of initial grain size on grain growth.

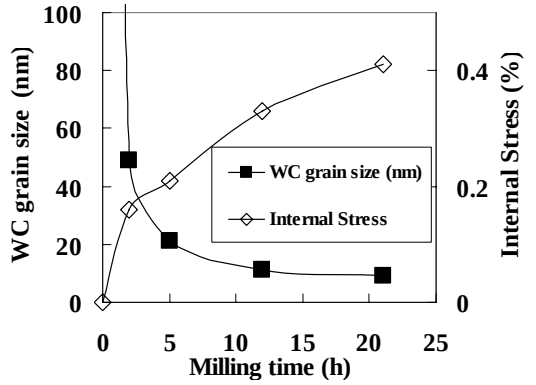

Fig. 14. Grain size and internal stress as a function of milling time, calculated by Stokes and Wilson's formula.

In order to confirm the grain size reported by X-ray diffraction results, high resolution TEM and SEM images of the dispersed WC powder were analyzed. Both the TEM and SEM images in Figures 15 and 16 showed very fine particles on the order of 10 nanometers as predicted by X-ray diffraction. However, there are very large or agglomerated particles on the order of approximately 100 nanometers or larger. As shown in the magnified image in Figure 16, the high resolution TEM images revealed the lattice planes and showed defined boundaries of single crystallites within the agglomerated particles. The figure showed a few bands of deformation twins providing direct evidence for significant lattice strains within tungsten carbide

powder, as estimated in Figure 14. The presence of significant lattice strain probably affects subsequent sintering.

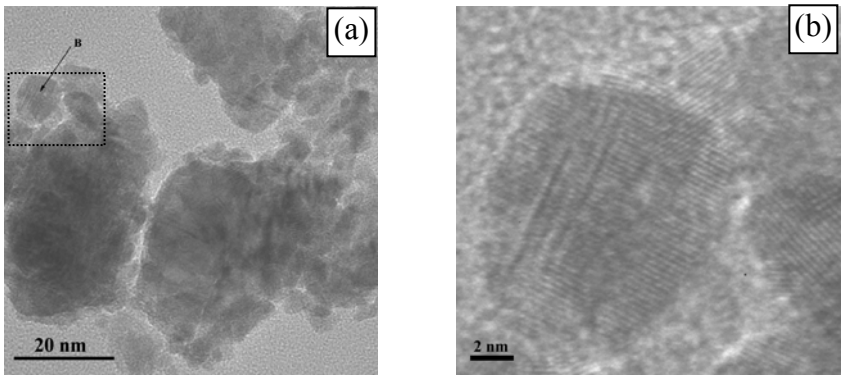

Fig. 15. High resolution TEM image of high energy milled powder (a), b) enlarged image for region B marked in (a).

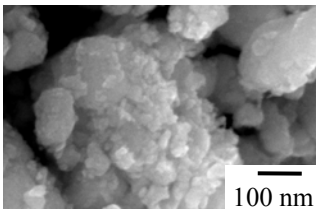

Fig. 16. The typical SEM morphology of high energy ball milled powders.

When grain sizes were larger than 100 nm, the SEM images were analyzed using Image Tool©, an image analysis software that is available via the web [79]. The particle size and grain size were measured by converting the measured cross-sectional area of a feature to the diameter of an equal area circle, which is termed the equivalent circle diameter (ECD).

Densification. Densification during sintering is defined as the % increase in density of the compact. It is measured by the following equation

$$\%\rho = \frac{\rho_{\sin tered} - \rho_{green}}{\rho_{theoretical} - \rho_{green}} \times 100 \qquad (6)$$

where $\rho_{theoretical}$ is the theoretical density of the 100% dense compact, $\rho_{\sin tered}$ is the density of the compact at the respective sintering temperature and ρ_{green} is the as pressed green density of the sample. The densities of the consolidated samples were measured using the Archimedes principle.

V.2.4 Mechanical Properties

Hardness and fracture toughness are the two most important mechanical properties of cemented tungsten carbide. Other mechanical properties, such as flexural strength, wear resistance and impact resistance, are fundamentally dependent on the hardness and fracture toughness.

Hardness. Vickers hardness was measured on polished surface by performing indentations at a load of 30 Kgf and a dwell time of 15 seconds.

Fracture toughness. In this work, two methods were used to measure the fracture toughness of sintered samples: one is Palmqvist method and the other one is standard short rod method.

V.2.4.a. Palmqvist Method

Palmqvist toughness was calculated from the Vickers hardness indentation according to the equation [80]:

$$K = 0.0889(HP/C)^{1/2} \qquad (7)$$

where K is the Palmqvist toughness, H is the hardness, P is the applied load, and C is the total length of cracks produced by the Vickers indentation.

V.2.4.b Short Rod Method

The plane strain fracture toughness, $K_{IC,}$ was measured by the standard short rod test according to ASTM B771 (Terra Tek Fractometer II).

It should noted that almost all reported fracture toughness data in the literature on sintered WC-Co using nanosized powders were measured using the Palmqvist method. It was not clear if these fracture toughness values can be reproduced using the standard true fracture toughness testing methods such as the short-rod method (ASTM-B771) and the SENB method (ASTM-E399).

VI. Presentation and Discussion of Results

VI.1. Chemical Vapor Synthesis of Nanocrystalline WC/Co Powder

VI.1.1 Tubular Reactor System

VI.1.1.a Preliminary Experiments

The preliminary experiments involved synthesizing WC and Co separately to find the optimum conditions under which WC and Co could be produced individually before attempting to produce the WC-Co composite. A mixture of 9 mol % CH_4-45 mol % H_2-Ar was fed at a total flow rate of 1.1 L/min (25 °C, 86.1 kPa), and the reaction temperature was 1400°C. The volatilizer in which the reactant precursors were vaporized was placed at a position inside the reactor where the temperature was 1000 °C. The feeding rate of WCl_6 was 0.04 g/min and that of $CoCl_2$ was 0.04 g/min. As shown in Figure 17, fully reduced Co was produced from $CoCl_2$, but a mixture of W_2C and WC was produced from WCl_6 under these conditions. Thus, conditions under which tungsten is fully carburized to WC were searched in subsequent experiments, as described in next section.

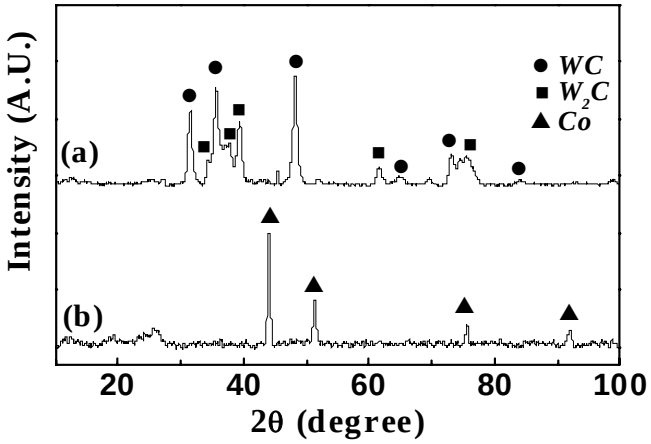

Fig. 17. X-ray diffraction patterns of the products obtained from (a) WCl_6 feeding rate of 0.04 g/min and (b) $CoCl_2$ feeding rate of 0.04 g/min.

VI.1.1.b Synthesis of Tungsten Carbide

According to Hojo et al. [11], WCl_6 is first reduced to metallic tungsten which in turn reacts with methane to form W_2C followed by its carburization to WC. It is thus expected that the extent of carburization will increase with increasing methane concentration as well as reaction temperature.

Accordingly, the system used for the preliminary experiments was modified to promote the production of WC with a minimal amount of W_2C by introducing CH_4 together with WCl_6 through the precursor delivery line as well as by placing the volatilizer at the position where the

temperature was 440°C. The volatilizer temperature was high enough to volatilize WCl_6 powder. However, it was sufficiently low to prevent the reduction and carburization of WCl_6 by hydrogen and methane in the volatilizer, which would result in a deposition of solids in the volatilizer.

This modification facilitated the mixing of the two reactants and the amount of W_2C in the product was minimized, as shown in Figure 18(a). The modification of the system effectively mixed the reactant gases at low temperature prior to reactions. Hojo et al. observed that W_2C yield was higher when reactant gases were mixed at high temperature prior to the reaction [11]. This phenomenon could be due to mixing efficiency of gaseous species affected by thermal expansion. Figure 18 also shows the XRD patterns of the products obtained with three different reaction temperatures. The product was WC but some W_2C formed with the decrease in reaction temperature, in agreement with a thermodynamic analysis presented by Hojo et al. The grain size of WC was calculated from the XRD data by applying the Scherrer equation (3). As the reaction temperature decreased from 1400°C to 1200°C, the grain size of WC decreased from 18±1 to 12±1 nm. Based on the fact that the amount of W_2C was least at 1400°C, the subsequent experiments were performed at this temperature.

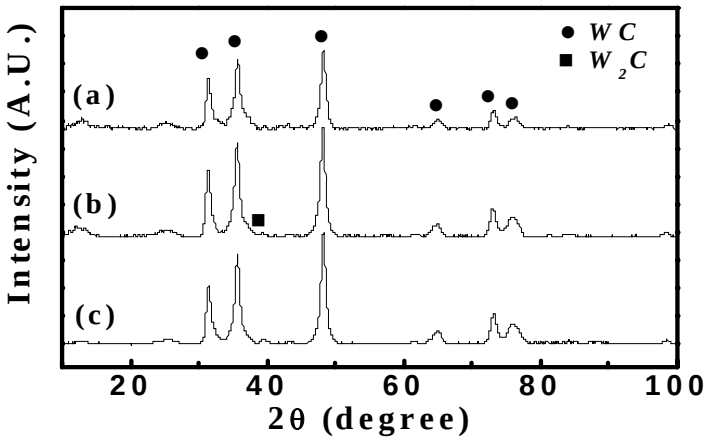

Fig. 18. X-ray diffraction patterns of the product obtained after the modification to feed WCl_6 and CH_4 together: (a) 1400°C, (b) 1300°C, and (C) 1200°C under the following conditions: CH_4 feeding rate = 0.1 L/min (25°C, 86.1 kPa), H_2 feeding rate = 0.25 L/min (25°C, 86.1 kPa), total flow rate = 1.1 L/min (25°C, 86.1 kPa), and WCl_6 feeding rate = 0.04 g/min.

The effect of the CH_4/H_2 ratio on the product composition is shown in Figure 19. The CH_4 flow rate was fixed at 0.1 L/min (25°C, 86.1 kPa) and the H_2 flow rate was varied in the feed stream. The amount of W_2C decreased as the CH_4/H_2 ratio increased, indicating that the degree of carburization increased with the increase in the CH_4/H_2 ratio, as discussed earlier. The grain size of WC was 18±1 nm and decreased to 12±1 nm when no H_2 was used. In the case of CH_4 feeding rate of 0.1 L/min (25°C, 86.1kPa) without H_2, CH_4 alone was enough to reduce and carburize WCl_6 to WC, in which CH_4 decomposes into C and H_2 at sufficiently high temperature. It seemed that the addition of H_2 in the feed along with CH_4 inhibited the decomposition of CH_4 to C and H_2, resulting the lower degree of carburization in the reaction.

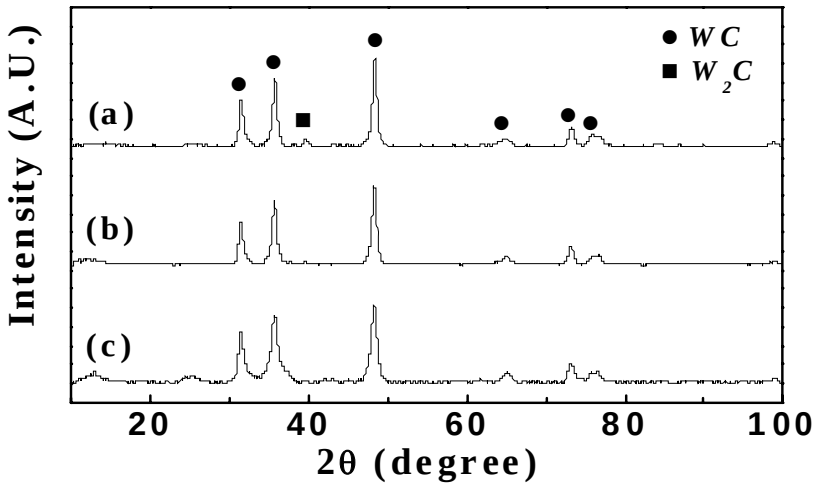

Fig. 19. X-ray diffraction patterns of the product obtained with different CH_4/H_2 molar ratios: (a) CH_4/H_2 = 0.2, (b) CH_4/H_2 = 0.4, and (c) only CH4 under the following conditions: reaction temperature = 1400°C, CH_4 feeding rate = 0.1 L/min (25°C, 86.1 kPa), total flow rate = 1.1 L/min (25°C, 86.1 kPa), and WCl_6 feeding rate = 0.04 g/min.

VI.1.1.c Synthesis of Tungsten Carbide-Cobalt Composite

A mixture of WCl_6 and $CoCl_2$ powders was fed to produce WC-Co composite powder. The volatilizer in which the reactant precursors were vaporized was placed at a position where the temperature was 1100°C, considering the boiling point of $CoCl_2$. The product under this condition was a mixture of WC, W_2C, and even some η-phase (Co_3W_3C), as shown in Figure 20(a). Thus, a modification was made to the reactant feeding arrangement to suppress the formation of Co_3W_3C and increase the degree of carburization [81]. In the modified system, separate feeders and volatilizers for WCl_6 and $CoCl_2$ were used to prevent the unreacted precursor gases from coming into contact with each other. Separate volatilizers for WCl_6 and $CoCl_2$ were placed where the temperatures were 440°C and 1400°C, respectively**.** With this modification, the degree of carburization was increased and the formation of Co_3W_3C was suppressed, and the product was a mixture of WC and Co with some free carbon, as shown in Figure 20(b). The grain size of WC was 24 ± 1 nm which was somewhat larger than that of WC synthesized without the addition of cobalt chloride. Since CH_4 was used in excess, free carbon was always present in the product of WC-Co composite.

In subsequent experiments, experimental conditions that can affect WC-Co composite formation significantly were further investigated, as described below.

Effect of CH_4 feeding rate

The effect of CH_4 concentration was investigated by varying its feeding rate from 0.1 L/min (25ºC, 86.1 kPa) to 0.01 L/min (25ºC, 86.1 kPa) while keeping all other conditions the same [reaction temperature of 1400ºC, total flow rate of 1.1 L/min (25°C, 86.1 kPa), WCl_6 feeding rate of 0.06 g/min, and $CoCl_2$ feeding rate of 0.02 g/min]. In the case of the lowest feeding rate of CH_4, the C/W (CH_4/WCl_6) ratio was 2.3 and the ratio of H_2 produced from CH_4 to H_2 required to reduce both precursors was 1.2.

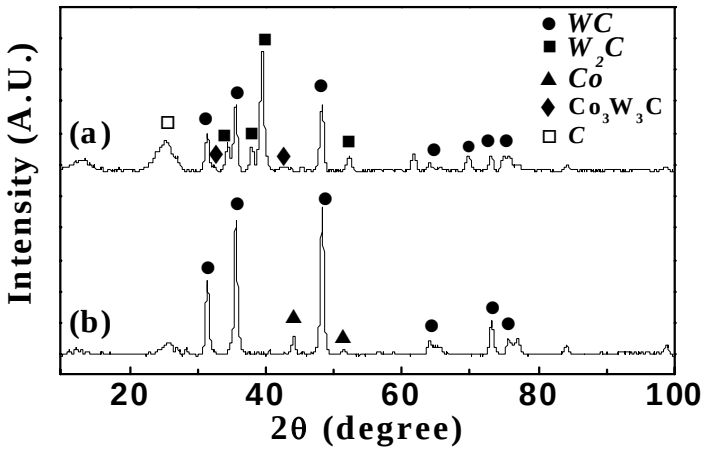

Fig. 20. X-ray diffraction patterns of the product obtained with (a) mixture feeding ($WCl_6/CoCl_2$ molar ratio of 1.1, and feeding rate of mixture of 0.053 g/min) and (b) modified arrangement (WCl_6 feeding rate of 0.06 g/min, and $CoCl_2$ feeding rate of 0.02 g/min) under the following conditions: reaction temperature = 1400°C, CH_4 feeding rate = 0.1 L/min (25°C, 86.1 kPa), H_2 feeding rate = 0 L/min, and total flow rate = 0.6 L/min (25°C, 86.1 kPa).

Figure 21 shows the $WC_{0.5}$/WC molar ratio versus the C/W molar ratio**.** [The $WC_{0.5}$/WC ratio is the same as twice the W_2C/WC ratio, but better represents how much of W is in each carbide phase.] The ratio was calculated from the peak intensity of W_2C at 2θ of 39.5 to that of WC at 2θ of 35.6, according to Equation (4). This calculation shows that the degree of carburization decreased with decreasing carbon potential. The main product was still WC and Co with a small amount of W_2C even at the lowest C/W molar ratio of 2.3. In addition, the amount of free carbon also can be decreased as the C/W molar ratio decreased. Thus, the C/W ratio of 2.3 was applied to the subsequent experiments. The grain size of WC produced under these conditions was 25 ± 1 nm, which was not affected by the change of carbon potential within the range tested. The particle size obtained at 2.3 of C/W ratio was examined using ZetaPALS and TEM. ZetaPALS gave an average particle size of 380 nm but examination using TEM showed that the actual WC particle size was 25 ± 5 nm from measurements on a limited number of particles.

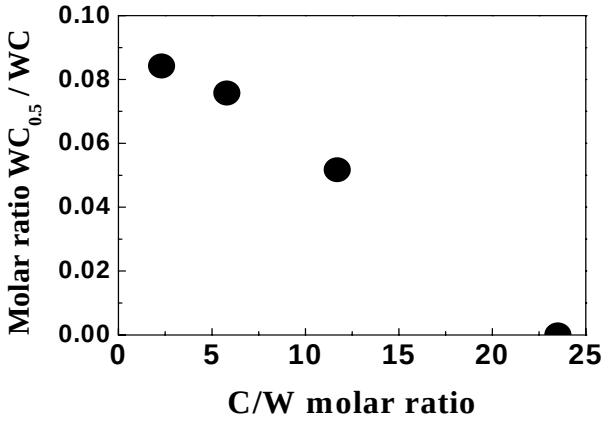

Fig. 21. Effect of the CH_4/WCl_6 molar ratio on the $WC_{0.5}$/WC molar ratio.

Figure 22 shows the TEM micrograph of the WC and Co powders obtained at 2.3 of C/W ratio. The difference of particle size obtained by ZetaPALS can be explained by the agglomeration of the synthesized powder as well as motion of the particles in liquid media that contributed to errors in particle size measurement.

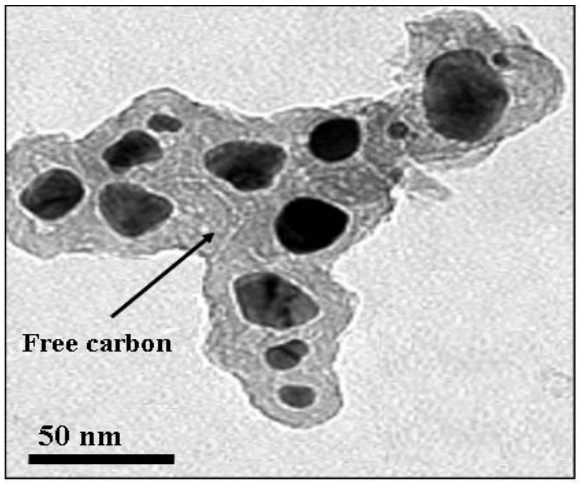

Fig. 22. TEM micrograph of WC-Co nanopowder synthesized at the reaction temperature of 1400°C.

In addition, as shown in the TEM micrograph, WC and Co particles are surrounded by excess carbon to form the agglomerate. The TEM examination of powders showed similar WC particle size to the grain size calculated by the Scherrer equation. Thus, the produced particles seem to be single crystals and it is reasonable to use the calculated grain size from XRD result as the particle size.

Effect of reactants concentration

The effect of reactants concentration was investigated by varying the feeding rate of WCl_6 from 0.06 g/min to 0.6 g/min and that of $CoCl_2$ from 0.02 g/min to 0.2 g/min. The experimental conditions were as follows: The WCl_6 volatilizer temperature was 440^{o}C, the feeding rate of CH_4 was controlled to keep the C/W molar ratio in the feed at 2.3, the $CoCl_2/WCl_6$ molar ratio in the feed was 1, the reaction temperature was 1400^{o}C, the total gas flow rate was made up by Ar to a constant value at 1.1 L/min (25°C, 86.1 kPa), and no H_2 was used in the feed stream since CH_4 alone gave high degree of carburization of W and was enough to reduce both chlorides. Figure 23 shows the XRD patterns of the products obtained with different feeding rates of precursors. The product under these conditions was WC and Co together with small amounts of W_2C and/or W depending on the feeding rate of each reactant. No intermediate phases such as Co_3W_3C or Co_6W_6C were present in the product. Again, the feeding arrangement discussed previously prevented the unreacted precursor gases from coming into contact with each other and forming intermediate phases, even when the concentration of precursors was increased.

The mole fractions of tungsten carbides phases are shown in Figure 24. The molar ratio was calculated from the XRD peak intensity of WC at 2θ of 35.6, that of W_2C at 2θ of 39.5, and that of W at 2θ of 40.2, according to Equation (4). The W_2C phase was represented as $WC_{0.5}$ to better show how much of W is in each carbide phase. As the feeding rate of WCl_6 was increased from 0.06 to 0.3 g/min, W_2C disappeared and a small amount of W was produced. The amount of produced W increased somewhat as the feeding rate was increased to 0.6 g/min. The degree of carburization was slightly decreased with the increase of reactants concentration considering that the carburization occurs from W to Co_3W_3C and W_2C and then WC in the presence of Co. The grain size of WC, 25 ± 1 nm at the lowest feeding rate, increased to 30 ± 1 nm at the highest feeding rate. It is likely that the increase in WCl_6 concentration leads to increased grain size of the reduced W, which resulted in a slower carburization rate. The morphology of the WC-Co composite powder is shown in Figure 25. EDS mapping of the composite powder confirmed that the WC and Co particles were uniformly mixed in the product.

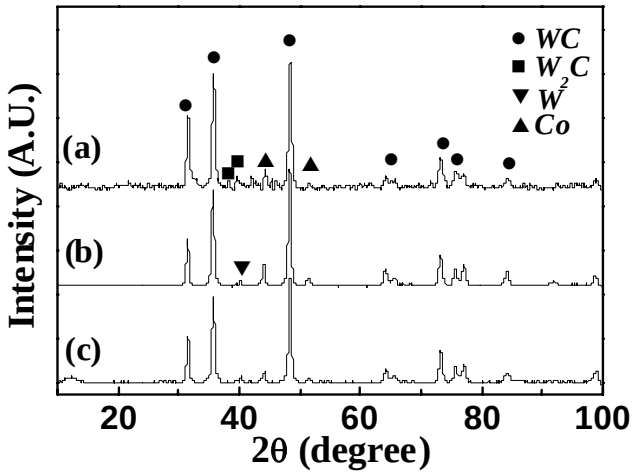

Fig. 23. X-ray diffraction patterns of the products obtained with different feeding rates of precursors in the feed stream: (a) 0.06 g/min for WCl6 and 0.02 g/min for CoCl2, (b) 0.3 g/min and 0.1 g/min, and (c) 0.6 g/min and 0.2 g/min, respectively.

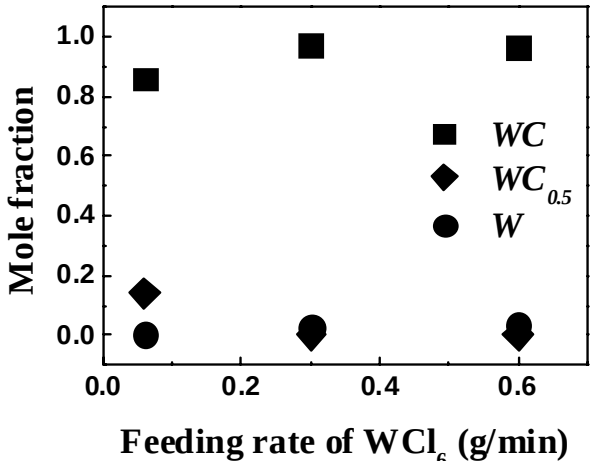

Fig. 24. Effect of precursor feeding rates on the mole fractions of tungsten carbides with $CoCl_2/WCl_6$ molar ratio = 1.

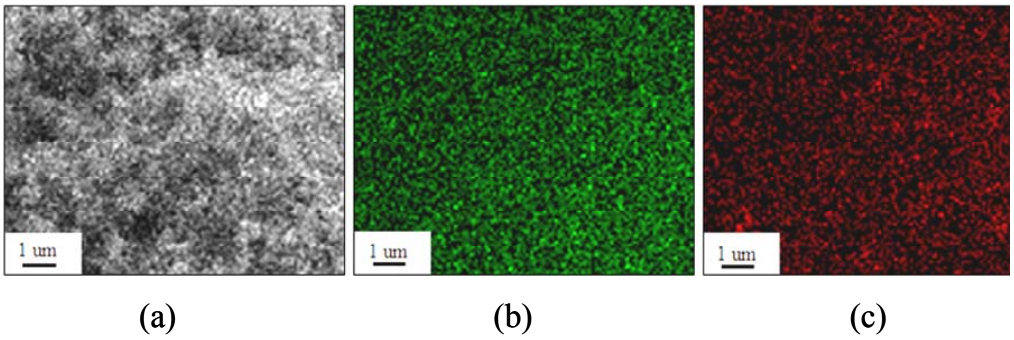

Fig. 25. SEM image of WC-Co composite powder with associated EDS maps for tungsten and cobalt: (a) WC-Co composite powder, (b) EDS map of W, and (c) EDS map of Co.

Effect of C/W molar ratio on the reduction of free carbon

The effect of CH_4 concentration in the feed stream was investigated by controlling C/W molar ratio from 2.7 to 2.1 while maintaining all other conditions constant [no H_2, reaction temperature of 1400°C, total gas flow rate of 1.1 L/min (25°C, 86.1 kPa), WCl_6 feeding rate of 0.6 g/min, and $CoCl_2$ feeding rate of 0.2 g/min]. Figure 26 shows the mole fraction of tungsten carbides depending on different C/W molar ratios in the feed stream, indicating that the degree of carburization decreased with the decrease of CH_4 concentration in the feed stream. The weight percentage of carbon in the product was converted to percent excess carbon, which is defined as the percentage of the excess carbon over the corresponding stoichiometric amount if all W was present as WC. The % excess carbon in the product decreased from 67.8 % to 3.13 % when the C/W molar ratio decreased from 2.7 to 2.1, as shown in Figure 27. The grain size of produced WC, 30±1 nm was not affected by carbon concentration in the feed stream within the range tested.

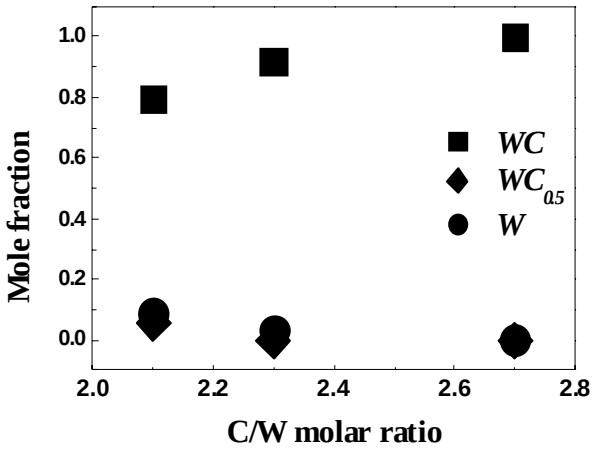

Fig. 26. Effect of C/W molar ratio in the feed stream on the mole fractions of tungsten carbides.

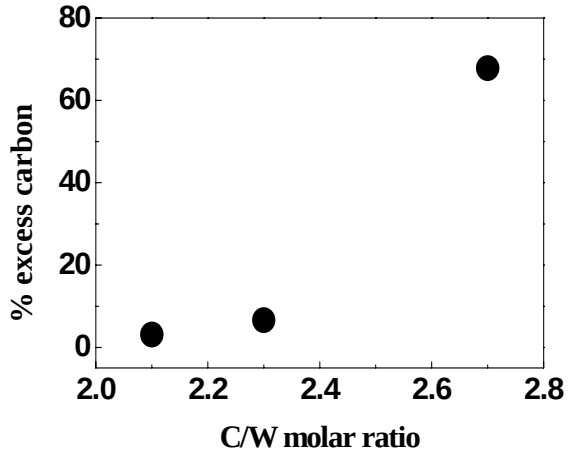

Fig. 27. Effect of C/W molar ratio in the feed stream on % excess carbon.

The results indicated that free carbon was still present in the product even at the lowest C/W molar ratio, which can be controlled in the feed stream. The ratio of H_2 produced from CH_4 to H_2 required to reduce both precursors was unity at C/W molar ratio of 2.1. Thus, other experimental conditions were investigated to reduce excess carbon in the product as described in the following sections.

Effect of H_2/CH_4 molar ratio on the reduction of free carbon

Since excess CH_4 was used to synthesize WC-Co composite powder, free carbon was always present in the product. Thus, hydrogen was added as the reducing gas as well as to reduce the amount of free carbon in the reaction. The effect of hydrogen concentration in the feed stream was investigated on the product composition and carbon content in the product by controlling the H_2/CH_4 molar ratio from 0 to 4.3 under otherwise identical conditions [C/W molar ratio of 2.7, reaction temperature of 1400 ^oC, total gas flow rate of 1.1 L/min (25°C, 86.1 kPa), WCl_6 feeding rate of 0.6 g/min, and $CoCl_2$ feeding rate of 0.2 g/min]. Figure 28 shows the mole fractions of tungsten carbides obtained with different H_2/CH_4 molar ratios, indicating that the degree of carburization decreased as the H_2/CH_4 molar ratio was increased. As mentioned earlier, hydrogen addition in the feed stream inhibited the decomposition of CH_4 into C and H_2. Thus, as the feeding rate of H_2 increased, the C potential decreased, which resulted in a lower degree of carburization and lower carbon content in the product as shown in Figure 29. The % excess carbon in the product decreased from 67.8 % to 17.5 % as the H_2/CH_4 ratio in the feed stream was increased from 0 to 4.3, as shown in Figure 29. The grain size of produced WC decreased from 30±1 nm with no H_2 to 26±1 nm with H_2/CH_4 ratio of 4.3.

Tungsten carbide powder is used mainly to make bulk components by a consolidation process. Therefore, the presence of incompletely carburized W_2C, W, or Co_3W_3C phases can be tolerated because they can be fully carburized during the subsequent sintering process. These phases can also be fully carburized during the separate post-treatment of the produced composite powder as discussed in the following section.

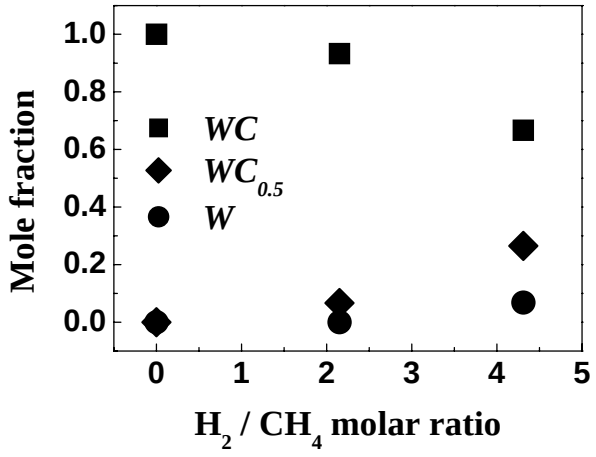

Fig. 28. Effect of H_2/CH_4 molar ratio in the feed stream on the mole fractions of tungsten carbides.

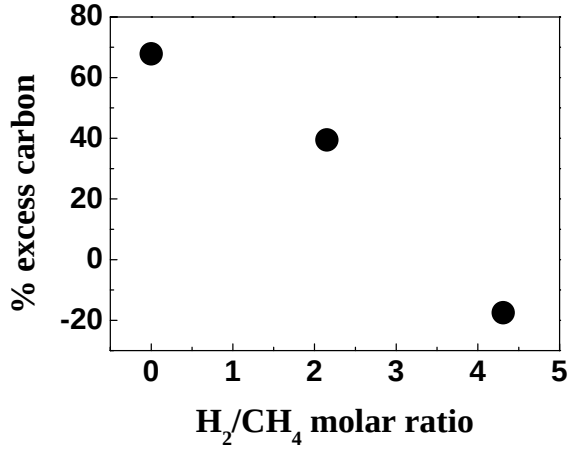

Fig. 29. Effect of H_2/CH_4 molar ratio in the feed stream on % excess carbon.

Post-treatment of produced powders

As mentioned earlier, free carbon was always present in the produced powders since excess methane was used in the reaction. Thus, the produced powders were subjected to the post-treatment to remove free carbon as well as to fully carburize unreacted tungsten carbide phases to the WC phase. Initially, the experiments were conducted to evaluate whether unreacted tungsten carbides can be fully carburized to the WC phase during the post-treatment. A sample of tungsten carbides containing relatively large amount of W and W_2C with the low excess carbon was prepared and it was placed in a ceramic boat of 1.5 cm W×9 cm L × 1.5 cm H in dimension, which in turn was placed in a tube furnace of 6 cm inner diameter under Ar atmosphere. The experimental conditions were as follows: The amount of powder treated was 2 g, the treatment temperature was 900°C, which was low enough to prevent rapid grain growth of particles, and the ramping rate of tube furnace to increase the temperature up to 900°C was 10 °C/min, and the cooling rate to the room temperature was also 10 °C/min, in which Ar flowed at a rate of 0.5 L/min (25°C, 86.1 kPa).

The result showed that W_2C and W phases were fully carburized to the WC phase after the powder was treated for 30 min, as shown in Figure 30. As mentioned earlier, it was confirmed that unreacted tungsten carbide phases, such as W_2C and W phases, are easily carburized to WC phase while being heated with free carbon. Therefore, in the subsequent experiments, the effect of hydrogen heat treatment on the product composition, grain growth, and carbon content was investigated. The experiments were conducted under the same conditions except that hydrogen was flowed at a rate of 0.5 L/min (25ºC, 86.1 kPa) after the temperature reached 900ºC. The result showed that the unreacted W_2C and W phases were also fully carburized to WC phase as well as the excess carbon was removed after the powder was treated by hydrogen, as shown in Figure 31 and Figure 32. The carburization of W_2C and W phases to the fully carburized WC phase also can be caused by highly mobile hydrocarbons, mainly CH_4, formed during the hydrogen heat treatment reacting with W_2C and W, which is more efficient than solid carbon on the carburization process [82].

The % excess carbon in the product, 112 % before the treatment, was down to 7 % after 1 hour of post-treatment, 3 % after 2 hours, and 0 % after 4 hours, as shown in Figure 32. Up to 4 % excess free carbon is not only tolerated but often need in the subsequent consolidation process to remove the small amount of oxygen present on the particle surface. Therefore, a post-treatment of 2 hours under the conditions used in this work was sufficient. The grain size of WC, 30±1 nm before the treatment, increased to 36 ± 1 nm after 4 hours of treatment. The particle size of composite powder before and after the hydrogen heat treatment was examined by TEM micrographs, as shown in Figures 33(a) and (b). EDS maps of the composite powder obtained after the hydrogen heat treatment are shown in Figures 33(c) and (d). The actual particle size, as opposed to the grain size, of the composite powder was less than 40 nm before the treatment and less than 70 nm after the treatment for 4 hours in hydrogen. It is noted that these values are from measurements on a rather limited number of particles. EDS maps also indicate that WC and Co particles were uniformly mixed in the product, which verifies the significant feature of the CVS process to produce very uniformly mixed powders.

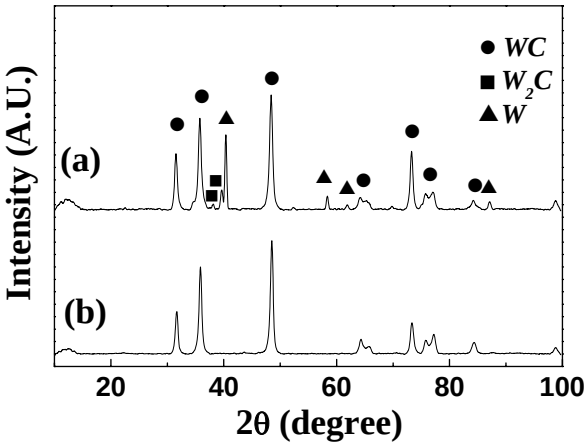

Fig. 30. X-ray diffraction patterns of the product obtained by post-treatment under Ar atmosphere: (a) before treatment and (b) after the treatment for 30 min under the following conditions: treatment temperature of 900°C, ramp rate of tubular furnace at 10 °C/min, and Ar flow rate of 0.5 L/min (25°C, 86.1 kPa).

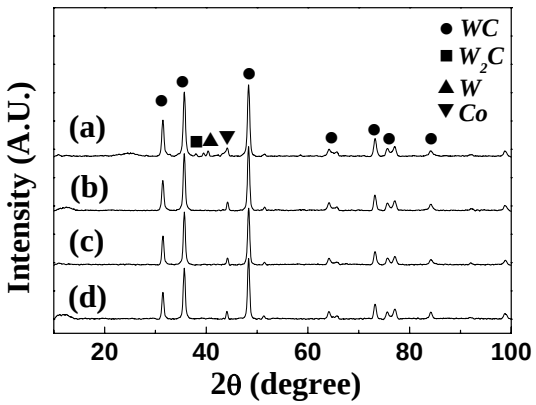

Fig. 31. X-ray diffraction patterns of the products obtained with different hydrogen treatment times at 900ºC using the powder produced from the tubular reactor: (a) before treatment, (b) 1 hour, (c) 2 hours, and (d) 4 hours of holding time.

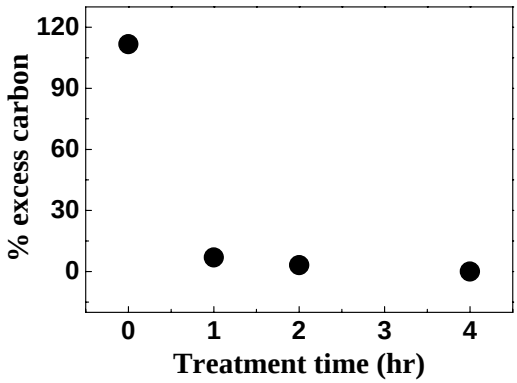

Fig. 32. Effect of hydrogen heat treatment time at 900ºC on % excess carbon.

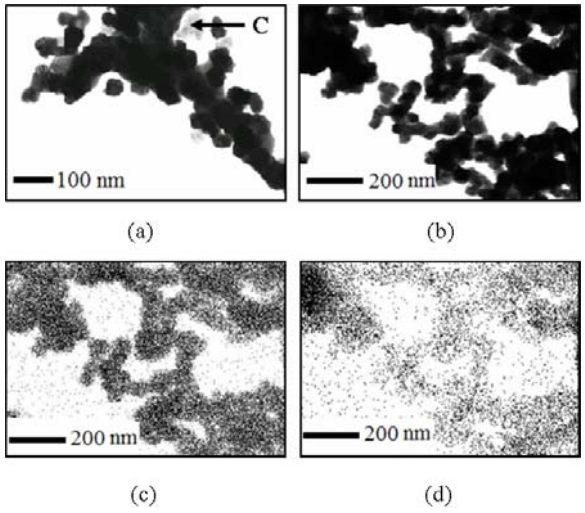

Fig. 33. TEM micrographs with EDS maps of WC-Co composite powders: (a) WC-Co composite powder obtained from the tubular reactor, (b) WC-Co composite powder after hydrogen heat treatment for 4 hours at 900ºC, (c) EDS map of posttreated sample (Tungsten, black area), and (d) EDS map of posttreated sample (Cobalt, black area).

*V**I**.1.2 Plasma Reactor System*

V.1.2.a Synthesis of Tungsten Carbide from Tungsten Hexachloride

Initial experiments were conducted to find optimum conditions at which tungsten carbide could be produced from WCl_6-H_2-CH_4 mixture in a plasma process. The experimental conditions were as follows: The feeding rate of WCl_6 was 3.5 g/min, the flow rate of Ar-H_2-CH_4 mixture to carry the WCl_6 powder was 4 L/min (25ºC, 86.1 kPa), the applied plasma torch power was 13 kW, and the flow rate of primary plasma gas (Ar) to generate plasma flame was controlled at 38 L/min (25ºC, 86.1 kPa) with no secondary plasma gas (H_2).

The main product under these conditions was WC_{1-x} with small amounts of W_2C and WC phases, as shown in Figure 34. This result is consistent with the phase diagram, as shown in Figure 35 [83], which indicates that WC_{1-x} is likely the first stable solid tungsten carbide phase formed as the W-C liquid solution cools towards solidification at 2710^{o}C. After the initial formation the WC_{1-x} phase may be carburized to WC. Further, this phase decomposes into WC and W_2C phases below 2530^{o}C. However, the rapid quenching of the synthesized particles, which provides little time for either decomposition or further carburization, resulted in the WC_{1-x} phase remaining as the major phase in the collected product. Figure 34 also shows the XRD patterns of the products obtained with different CH_4/H_2 molar ratios in the feed stream. The amount of W_2C and WC decreased as the CH_4/H_2 ratio was increased and when CH_4 alone was used as the reaction gas, the product was WC_{1-x}. The grain size of WC_{1-x}, 13±1 nm, decreased to 9±1 nm when no H_2 was used. The results of these experiments indicated that methane alone was enough to reduce and carburize tungsten hexachloride to tungsten carbide. Thus, the subsequent experiments were performed without the hydrogen addition in the feed stream. Further, these and the subsequent experiments showed that the conversion of WCl_6 to tungsten carbides was complete in the plasma reactor as long as methane was added in excess of the stoichiometric amount.

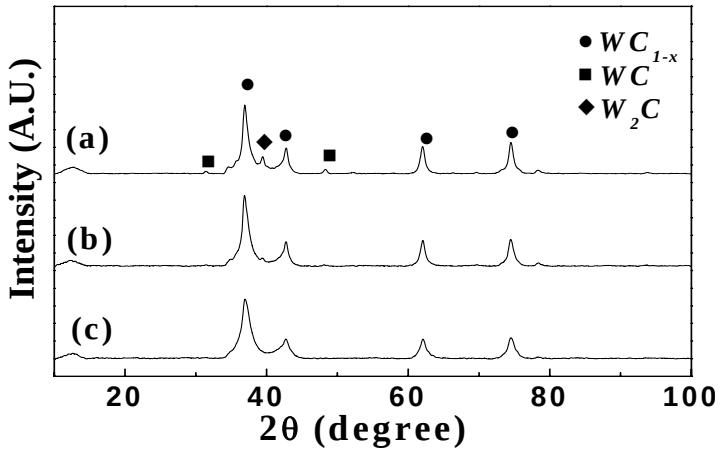

Fig. 34. X-ray diffraction patterns of the products obtained from different CH_4/H_2 molar ratios: (a) [CH_4/H_2] = 0.5, (b) [CH_4/H_2] = 1, and (c) only CH_4.

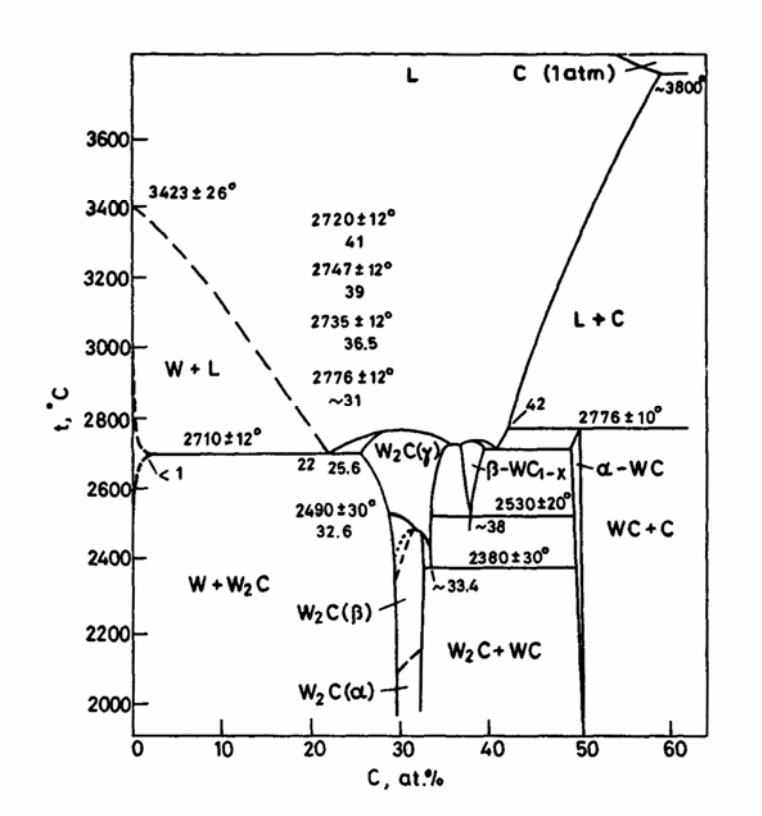

Fig. 35. Phase diagram of W-C system [58].

The results obtained from the preliminary experiments conducted in the thermal plasma process showed a considerable promise compared with other conventional processes, owing to the high temperature generated by the plasma flame to rapidly volatilize the precursor (WCl_6) and the rapid quenching of the product to yield nanosized tungsten carbide powder.

Experiments were conducted to synthesize WC_{1-x}-Co composite powder using a premixed tungsten hexachloride and cobalt chloride with a Co/W ratio of 0.8. The products obtained from the plasma reactor in these runs were a mixture of WC_{1-x}-Co and W_2C with a very small amount of Co, indicating that the degree of carburization was decreased by the addition of cobalt chloride. When cobalt chloride alone was used in the plasma process the Co was obtained. The runs were repeated many times, but the results were the same. At this point, this approach was abandoned.

In the next runs, ammonium paratungstate (APT) and cobalt oxide (Co_3O_4) were used as the precursors to synthesize WC1-x-Co composite powder in the plasma process. These materials can be volatilized in the plasma flame owing to the high temperature, and followed by subsequent vapor phase reactions. These materials are also more suitable for industrial applications than metal chlorides because of the latter's undesirable properties that were discussed earlier. Also, a post-treatment of synthesized powders using these materials to produce WC-Co composite powder was tested, as will be discussed later.

VI.1.2.b Synthesis of Tungsten Carbide from APT

Initial experiments were conducted to evaluate whether vaporized APT precursor could be reduced to tungsten before attempting to produce tungsten carbide. The experimental conditions were as follows: The feeding rate of APT was 3.1 g/min, the flow rate of carrier gas to feed the APT powder into the plasma flame was 4 L/min (25ºC, 86.1 kPa), the flow rate of primary plasma gas (Ar) to generate the plasma flame was 48 L/min (25ºC, 86.1 kPa) with no secondary plasma gas (H_2) and the applied power of the plasma torch was 13 kW. When APT powder was delivered with only Ar as a carrier gas into the plasma flame, WO_3 was produced as observed in the result of heating APT in Ar atmosphere, as shown in Figure 36(a).

Tungsten powder was produced by the addition of H_2 gas as the reducing agent in the feed stream together with APT powder as received without pre-treatment, as shown in Figure 36(b). The produced W powder had a grain size of less than 25 nm determined by applying the Scherrer equation to the XRD data and its morphology was mostly round. XRD results showed that the product was tungsten without any detectable oxides. When CH_4 was fed as the carburizing agent with H_2 in the feed stream together with APT powder, tungsten carbide (WC_{1-x}) was produced, as shown in Figure 36(c). The grain size of WC_{1-x} powder was determined by applying the Scherrer equation to the XRD data and it was found to be less than 20 nm.

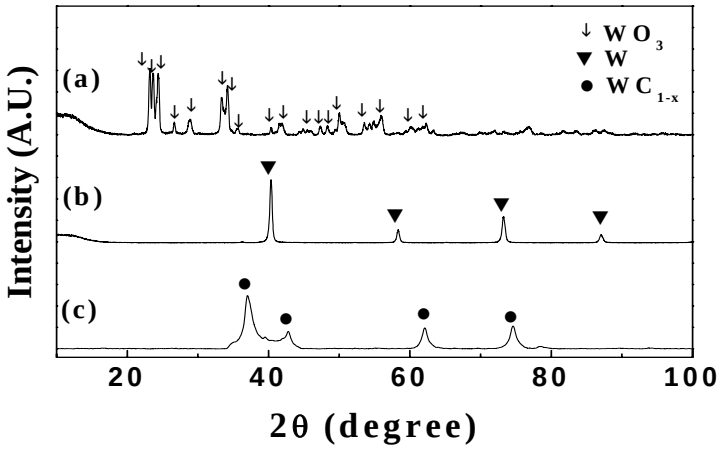

Fig. 36. X-ray diffraction patterns of products obtained by thermal plasma process of APT ($(NH_4)_{10}W_{12}O_{41}\cdot xH_2O$) with different reactant gases: (a) Ar, (b) Ar and H_2, and (c) H_2 and CH_4.

The results thus obtained for the direct reduction and carburization of APT showed a considerable promise of the thermal plasma process conducted in this work compared with other conventional processes. This is largely due to the high temperature generated by the plasma flame to rapidly volatilize the APT powder and the rapid quenching of the product to yield nanosized tungsten and/or tungsten carbide powder. Thus, it is expected that this process is suitable for large-scale production of nanosized tungsten carbide powders since the plasma process can work continuously.

VI.1.2.c Synthesis of Tungsten Carbide-Cobalt Composite Powder from APT and Cobalt Oxide

In the preliminary experiments, cobalt oxide (Co_3O_4) was tested as a Co precursor before attempting to produce WC_{1-x}-Co composite powder, in which ammonium paratungstate and cobalt oxide were used as the precursors.

Experiments were first conducted to evaluate whether cobalt oxide can be reduced in the plasma process. The experimental conditions were as follows: The feeding rate of Co_3O_4 was 2 g/min, plasma torch power was 9 kW, the flow rate of plasma gas (Ar) was 38 L/min (25ºC, 86.1 kPa) with no secondary plasma gas (H_2), and the flow rate of H_2 to carry Co_3O_4 powder was 4 L/min (25ºC, 86.1 kPa) without Ar addition as a carrier gas. From the result, Co powder was obtained, as shown in Figure 37(a). Thus, subsequent experiments, in which premixed AP-Co_3O_4 powder with a Co/W ratio of 0.7 was fed into the plasma flame at a feeding rate of 3.5 g/min, were conducted under the same condition. The product was W-Co composite powder, as shown in Figure 37(b). In order to synthesize WC_{1-x}-Co composite powder, CH_4 and H_2 were fed with premixed APT and Co_3O_4. The experiments were conducted under the same conditions as those of synthesizing W-Co composite powder except that CH_4 and H_2 flow rates were each 2 L/min (25ºC, 86.1 kPa). The product obtained under these conditions was a mixture of W, W_2C, and WC_{1-x} with Co, as shown in Figure 37(c). From the results, the addition of cobalt oxide in the feed stream resulted in a lower degree of carburization considering that the product was WC_{1-x} when no Co_3O_4 was added in the feed stream. Therefore, conditions to increase the degree of carburization were further investigated in subsequent experiments, as described in the following sections.

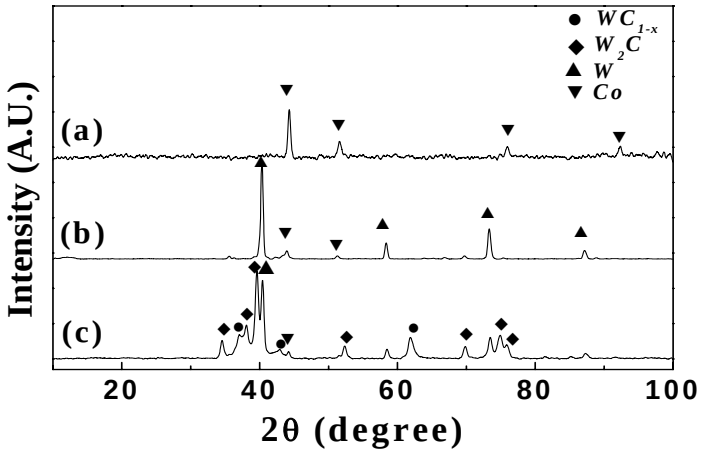

Fig. 37. X-ray diffraction patterns of products obtained by thermal plasma process from (a) Co_3O_4-H_2 mixture, (b) APT-Co_3O_4-H_2 mixture, and (c) APT-Co_3O_4-H_2-CH_4 mixture.

Effect of plasma torch power

As mentioned earlier, the degree of carburization is highly dependent on the reaction temperature as well as the methane concentration in the reaction. Therefore, experiments were first conducted to investigate the effect of plasma torch power, in which the temperature of

plasma flame increased with an increase in plasma torch power, on the degree of carburization by varying it from 9 kW to 18 kW while maintaining all other conditions constant [flow rate of primary plasma gas (Ar) of 38 L/min (25ºC, 86.1 kPa) with no secondary plasma gas (H_2), feeding rate of premixed APT-Co_3O_4 powder of 3.5 g/min in which Co/W ratio was 0.7, C/W ratio of 6.2, and the flow rate of H_2-CH_4 mixture to carry the premixed APT-Co_3O_4 powder of 4 L/min (25ºC, 86.1 kPa)]. Figure 38 shows the XRD patterns of the products obtained with different power levels of the plasma torch. The product obtained under these conditions was a mixture of W, W2C, and WC_{1-x} with Co and the product composition was not affected by the plasma torch power within the range tested.

The grain size of WC_{1-x} obtained at a plasma torch power of 9 kW was 9±1 nm and it slightly increased to 11±1 nm as the plasma torch power was increased to 18 kW. Since the plasma torch power applied to the synthesis of tungsten carbide-cobalt composite powder was high enough in these experiments, considering that the product was WC_{1-x} phase at a plasma torch power of 13 kW when APT alone was used, no further experiment to increase the plasma torch power above 18 kW was conducted. In subsequent experiments, other factors which can increase the degree of carburization such as methane concentration in the feed stream as well as the plasma gas flow rate were tested.

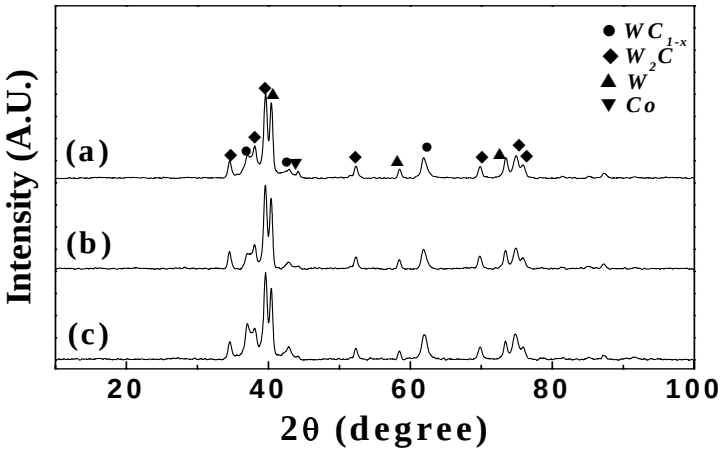

Fig. 38. X-ray diffraction patterns of the products obtained with different power levels of plasma torch: (a) 9 kW, (b) 12 kW, and (c) 18 kW.

Effect of methane concentration in the feed stream

The effect of methane concentration in the feed stream was investigated on the degree of carburization by varying the C/W ratio from 6.2 to 12.4 while maintaining all other conditions the same [plasma torch power of 9 kW, the flow rate of primary plasma gas (Ar) of 38 L/min (25ºC, 86.1 kPa) with no secondary plasma gas (H_2), feeding rate of premixed APT-Co_3O_4 powder of 3.5 g/min with Co/W ratio of 0.7, and the flow rate of H_2-CH_4 mixture to carry the premixed APT-Co_3O_4 powder of 4 L/min (25ºC, 86.1 kPa)]. Figure 39 shows the XRD patterns of the products obtained with different C/W ratios in the feed stream. The product obtained at a C/W ratio of 6.2 was a mixture of W, W_2C, and WC_{1-x} with Co and the amount of W and W_2C phases decreased with an increase in the C/W ratio in the feed stream, indicating the degree of carburization increased with increasing C/W ratio. Since excess methane was used in the

reaction, free carbon was always present in the produced powder. However, the free carbon can be removed by the post-treatment as discussed earlier. The grain size of WC_{1-x}, 8±1 nm, was not affected by methane concentration in the feed stream within the range tested. Since the highest degree of carburization was observed when no H_2 was used in the feed stream and methane alone used in excess was enough to reduce and carburize APT and Co_3O_4 to tungsten carbide with cobalt, no H_2 was used in the subsequent experiments.

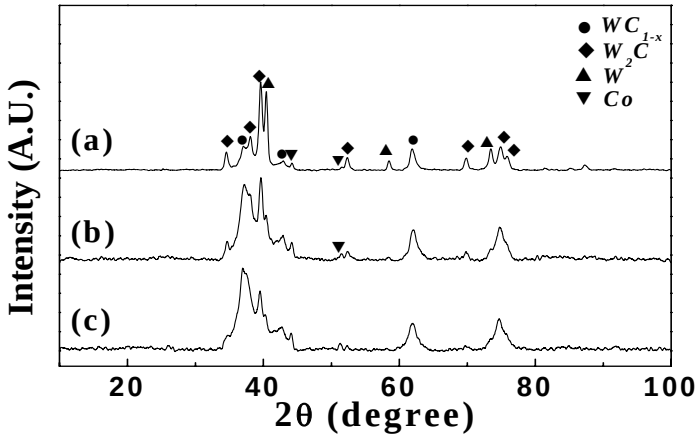

Fig. 39. X-ray diffraction patterns of the products obtained with different C/W molar ratios: (a) 6.2, (b) 9.3, and (c) 12.4.

Effect of plasma gas flow rate

Experiments were performed to determine the effect of plasma gas flow rate on the degree of carburization by varying the flow rate of the primary plasma gas (Ar) from 29 L/min (25ºC, 86.1 kPa) to 57 L/min (25ºC, 86.1 kPa) with no secondary plasma gas (H_2), under otherwise identical conditions [plasma torch power of 9 kW, feeding rate of premixed APT-Co_3O_4 powder of 3.5 g/min with Co/W ratio of 0.7, and the flow rate of CH_4 to carry the premixed APT-Co_3O_4 powder of 4 L/min (25ºC, 86.1 kPa) in which no H_2 was used]. Figure 40 shows the XRD patterns of the products obtained with different plasma gas flow rates.

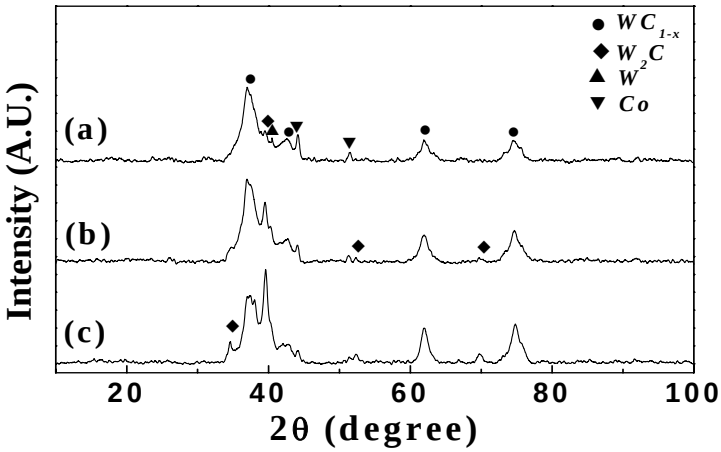

Fig. 40. X-ray diffraction patterns of the products obtained from (a) 29 L/min (25ºC, 86.1 kPa), (b) 38 L/min (25ºC, 86.1 kPa), and (c) 57 L/min (25ºC, 86.1 kPa).

The main product obtained at the lowest flow rate of plasma gas of 29 L/min (25ºC, 86.1 kPa) was WC_{1-x} and Co with small amounts of W and W_2C. The amount of W and W_2C increased with an increase in plasma gas flow rate, indicating that the degree of carburization decreased with the increase of the plasma gas flow rate. The grain size of WC_{1-x} obtained at the plasma gas flow rate of 29 L/min (25ºC, 86.1 kPa) was10 ±1 nm and it slightly decreased to 7±1 nm as the plasma gas flow rate was increased to 57 L/min (25ºC, 86.1 kPa). EDS mapping of the composite powder obtained at a plasma gas flow rate of 29 L/min (25ºC, 86.1 kPa) was conducted and it confirmed that the WC_{1-x} and Co particles were uniformly mixed in the product, as shown in Figure 41.

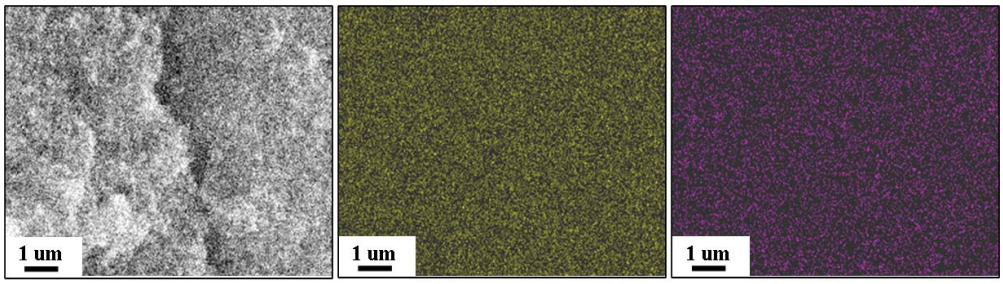

Fig. 41. SEM image of WC_{1-x}-Co composite powder with associated EDS maps for tungsten and cobalt: (a) WC_{1-x}-Co composite powder, (b) EDS map of W, and (c) EDS map of Co.

Effect of secondary plasma gas (H_2) addition

Experiments were conducted to evaluate the effect of adding hydrogen in the plasma flame while keeping all other conditions the same [flow rate of the primary plasma gas (Ar) of 29 L/min (25ºC, 86.1 kPa), feeding rate of premixed APT-Co_3O_4 powder of 3.5 g/min with Co/W ratio of 0.7, and CH_4 flow rate to carry the premixed APT-Co_3O_4 powder of 4 L/min (25ºC, 86.1 kPa) with no H_2]. The secondary plasma gas (H_2) was added at a composition of Ar-1.2 mol % H_2, or Ar-4.1 mol % H_2 in the plasma flame, which resulted in a H_2 flow rate of 0.36 L/min (25ºC, 86.1 kPa), or 1.27 L/min (25ºC, 86.1 kPa), respectively. The applied power of the plasma torch was 9 kW when no secondary plasma gas (H_2) was added and increased to about 12 kW when the secondary plasma gas (H_2) was added at 0.36 L/min (25ºC, 86.1 kPa), or 1.27 L/min (25ºC, 86.1 kPa). Figure 42 shows the XRD patterns of the products obtained with the additions of secondary plasma gas (H_2). The main product obtained with no secondary plasma gas (H_2) addition was WC_{1-x} and Co with a small amount of W_2C. The amount of W2C increased when the flow rate of secondary plasma gas was increased to 0.36 L/min (25ºC, 86.1 kPa). When the flow rate of secondary plasma gas was increased to 1.27 L/min (25ºC, 86.1 kPa) the formation of W occurred. It seemed that the addition of secondary plasma gas increased the plasma flame length, leading to an increased reaction time, but it also resulted in the lower carbon concentration in the reaction, which lowered the degree of carburization. The grain size of WC_{1-x} obtained without secondary plasma gas (H_2) addition was 10±1 nm and it slightly increased to 12±1 nm as the flow rate of secondary plasma gas was increased to 1.27 L/min (25ºC, 86.1 kPa).

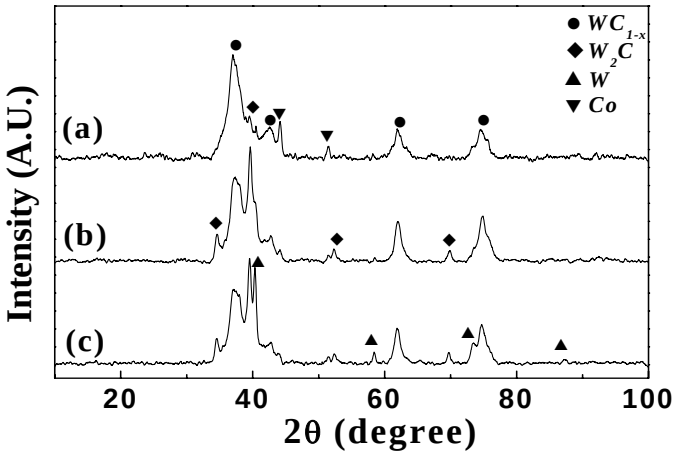

Fig. 42. X-ray diffraction patterns of the products obtained by the addition of secondary plasma gas (H2) in the plasma flame: (a) 0, (b) 0.36 L/min (25ºC, 86.1 kPa), and (c) 1.27 L/min (25ºC, 86.1 kPa).

Post-treatment of produced composite powders

The produced composite powders were subjected to post-treatment to remove free carbon as well as to fully carburize unreacted tungsten carbide phases, WC_{1-x}, W_2C, or W phases to the WC phase. The powder obtained from the plasma reactor was placed in a ceramic boat of 3.6 cm W x 9 cm L x 1.5 cm H in dimensions, which in turn was placed in a tube furnace of 6 cm inner diameter under H_2 atmosphere. The effect of hydrogen heat treatment on the product composition, grain growth, and carbon content was investigated. The amount of composite powder treated was 5 g, the treatment temperature was 900 ºC, which was low enough to prevent rapid grain growth of particles, the ramping rate of tube furnace to increase the temperature up to 900 ºC was 10 ºC /min and the cooling rate to room temperature was also 10 ºC /min, and hydrogen was flowed at a rate of 0.5 L/min (25ºC, 86.1 kPa) after the temperature reached 900ºC. The result showed that the incompletely carburized WC_{1-x}, W_2C, W phases were fully carburized to the WC phase, which resulted in the formation of WC-Co composite powder after the treatment time of 2 hours, as shown in Figure 43. The grain size of WC in the composite powder obtained after the post-treatment for 2 hours was 40±1 nm. Figure 44 shows the TEM micrographs of composite powder, which mainly consisted of WC_{1-x} and Co particles, obtained at 9 kW torch power and the WC-Co composite powder obtained after the hydrogen heat treatment for 2 hours. The particle size of composite powder before the treatment was less than 10 nm and after the treatment it grew to somewhat less than 100 nm, based on measurements on a limited number of particles. The carbon in the product, 138 % excess before the treatment was close to the stoichiometric amount to form WC phase after 2 hours treatment.

In this project, WC-Co composite powders of particle size less than 70 nm and 100 nm with a stoichiometric amount of carbon were obtained from the tubular reactor system and the plasma reactor system, respectively, after the post-treatment. This investigation has achieved the simultaneous synthesis of WC-Co nanocomposite powder, unlike with other gas phase reaction methods. Under certain synthesis conditions, the WC-Co composite powder obtained from the tubular reactor did not require a post-treatment. The CVS process carried out in a tubular reactor

system and a plasma reactor system has confirmed that it is feasible to produce nanosized WC-Co composite powder by this method.

The plasma reactor system is particularly suitable for industrial application because it is easy to scale up, even though it requires post-treatment. Such a treatment, however, is rather simple. The composite powders thus produced can be used directly for compaction into bulk cemented tungsten carbide. This method for producing WC-Co nanocomposite powder is superior to other existing processes in that it uses readily available and inexpensive raw materials and requires rather simple process steps.

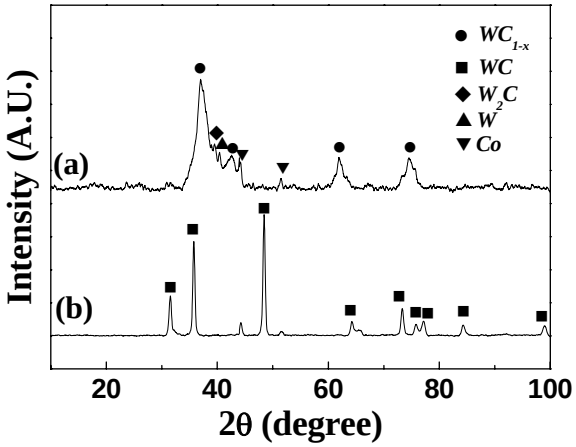

Fig. 43. X-ray diffraction patterns of the products obtained by hydrogen treatment at 900°C using the composite powder produced from the plasma reactor: (a) before treatment and (b) 2 hours of holding time.

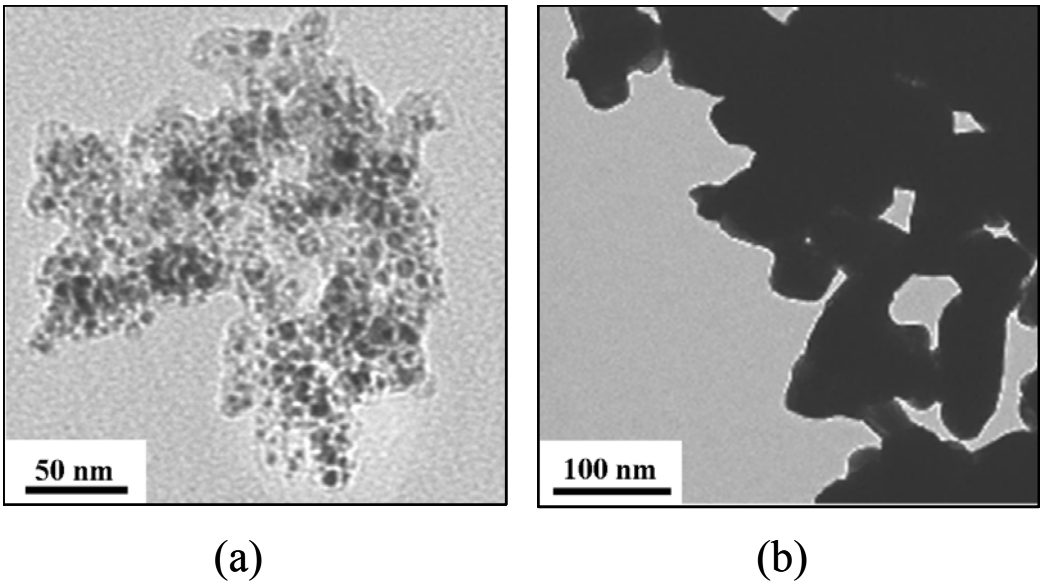

Fig. 44. TEM micrographs of powders: (a) WC_{1-x}-Co composite powder obtained from the plasma reactor and (b) WC-Co composite powder obtained after the hydrogen treatment for 2 hours at 900°C.

VI.2 Densification and Grain Growth during Sintering of Nanosized WC-Co Powders

VI.2.1 Grain Growth Behavior during the Early Stage of Sintering

Compared to conventional micron-sized powders, the nanocrystalline WC-Co powders have an additional challenge of retaining nanoscale WC grain sizes upon achieving full densification during sintering. Cemented tungsten carbide is typically sintered via liquid phase sintering in vacuum at approximately 1400^{o}C. Previous studies on the sintering of nanosized WC-Co powders have shown that significant grain growth occurs during the early stage of sintering before the liquid phase sintering temperature is reached, suggesting a rapid grain growth process in the solid state. In fact, the grain size at the first data point of the isothermal hold experiment in a comparative study by Fang et al. of the grain growth of nanosized WC-Co with conventional powders was several times larger than the original grain size of the powder [18]. The rapid grain growth during the early stage of sintering of nanocrystalline WC-Co powders is also evident in many other studies, which have repeatedly shown that the finest sintered grain sizes are approximately 100 to 200 nanometers even when the materials are sintered under high pressure in solid state [15, 24, 41].

The rapid grain growth during early stage of sintering has also been observed in many other materials. Malow and Koch [84] conducted studies on the stability of nanosized iron powders during isothermal annealing at various temperatures. Their data showed that the grain sizes at the beginning of the isothermal experiments were several times larger than the original size of the nanosized powder. Krill et al. [85] further demonstrated how the "initial growth spurt" of nanocrystalline Fe during annealing was not captured by isothermal studies. In another work on two-step sintering of nanosized ceramic powders, Chen and Wang [86] successfully minimized the latter stage grain growth during sintering by exploiting differences in grain boundary migration and grain boundary diffusion. However, they explicitly showed that the grain size at the beginning of the second sintering step is four to six times larger than the original size of the powder during the first sintering step. This phenomenon was also mentioned in the publication of Lee et al. [87]. In short, the grain growth of nanosized particles during sintering should be treated as consisting of at least two parts: an initial stage of grain growth that occurs during heating and the later stage of sintering during isothermal holding.

To date, however, there have been few reported studies in the literature that directly deal with the kinetics or the mechanisms of this part of grain growth. In order to understand the mechanisms for grain growth during the early stage of sintering of nanocrystalline WC-Co powders, systematic microstructural examinations were conducted to study the evolution of microstructure versus temperature during heat-up. The grain growth of nanocrystalline WC-Co powders was studied by tracking the changes of grain sizes and morphology of grains during heat-up as well as isothermal hold. The effects of temperature, holding time, initial grain size, cobalt content and grain growth inhibitor on the initial stage grain growth are discussed.

VI.2.1.a Effect of Temperature and Holding Time

The as-milled nanocrystalline WC-10Co powder (denoted by WC-10Co_10nm) was heated up to 800 °C, 1000 °C, 1100 °C, 1200 °C, 1300 °C with heating rate 10°C/min. Using the XRD line broadening technique, the calculated average grain sizes of WC powders after milling for 2, 5, and 12 hours were approximately 49, 21 and 11 nm, respectively. Correspondingly, the WC-Co powders are denoted by WC-10Co_50 nm, WC-10Co_20 nm, and WC-10Co_10 nm in the following descriptions of results and discussions.

Constant Heating Rate Experiment. The plot of WC grain size of WC-10Co_10 nm powder as a function of temperature during heat-up from 800 °C to 1400 °C is shown in Figure 45. It can be seen from this figure that WC grains grow slowly and steadily below 1000 °C. Above 1000 °C, the grain growth accelerated dramatically. In the range of 1100 °C to 1300 °C, the grain size has grown to greater than 100 nm. It is shown that the WC grain size, which is initially as large as 10 nm, increased to about 400 nm, i.e., by a factor of 40 during heat-up to the standard liquid phase sintering temperature 1400 °C. This grain growth could not be explained by the classic theories. Clearly, the rapid grain growth during this stage of sintering must be understood and controlled to obtain grain sizes that are less than 100 nm at fully sintered states.

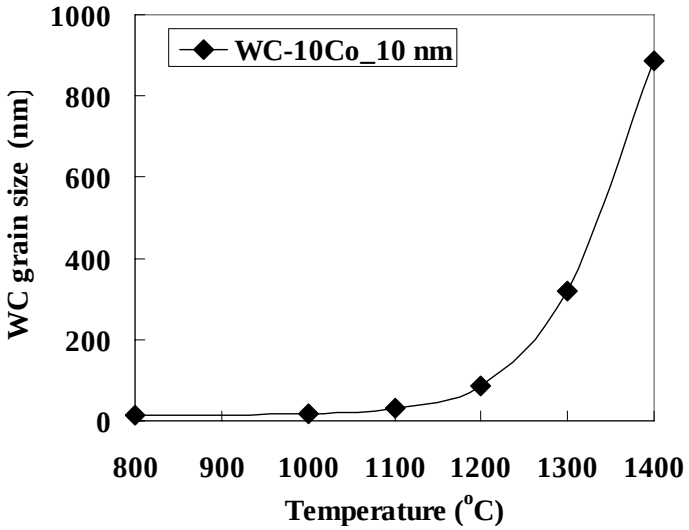

Fig. 45. WC grain growth curve of WC-10Co_10 nm powder during heat-up.

Isothermal Experiment. In order to understand the entire grain growth process, isothermal sintering experiments were carried out at 1100 °C, 1200 °C, and 1300 °C following heat-up at 10 °C /min. Figure 46 shows the isothermal grain growth curve of grain size vs. time at the three temperatures for the WC-10Co_10 nm powder. It demonstrates that the grain size increases with increasing of temperature and holding time. Compare the grain growth behavior of isothermal hold to that during heat-up. It can be seen that the grain growth is more dependent on the temperature than holding time. Thus, temperature is the most important process parameter to control grain growth.

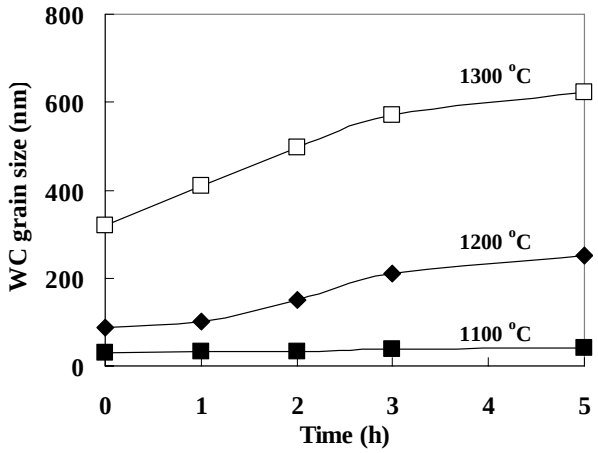

Fig. 46. Isothermal WC grain growth of WC-10Co_10 nm at 1100, 1200, 1300 °C.

VI.2.1.b Evolution of Grain Morphology and Growth Process

To study the WC grain growth process, high resolution SEM microstructural examinations were conducted to observe the evolution of the grain structure versus temperature during heat-up of WC-10Co_10nm powders, as shown in Figure 47. Figures 47 (a) and (b) show that there was little change of microstructure from room temperature to 800 °C. With the increase of temperature from 800 °C to 1000 °C, the sizes of primary particles within aggregates and the size of aggregates increased significantly. The surface morphologies of particles were smoothed. Small particles that were attached on the surface of large aggregates disappeared. Considerable WC grain growth also occurred. The average grain size increased from approximately 12 nm to 19 nm based on the XRD data. Between 1000 °C and 1100 °C, the aggregates developed a multifaceted surface morphology that has the layered structure of crystal platelets, suggesting a preferred orientation of particles during aggregation. At 1200 °C, the aggregates have become much larger grains with angular shapes and smooth surfaces. At 1300 °C, the WC grains have grown to several hundred nanometers and transformed to triangular prism with truncated corners. It is also evident that liquid phase sintering occurred at approximately 1300 °C.

It showed that the shape change and surface faceting of WC grains of WC-10Co_10 nm powders during heat up were observed at much lower temperature (below 1000 °C) compared to coarse powders (For micron size powder, the changes occur above 1200 °C). This result indicated that the mass transport through dissolution or surface diffusion of the WC grains takes place very fast even at a low temperature with small grain size.

VI.2.1.c Effect of Initial Grain Size

The effect of the initial WC grain size of the starting powder on grain growth during heat-up is shown in Figure 48. For all the powders, the grain growth started around 800°C, while rapid grain growth took place between 1000 and 1200 °C. Figure 48 shows that the finer the initial grain size of the powder, the smaller the final grain size. It is interesting to note that the relative grain growth (the ratio of sintered grain size to initial grain size G/G_0) of the finer size powder is greater than that of the larger one, as shown in Figure 49.

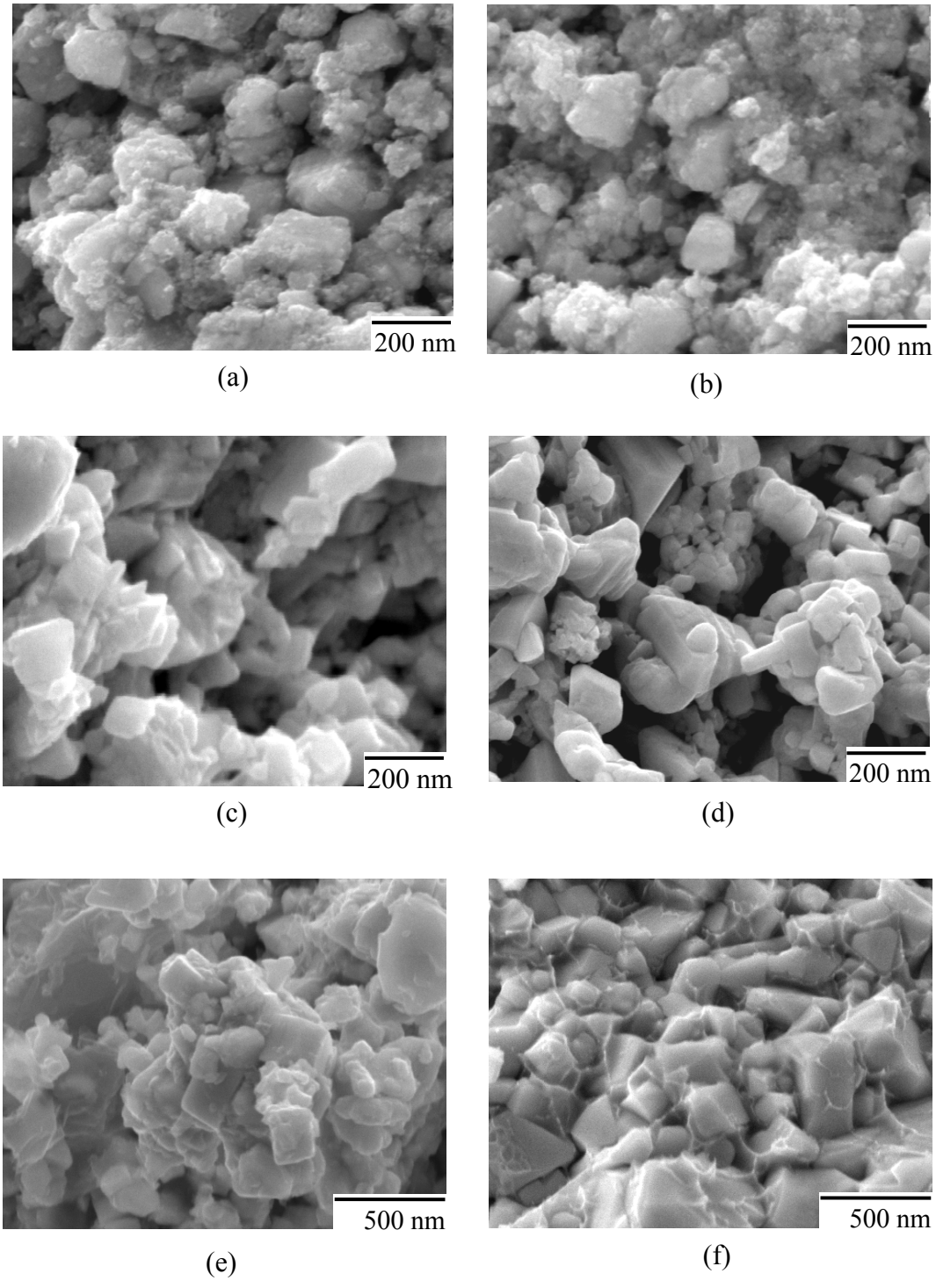

Fig. 47. The SEM observation of the evolution of the morphologies of WC-10Co_10 nm powders when heated to different temperatures: (a) as-milled power, (b) 800 ^{o}C, (c) 1000 ^{o}C (Co leached), (d)1100 ^{o}C (Co leached), (e) 1200 ^{o}C , and (f) 1300 ^{o}C.

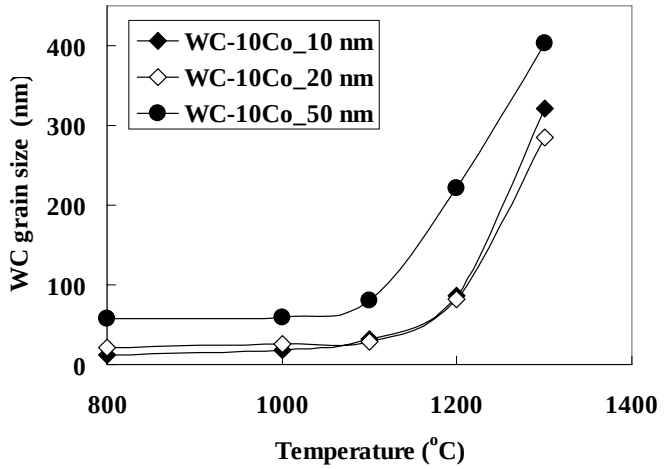

Fig. 48. WC grain growth curve during heat-up of WC-10Co powders with different initial grain sizes.

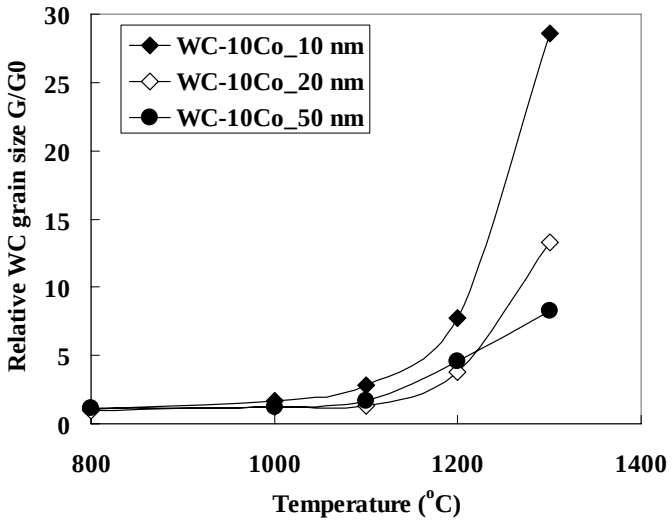

Fig. 49. WC grain growth curve during heat-up of WC-10Co powders with different initial grain sizes.

VI.2.1.d Effect of Co

The role of cobalt during liquid phase sintering of cemented tungsten carbide WC-Co was well documented. The role of cobalt on densification during solid state sintering of WC-Co has been examined by various authors [47, 88, 89]. Its effect on grain growth during solid state sintering, however, has not been explicitly studied. Therefore, pure nanocrystalline WC powder was sintered under the same conditions as that for WC-10Co powders to investigate the influence of Co. The change of grain size versus temperature and the change of the morphology of pure WC during heat-up are shown in Figures 50 and 51, respectively, in comparison with that of the WC-10Co powder (Figure 47).

The pure WC powder did not have any significant changes in grain sizes until 1300 °C. Furthermore, the sizes of the aggregates that formed during sintering are smaller. The temperature for the grains within the aggregates becoming faceted is much higher. Evidently, the

addition of Co to WC reduces the temperature at which rapid grain growth occurs. The effect of cobalt is logically related to the solubility of W and C in the cobalt phase. The exact mechanism by which cobalt promotes grain growth, however, is worthy of exploring in light of the need to understand the processes of grain growth. Based on the theories of activated sintering [90], cobalt metal that coats WC grains during milling may serve as a conduit for W and C diffusion, which results in densification as well as grain growth.

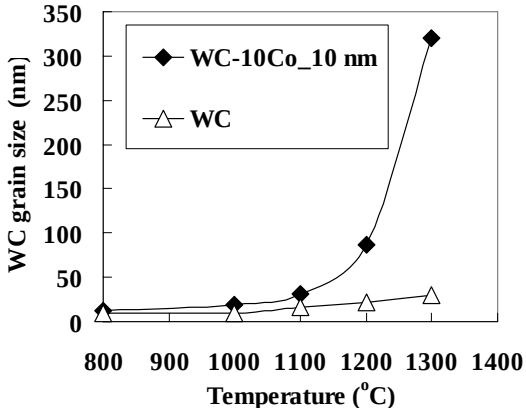

Fig. 50. Comparison of WC grain growth during heat-up of nanosized pure WC and WC-Co_10 nm powders.

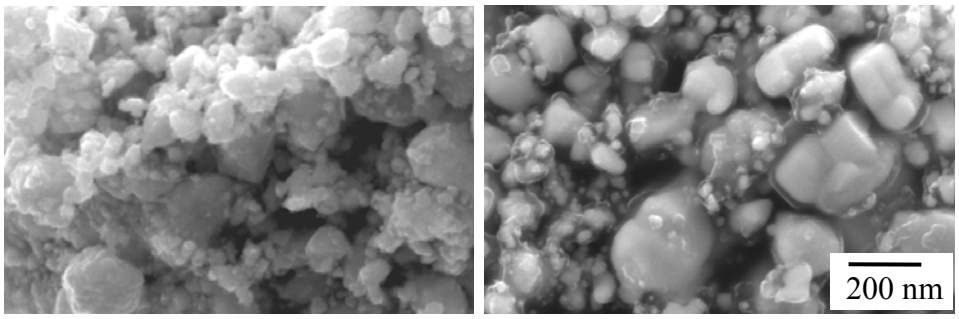

(a) (b)

Fig. 51. The SEM micrograph of pure 10 nm WC powder heated to (a) 1300 °C; (b) 1400 °C.

VI.2.1.f Effect of Grain Growth Inhibitor

It has been well documented in the literature that the grain growth of WC-Co materials can be mitigated by adding inhibitors such as Cr_3C_2, TaC, and VC during liquid phase sintering. Among them, VC is the most effective one. Inhibition of the grain growth by VC is typically attributed to its effect on the solution-reprecipitation process during liquid phase sintering. However, the role of VC on grain growth during solid state sintering is not clear yet.

In this work we investigated the effects of VC by doping the WC-10Co_10 nm powder with 1wt% VC and studied its effect on the grain growth during heat up, mostly solid state sintering. As shown in Figure 52, the rapid grain growth did not start until 1300 °C with VC doping. In other words, VC effectively prevented the rapid growth from taking place until 1400 °C. This is a very significant finding because it implies that the initial grain growth can be

minimized. Figure 53 shows the morphology of the WC grains of VC doped WC-10Co_10 nm powders at 1300 ^{o}C. Clearly, compared to un-doped WC-10Co_10 nm powders (Figure 47f), the doped WC grains exhibit multi-faceted characteristics of layered structure, while WC without doping becomes fully developed prism shaped grains. This result suggests that VC has effectively delayed the aggregation of nanosized particles and the transformation of aggregates to single crystals to higher temperatures. From Figure 52, it is noted that VC seems more effective above 1100 ^{o}C. This may relate to the interaction between VC and Co: the solubility of VC in Co and VC could hinder Co spreading, etc.

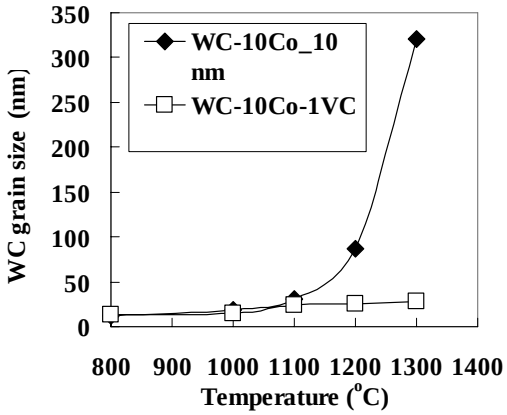

Fig. 52. Comparison of WC grain growth during heat-up in WC-Co powder with and without VC-doping.

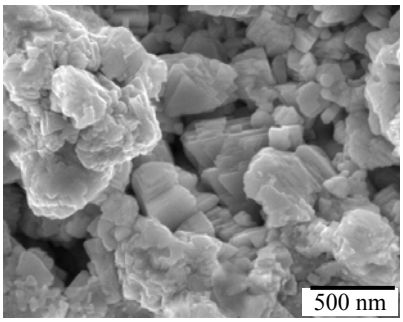

Fig. 53. The SEM micrograph of WC-10Co-1VC powders heated to 1300^{o}C (Co leached).

VI.2.2 Densification during the Early Stage of Sintering

Previous studies have shown that although cemented tungsten carbides are typically produced by standard liquid phase sintering at about 1400 ^{o}C, a large amount of densification can occur below the eutectic temperature of WC-Co system, especially for nanocrystalline powders. In the meanwhile, the grain growth takes place significantly during the early stage of sintering as shown in the last section. It is necessary to find ways to decouple the densification and grain growth to obtain dense bulk materials with nanostructure. One of the ways to decrease the WC grain growth is by lowering the sintering temperature. It seems that this is the reason for the increasing attention to study the densification during solid state sintering, during heat-up. In the following section, the factors influencing densification will be discussed, including initial grain size, Co content, grain growth inhibitor.

VI.2.2.a Effect of Initial Grain Size

Figure 54 shows the densification behavior of WC-Co with different initial grain sizes: 10 nm, 50 nm, and 1000 nm as function of temperature during heat up. For all the three samples, the densification during solid state sintering at least took three stages separated by two temperatures: 1000 ^{o}C and 1200 ^{o}C. The two representative temperature points correspond to two densification rate inflection. Before 1000 ^{o}C, in stage I, the densification was gradually accelerated. The smaller the initial grain size, the faster the densification was. In stage II, the densification of nanosized powders was significantly faster than that of the coarse powders. Compared to coarse powder, the densification of nanosized powders took place much faster, which reached 80% (about 90% relative density) at 1200 ^{o}C.

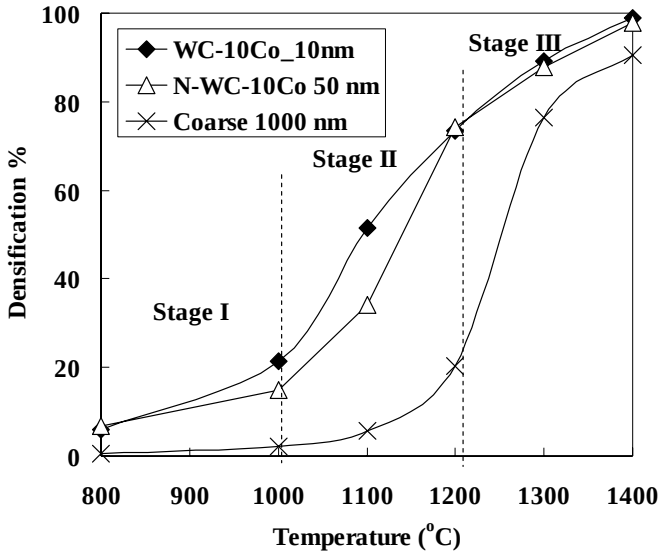

Fig. 54. Plot of % densification vs. temperature for all the grades of powders, i.e., 10 nm, 50 nm, 1000 nm during continuous heat-up to different temperatures.

It is interesting to note that the nanosized powders reached almost the same densification value at 1200 ^{o}C, no matter the initial size difference for the two powders. After 1200 ^{o}C, in stage III, the densification of coarse powders started accelerating; the densification rate of nanosized powder decreases as the material approaches the full density. The different temperature ranges for the rapid densification, which are responsible for the major fraction of entire densification, imply there are different mechanisms for the densification process due to the effect of initial grain size.

VI.2.2.b Effect of Co Content

Previous studies have shown that the binder phase cobalt is responsible for the densification of coarse size powders. WC-1Co and WC-10Co were used to demonstrate the effect of cobalt content on the densification behavior of nanocrystalline WC-Co powders during heat up. It can be seen in Figure 55 that the densification of the powder with 1 wt% Co is faster than that of powder with 10 wt% Co before 1200 ^{o}C. After 1200 ^{o}C, the densification rate of WC-1Co powder is suddenly decreased. The achieved densification is less than that of WC-10Co

powder.

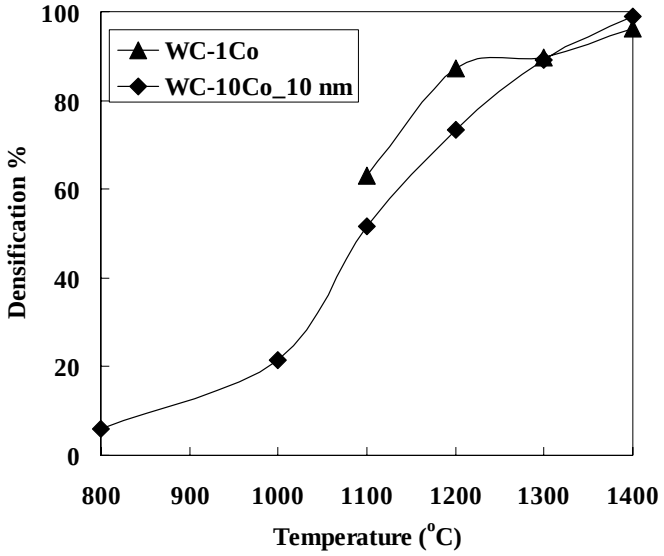

Fig. 55. Effect of cobalt on densification of nanocrystalline WC-Co powder during heat up.

VI.2.2.c Effect of Grain Growth Inhibitor

The grain growth inhibitors significantly affect the densification during sintering of nanocrystalline WC-Co powders. Figure 56 shows the effect of VC addition on the densification of nanocrystalline WC-Co powders with different initial grain sizes (10 nm and 50 nm) during heat-up. With 1wt% VC addition, the densification rate decreases dramatically before 1200 °C. The addition of VC shifts the temperature range for rapid densification to higher temperature. Furthermore, with the decrease of initial grain size, the inhibition effect of VC on densification decreases.

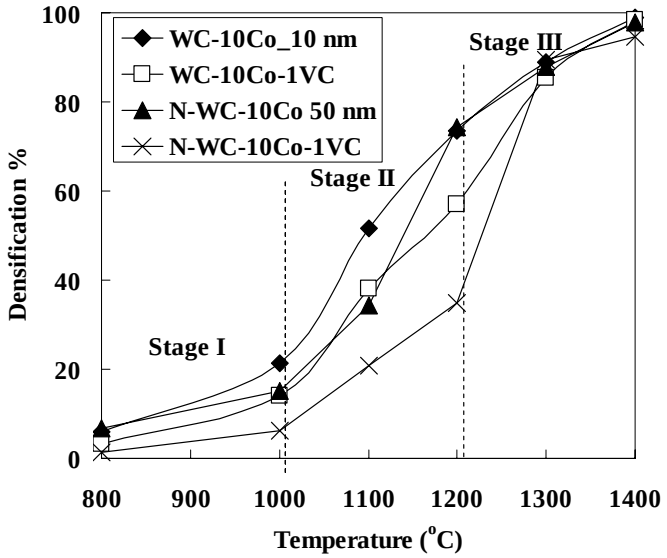

Fig. 56. Effect of grain growth inhibitor on densification of nanocrystalline WC-Co powder during heat up.

VI.3. Consolidation of Nanosized WC-Co Powders Using the Ultrahigh Pressure RapidHot Consolidation Process

In view of the above results, the project team decided to develop a new consolidation process for sintering nanocrystalline WC-Co powders at lower temperatures, i.e., sintering in solid state, without use of grain growth inhibitors. The process should be capable of enhancing the densification and limiting grain growth at the same time. Many attempts have focused on developing alternative processes to liquid phase sintering, which allow full densification of WC-Co materials at a lower sintering temperature and/or within a shorter thermal cycle time, such as Microwave Sintering (MS), Spark Plasma Sintering (SPS), High Frequency Induction Heated Sintering (HFIHS), and so on. Compared to conventional sintering techniques, these techniques are characterized by shorter densification time at lower temperatures during the consolidation processes, resulting from external field coupled with applying pressure. SPS, for example, by application of electrical fields, can generate rapid and simultaneous heating within samples due to the pulse electrical current through the graphite die and/or samples. During SPS, the rapid heating allows avoidance of the temperature range of rapid coarsening of grains resulting from the grain/particle coalescence controlled by surface diffusion. Applied pressure aids the densification process at relatively low temperature. However, the maximum pressure of typical SPS is limited (150 MPa). Using these techniques, the finest average grain size that has been achievable until now is still in the range 100-300 nm.

In this project, an ultrahigh pressure rapid hot consolidation (UPRC) process, which combines rapid heating (>100 ^{o}C/min) and ultrahigh pressure, was designed and developed. Ultrahigh pressure is defined as pressure greater than 400MPa, which is typically the upper limit of commercial Hot Isostatic Press (HIP) processes. The process was successfully applied to producing dense nanocrystalline WC-Co with no grain growth inhibitors in a short cycle.

In this section, the grain growth and densification behaviors during UPRC are discussed. The obtained results are compared to previous pressure-less vacuum sintering results to further reveal the effects of the process variables (including temperature, holding time, pressure, and heating rate) on the grain growth and densification during the sintering of nanocrystalline WC-Co powders.

VI.3.1 Grain Growth and Densification Behaviors during UPRC

The samples were sintered at 1100 °C, 1200 °C, and 1300 °C for 15 min with a heating rate of 200 ^{o}C/min, under a pressure 800 of MPa. The plots of WC grain size and densification as a function of temperature is shown in Figure 57. The sintered density increased with the increased sintering temperature and densification was completed at about 1200 ^{o}C. After 1200 ^{o}C, the densification changed little. For the grain growth, it is shown that the WC grain size rapidly increased by a factor of 4 from 1200 ^{o}C to 1300 ^{o}C. This is similar to the pressure-less vacuum sintering. It is justified to conclude that the critical temperature exists above which the grain growth accelerates dramatically.

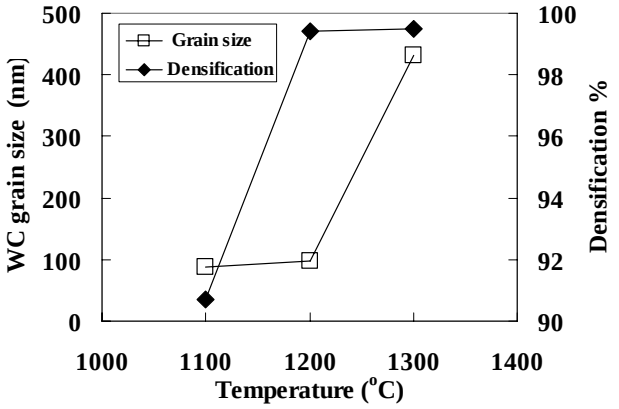

Fig. 57. Plots of grain size and densification as function of sintering temperature of sintering N-WC-10Co powder by UPRC process.

VI.3.2 Effect of Process Variables

A series of experiments were carried out to study the sintering process of UPRC. Comparing the results between UPRC and vacuum sintering reveals the effects of the process variables (including pressure, heating rate, temperature, and holding time) on grain growth and densification behavior of the nanocrystalline WC-Co powders.

As shown in Table 4, both the rapid heating (samples 6, 7) and the application of pressure (samples 2, 4) are effective to limit the grain growth. Sample 2 demonstrated that with combined rapid heating and ultrahigh pressure, dense bulk WC-Co with less than 100 nm grain size was obtained in a short sintering time.

Table 4. The variation of relative density and grain size with process variables during UPRC process and vacuum sintering.

Process	*Sample No.*	*Temperature (°C)*	*Heating Rate (°C/min)*	*Holding Time (min)*	*Pressure Application (MPa)*	*Relative Density (%)*	*Grain Size (nm)*
UPRC	1	1100	200	15	800	90.7	
	2	1200	200	15	800	99.4	97
	3	1300	200	15	800	99.2	432
	4	1200	200	0	800	98.9	90
	5	1200	200	15	0	79.7	250
	6	1200	200	0	0	77.7	121
Vacuum sintering	7	1200	10	0	0	87	280
	8	1400	10	0	0	98.9	502

As mentioned earlier, between 1200 and 1300 ^{o}C, the grain growth took place very rapidly even under ultrahigh pressure, similar to the pressure-less vacuum sintering. The temperature range for the rapid grain growth, however, was shifted to higher temperature. It appears that the critical temperature for the grain growth was delayed.

The ultrahigh pressure plays significant role in enhancing densification kinetics in the sintering of nanocrystalline WC-10Co powders. A high relative density was achieved in 1 min under a pressure of 800 MPa (Sample 4). In the meanwhile, the densification temperature was 200 ^{o}C lower than that of Sample 8. At a given temperature, density increases with holding time. It seems that temperature is a more important factor than holding time in influencing densification (Samples 1, 2, 4). According to Samples 6 and 7, the higher heating rate does not lead to immediate densification.

VI.3.3 Effect on Microstructure Evolution

The microstructures at different process conditions during sintering by UPRC and vacuum sintering are shown in Figure 58. The aggregates of original powder in Figure 58(a) transformed into the grains in Figure 58(e) when the powder was heated up to at 1200 ^{o}C by vacuum sintering. Comparing Figures 58 (f) to (e), it shows that the rapid heating inhibits the transformation within the aggregates. In Figure 58(b), it seems that the ultrahigh pressure can break up the aggregates and further decrease the grain size.

Shape change and surface faceting in WC particles were observed with a very fast heating rate of 200 ^{o}C/min during the UPRC process, as shown in Figure 58(f). This result confirmed that the mass transport via dissolution or surface diffusion of the WC particles takes place very fast even at a low temperature for small grain size powder. It is noted that the changes of WC particles seem different with rapid heating. The surface of particles is not as flat and smooth as with slow heating.

It is clear that the aggregates in Figure 58(a) coalesced into the grains in Figure 58(e) when the powder was heated up to 1200 ^{o}C by vacuum sintering. It has been shown that the rapid heating inhibits the transformation within the aggregates and applied ultrahigh pressure can break up the aggregates and further decrease the grain size.

VI.3.4 Rapid Heating Experiments

To further study the effect of heating rate on the grain growth and densification of sintering nanocrystalline WC-Co powders, samples from WC-10Co_10 nm powder were sintered by UPRC at a heating rate of 200 °C/min without the application of pressure. Compared to the sintering results from vacuum sintering at a heating rate of 10 °C/min, it was found out that the samples sintered at the higher heating rate (200 °C/min) possess lower density and smaller grain size than samples sintered at the lower heating rate (10 °C/min). Figure 59 shows the difference in the densification and grain sizes of the samples sintered at different heating rates. It is seen that the effects of rapid heating on grain growth is more evident after 1100 °C.

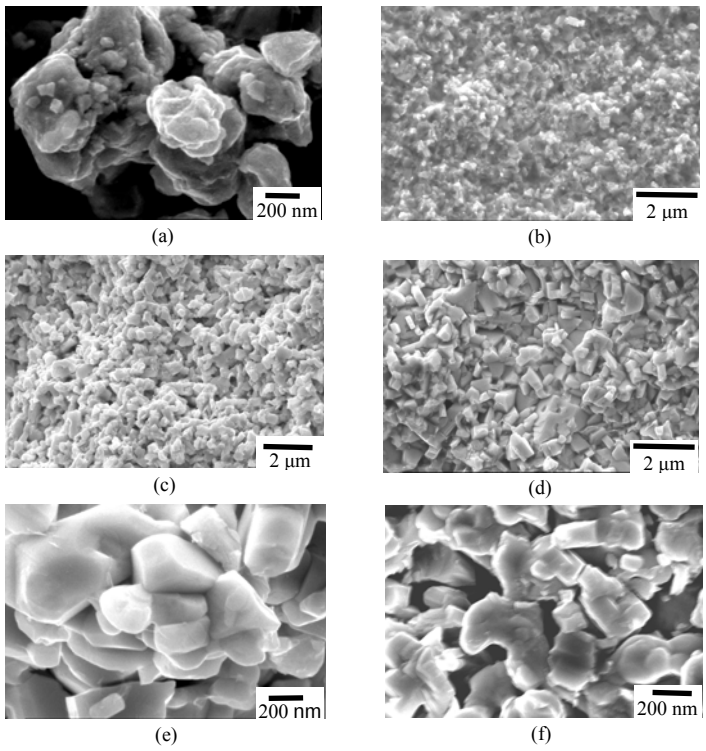

Fig. 58. The SEM micrograph of (a) As-milled nanocrystalline WC-10 Powders (b) Fracture surface of WC-10Co sintered by UPRC at 1200 °C for 15 min, under pressure of 800 MPa (*Sample 2*). (c) Fracture surface of WC-10Co sintered by UPRC at 1300 °C for 15 min, under pressure of 800 MPa (*Sample 3*). (d) Fracture surface of WC-10Co sintered by UPRC at 1200 °C for 15 min, under pressure of 0 MPa (*Sample 5*). (e) Fracture surface of WC-10Co sintered by vacuum sintering at 1200 °C for 0 min, heating rate 10 °C/min (*Sample 7*). (f) Fracture surface of WC-10Co sintered by UPRC at 1200 °C for 0 min, heating rate 200 °C/min, under pressure of 0 MPa (*Sample 6*).

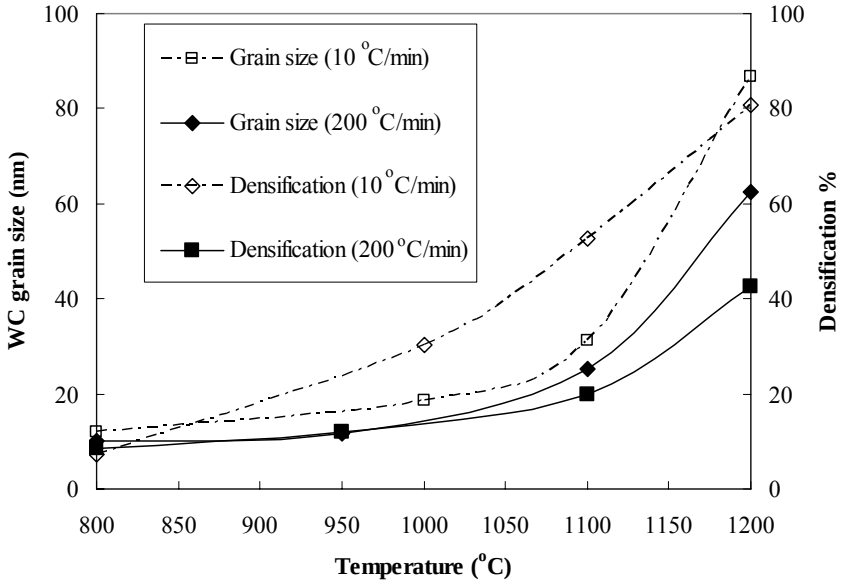

Fig. 59. The plots of grain size and densification as function of sintering temperature of sintering WC-10Co_10 nm powder by UPRC process and vacuum sintering.

VI.4. Sintering of Binder-less Nanosized WC

For cemented tungsten carbide, the binder phase Co is used to improve the sinterability of WC to fully dense materials. The addition of Co, however, causes significant WC grain growth, reduces the hardness and corrosion/oxidation resistance of the material. To avoid those problems, the amount of Co binder phase needs to be reduced as much as possible.

Considering the high melting point of WC, by conventional process, it is difficult to sinter pure WC without use of very high temperature (>1700 ^{o}C) or high pressure. The outcome of the processes results in very large grain size. In this work, another method to enhance the sinterability of WC was studied by reducing the grain size of initial powder. The finer the initial powder grain size, the lower the sintering temperature and the shorter the sintering time are.

Figure 60 shows the densification behavior of nanosized binderless WC sintered between 1400~1500 ^{o}C. The density of the samples was increased with the increase of the sintering temperature. The binderless WC sintered above 1450 ^{o}C for 1 hour showed nearly full densification, more than 99% theoretical density. The Vickers hardness of the samples sintered at 1470 ^{o}C was HV_{30}=2620. The average grain size is measured as 158 nm, as shown in figure 61.

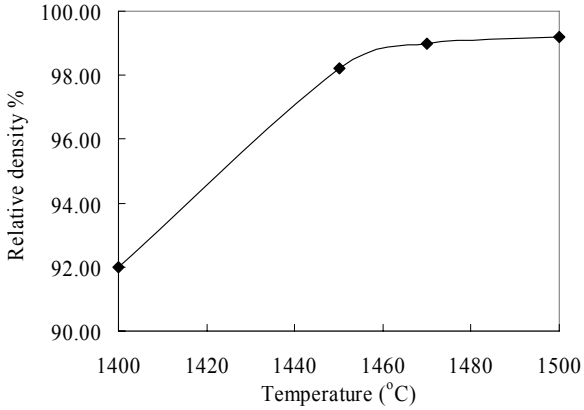

Fig. 60. The variation of sintered relative density of binderless WC with vary sintering temperature.

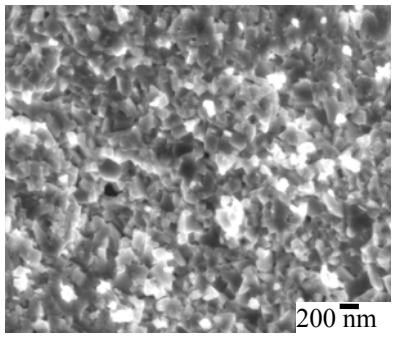

Fig. 61. SEM morphology of Nanocrystalline pure WC sintered at 1470 ^{o}C for 1 hour.

VI.5. Manufacturing of Functionally Graded WC-Co Using Nanosized WC-Co Powders

Considering the fact that the fracture toughness of WC-Co materials always decrease with the increase of the hardness, there is always a concern regarding the broadness of potential applications of WC-Co made from nanosized WC-Co powders. A potential solution to take the advantages of nanocrystalline structure without significantly sacrificing the impact resistance of the material is to make engineering components of which the surface layer is nanocrystalline while the bulk may remain to be a micro-grain sized material with lower hardness and higher toughness. Based on this view point, a series of effort were made toward making WC-Co with graded microstructure in which the grain size near surface layer is ultrafine while the grain size in the interior is normal (submicron to micron size).

To manufacture functionally graded WC-Co with grain size gradient, we prepared two different powder mixtures: one is the standard grade to be used as the bulk substrate, and the other is the fine grain grade which will be on the surface providing superior wear resistance. During sintering of a green structure which consists of layers with different grain sizes, there is an issue of the cobalt migration. In general, during sintering, liquid phase cobalt will migrate from areas with more cobalt to areas with less cobalt, and from areas with coarser grain size to areas with finer grain size. Carbon content is another factor that affects the direction of cobalt migration. Liquid phase tends to migrate in the same direction of carbon diffusion. Figure 62 illustrates the general trend of cobalt migration during sintering of WC-Co materials.

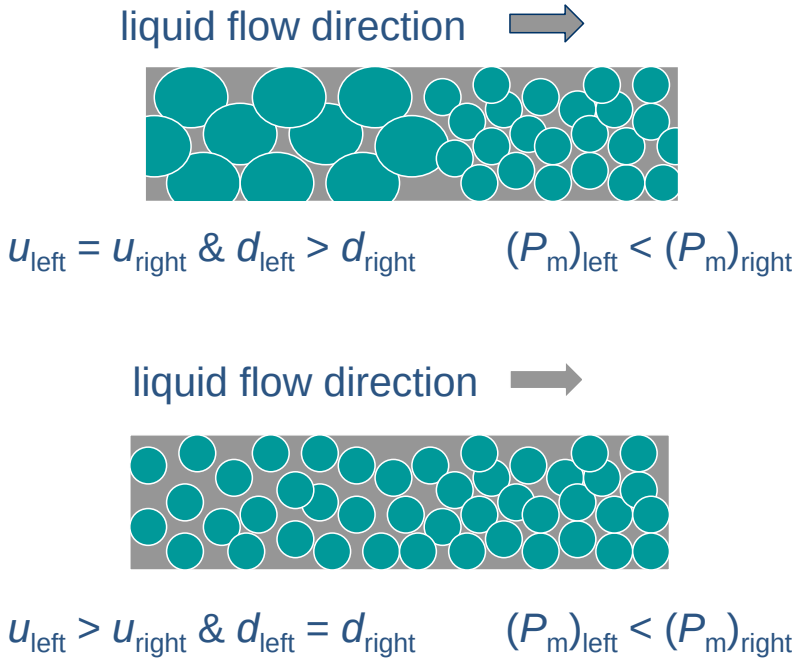

Fig. 62. Illustration of the trend of cobalt migration during sintering of FGM WC-Co.

In order to produce FGM WC-Co with grain size difference, we must therefore understand the interactions of cobalt content and grain size and the evolution of microstructure during sintering. Based on a model that was established in our previous work and literature, as shown below, we designed a series of experiments with different grain size and cobalt content to obtain FGM WC-Co.

$$P_m = k_1\left[(\frac{1}{u}-1)^{1/3}-1.41u\right]\Big/ d^n \qquad (8)$$

where u is volume fraction of liquid, d is grain size, k and n are constants. Pm is defined as the migration pressure. It is determined by the balance of interfacial energies in the WC-Co system. Liquid migrates from areas with lower Pm to areas with higher Pm. It is known that WC/WC interface has higher energy than that of the WC/Co interface, which is why cobalt will penetrate in between WC grains to minimize the energy. When grain size decreases, it requires more liquid to cover all the surfaces of WC grains, hence liquid migrates from regions with coarser grain size (lower Pm) to regions with finer grain size (higher Pm). Liquid migration will cease once Pm across the system is equilibrated.

After sintering, by measuring final distribution of cobalt phase of all the samples, we were able to determine using numerical techniques the parameters in the model as shown below:

$$P_m = 2048\left[(\frac{1}{u}-1)^{1/3}-1.41u\right]\Big/ d^{0.4} \qquad (9)$$

This model can then be used to design FGM based on different grain sizes. Figure 63 illustrates the design method.

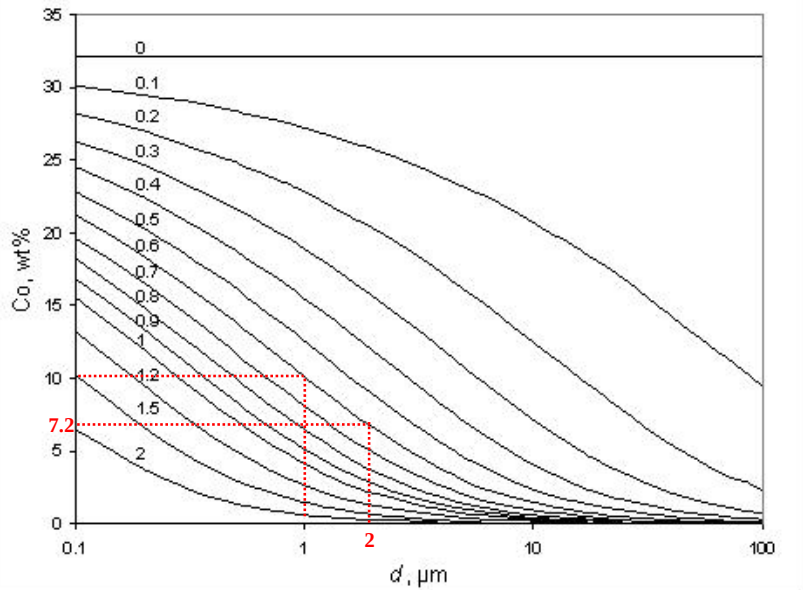

Fig. 63. Liquid migration pressure contours as a function of grain size and volume fraction of cobalt.

The solid lines in the figure are liquid migration pressure contour lines as a function of grain size and volume fraction of the cobalt phase. By finding two points on a single line, one can identify two pairs of cobalt content vs. grain size. For these two pairs of Co% and d values, the liquid migration pressures are equal. Therefore, if two layer of materials made of those two compositions are pressed together, there will be no liquid migration between the two layers. A FGM is thus successfully fabricated. For example, if the bulk substrate has 1 micron grain size and 6wt% cobalt and the surface layer has 100 nm grain size and 15% cobalt, the system would be at equilibrium during sintering. A FGM WC-Co using nanosized WC/Co powders are thus designed and fabricated. We plan to test these FGM for potential applications.

VI.6. Evaluation of Mechanical Properties of WC-Co Material Made from Nanosized Powders

The conventional WC-Co material combines a high hardness with a moderate toughness making them suitable for a wide range of applications including tooling and wear parts. Its performance, however, is limited by its relatively low toughness. When the WC grain size is in the nanoscale, there is significant potential to improve both the hardness and the fracture toughness of the material. Previous results of sintering nanosized WC-Co powders have shown that at any given harness, WC-Co samples produced from nanocrystalline powders had higher toughness than those produced from conventional powders. So far, all the reported grain sizes of the sintered samples from nanocrystalline powders, however, are larger than 100 nm. In order to evaluate the true mechanical properties of nanocrystalline WC-Co materials, the dense bulk WC-Co materials with nanocrystalline grain size have to be produced first.

In this research, the almost fully dense nanocrystalline WC-Co materials were successfully made by the UPRC process. The two very important properties, hardness and fracture toughness, were measured to evaluate the mechanical properties of nanocrystalline WC-Co materials.

VI.6.1. UPRC Results

The nanocrystalline WC-10Co powder, N-WC-10Co (initial grain size 50 nm) was used to optimize the conditions of UPRC. Figure 64 shows the Vickers harnesses of sintered samples by UPRC as a function of temperature. With increasing the temperature to 1200 °C, the hardness increased with the increase of density (Figure 57). The hardness value at 1300 °C decreased dramatically due to the significant grain growth, from 97 nm (at 1200 °C) to 423 nm. The temperature of 1200 °C was chosen to produce the samples for the mechanical property tests.

To evaluate the fracture toughness of the samples, the Palmqvist toughness was used as a toughness parameter. Figure 65 shows the Vickers indentation on the sample sintered at 1200 °C. Using the Equation (7), the Palmqvist toughness of the sample is calculated as 9.8 $MPa \cdot m^{1/2}$.

The fracture surface of sintered sample from WC-10Co_10 nm powders is shown in Figure 66. The grain size is 76 nm measured by XRD. Table 5 compares the mechanical properties of the samples made of powders with different initial grain sizes: 10 nm and 50 nm. The smaller the initial grain size, the smaller the sintered grain size and the higher hardness. The toughness is still at the same level. It means that the nanocrystalline WC-Co materials can have high hardness

without sacrificing the toughness.

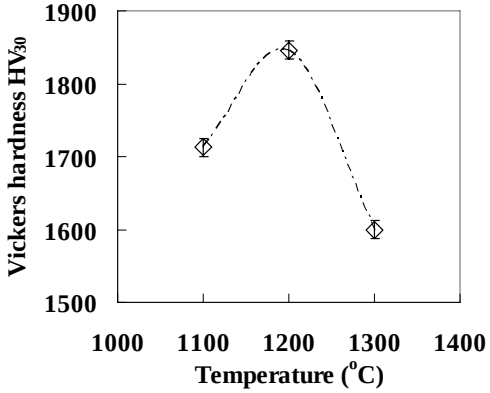

Fig. 64. Variation of Vickers hardness of N-WC-10Co sintered by UPRC with temperatures: 1100 °C, 1200 °C and 1300 °C for 15 min, under 800 MPa.

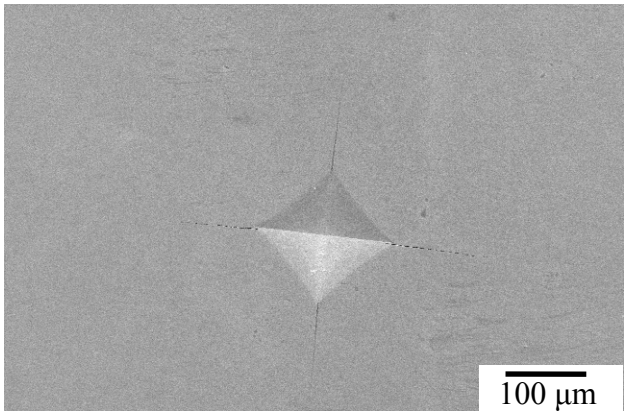

Fig. 65. Vickers's hardness indention of N-WC-10Co sintered at 1200 °C for 15 min. Under pressure 800 MPa.

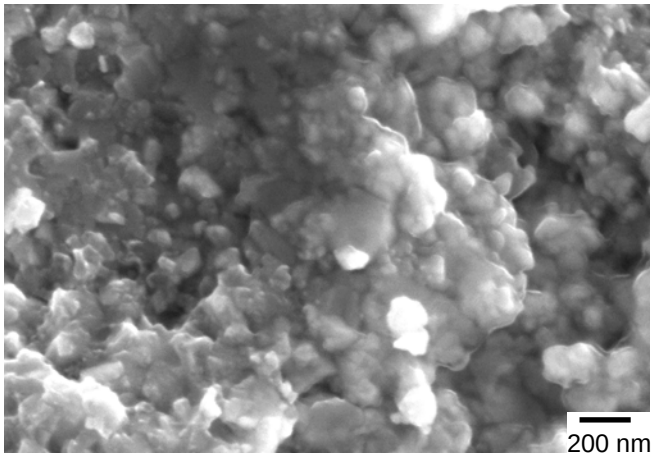

Fig. 66. SEM fracture morphology of WC-10Co_10 nm powder sintered by UPRC at 1200 °C for 15 min. Under pressure 800 MPa.

Table 5. Mechanical properties of samples consolidated by UPRC from initial grain sizes: 10 nm and 50 nm.

Process	*samples*	*Grain size (nm)*	*Vickers Hardness HV_{30}*	*Palmqvist toughness $MPa{\cdot}m^{1/2}$*
UPRC	WC-10Co 10 nm	76	1960	9.7
	N-WC-10Co 50 nm	97	1845.3	9.8

VI.6.2. Comparison of Mechanical Properties

To better evaluate the mechanical properties of samples produced by UPRC, the Vickers hardness and fracture toughness tests by using the standard short rod method (ASTM-B771) were conducted on the samples consolidated by UPRC and vacuum sintering from the same grade of WC-10Co_10 nm powders. Table 6 shows the test results. The hardness values of the samples produced by UPRC are much higher than those by vacuum sintering. The fracture toughness values are comparable.

Figure 67 compares the relationship of the fracture toughness and hardness of between conventional WC-Co materials and samples made by UPRC [71]. It is clear from Figure 67 that the hardness value significantly increased at identical facture toughness level.

Table 6. Mechanical properties of samples consolidated by UPRC and vacuum sintering.

Process	*samples*	*Vickers Hardness HV_{30}*	*Fracture toughness K_{IC} $MPa{\cdot}m^{1/2}$*
UPRC	WC-10Co 10 nm	1830.2	9.81
	WC-10Co-1L*	2038.3	7.15
Vacuum sintering 1360 ^{O}C, 1h	WC-10Co	1547.6	10.04
	WC-10Co-1L	1788.8	9.65

** L represents grain growth inhibitors: 1L=0.6 wt% VC + 0.4 wt% Cr_3C_2*

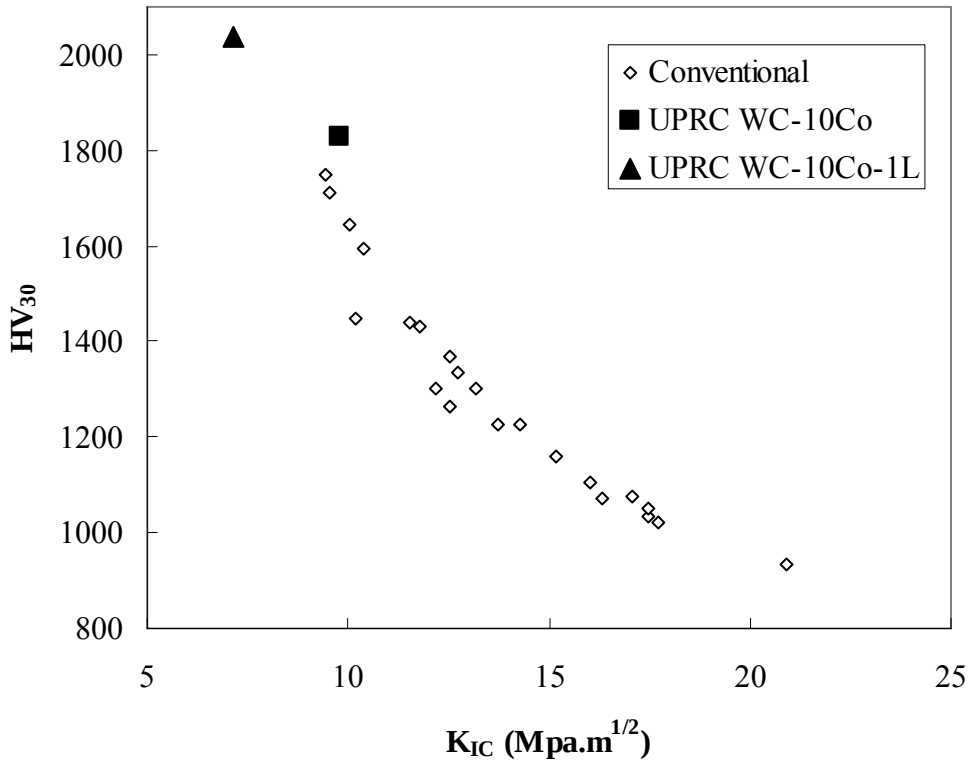

Fig. 67. Fracture toughness K_{IC} vs. hardness HV_{30} relationship from UPRC and conventional sintering.

Conclusions

Based on the results presented above, the following conclusions are drawn:

1. The CVS process was investigated in this project with an electrically heated tubular reactor and a plasma reactor. The latter has a greater potential for an industrial process because a plasma process can use readily available and inexpensive raw materials such as APT and cobalt oxide instead of chlorides; can more readily be scaled-up; and requires fewer and simpler process steps than existing processes. As-processed powders usually have a particle size of 20 nm. CVS WC and WC/Co powders are likely to contain excess carbon which can be removed by a hear treatment in H_2. Particle size increases to approximately 40 to 50 nm after the treatment. The yield of CVS process is low in the current laboratory process. We believe that the yield of such processes can only be demonstrated in an industrial pilot production set up.

2. The capability of ultrahigh pressure rapid heating and consolidation (UPRC) process is proven. Similar to the popular SPS process, UPRC process is capable of rapid heating. However, different from the SPS process, the UPRC process is capable of much higher pressure (up to 1 GPa depending on die design) and the pressure is applied iso-statically. The process can be used to consolidate and manufacture a range of bulk nanocrystalline materials.

3. Given the present state-of-the-art technology, it is not feasible to make bulk WC-Co materials with less than 50 nm average grain size in the sintered states. However, it is proven by this program that fully sintered bulk WC-Co can be made with final grain size between 50 to 100 nm without relying on grain growth inhibitor.

4. Binderless (i.e. pure WC with less than 1% metal content) tungsten carbide can be manufactured using nanosized WC powders produced by the custom-designed high energy planetary ball milling process. The powder can be sintered to near-full density (>99%) at below 1500 °C.

Recommendations

This program has met its initial basic goal of demonstrating the feasibility and viability of developing processes for making nano WC/Co composite powders and sintering nanosized WC/Co to make bulk nanocrystalline WC-Co materials. However, the mechanical properties of the resultant material follow the conventional trend with respect to the relationship between hardness and fracture toughness. Albeit that fact, a number of materials and processes that were developed as parts of this program have commercial potentials. We recommend the following:

1. Individual pieces of technologies developed in this program should be further investigated and tested in pilot production scale through government and private industry sponsored programs geared toward commercialization. As it was pointed out earlier, the CVS process needs to demonstrate its viability by achieving certain threshold value of yield. The UPRC process can be applied for consolidation of high temperature ceramics. The binderless tungsten carbide can be used for water jet nozzles and other applications requiring extreme wear resistance. We will recommend the management of Kennametal Inc. and Smith International Inc. to consider development of products based on these technologies.

2. Fundamental studies on mechanisms of nano grain growth during sintering and means to control and minimize the initial dynamic grain growth should be continued. Until then, a rule-of-thumb is that the finest grain size in a sintered material from nanosized powders is approximately 50-100 nm. To obtain bulk nanocrystalline materials with grain size finer than 50 nm, more in-depth research is still needed.

Accomplishments

1. Publications

Peer-reviewed Journal papers:

1) Z. Zak Fang，Wang X, Taegong Ryu, Kyu Sup Hwang, and H. Y. Sohn. "Synthesis, Sintering, and Mechanical Properties of Nanocrystalline Tungsten Carbide –A Review". *Inter. J. Refract. Met. Hard Mater*, **2009**, 27, 288-299.

2) Xu Wang, Zhigang Zak Fang, and H. Y. Sohn, "Grain Growth During Early Stages of Sintering of Nano Size WC-Co", *Inter. J. Refract. Met. Hard Mater.*, **2008,** 26(3), 232-241**.**

3) Taegong Ryu, H. Y. Sohn, Kyu Sup Hwang, and Z. Z. Fang, "Plasma synthesis of tungsten carbide and cobalt nanocomposite powder and post-treatment," *J. Alloys Compounds*, submitted. (**2008**)

4) Taegong Ryu, H. Y. Sohn, Kyu Sup Hwang, and Z. Z. Fang, "Plasma Synthesis of Tungsten Carbide Nanopowder from Ammonium Paratungstate," *J. Amer. Ceram. Soc.*, accepted.

5) Taegong Ryu, H. Y. Sohn, Kyu Sup Hwang, and Z. Z. Fang, "Chemical Vapor Synthesis and Characterization of Nanosized WC-Co Composite Powder and Post-Treatment," *Ind. Eng. Chem. Research*, **2008**,47, 9384-9388.

6) Taegong Ryu, H.Y. Sohn, Kyu Sup Hwang, and Zhigang Z. Fang, "Tungsten carbide nanopowder by plasma assisted chemical vapor synthesis from WCl6-CH4-H2 mixtures," *J. Mater. Sci.*, **2008**, 43, 5185-5192.

7) Taegong Ryu, H. Y. Sohn, Kyu Sup Hwang, and Z. Z. Fang, "Plasma Synthesis of Tungsten Carbide Nanopowder from Tungsten Hexachloride," *High Temp. Materials and Processes*, **2008**,27, 91-96.

8) Oladapo Eso, Peng Fan and Zhigang Zak Fang, "A Kinetic Model for Cobalt Gradient Formation During Liquid Phase Sintering of Functionally Graded WC-Co", *Int. J. Refract. Met. Hard Mater.*, **2008,** *26(2)*, 91-97.

9) Peng Fan, Oladapo Eso, Zhigang Zak Fang and H.Y. Sohn, "Effect of WC Particle Size on Co Distribution in Liquid-Phase-Sintered Functionally Graded WC-Co Composite", *Inter. J. Refract. Met. Hard Mater.*, **2008,** *26(2)*, 98-105.

10) Peng Fan and Zhigang Zak Fang, "Numerical simulation of kinetics of the cobalt gradient change in WC-Co during liquid phase sintering", *Int. J. Refract. Met. Hard Mater.*, **2008,** in press.

11) Taegong Ryu, H.Y. Sohn, Gilsoo Han, Young-Ugk. Kim, Kyu Sup Hwang, M. Mena, and Zhigang Z. Fang, "Nanograined WC-Co composite powder by chemical vapor synthesis," Metall. Mater. Trans. B, **2007**, 39B, 1-6.

12) H.Y. Sohn, Taegong Ryu, Jin Won Choi, Kyu Sup Hwang, Gilsoo. Han, Young Joon Choi, and Zhigang Z. Fang, "Chemical Vapor Synthesis (CVS) of Inorganic Nanopowders" JOM, **2007**, 59, 44-49.

13) Oladapo Eso, Zhigang Zak Fang, and Anthony Griffo, "Kinetics of Cobalt Gradient Formation during Liquid Phase sintering of functionally graded Wc-Co", *Int. J.*

Powder Metallurgy, **2007, 43***(3)*, 57-63.

14) Peng Fan, Zhigang Zak Fang and H.Y. Sohn, "Mathematical Modeling of Liquid Phase Migration in Solid-Liquid Mixtures: Application to the Sintering of Functionally Graded WC-Co Composites", Acta Materialia, **2007,** *55(9)*, 3111-3119.

15) Praveen, Maheshwari, Zhigang Zak Fang and H.Y. Sohn, "Early-stage Sintering Densification and Grain Growth of Nanosized WC-Co Powders", *Int. J. Powder Metall.*, **2007**, *43(2),* 41-47.

16) Oladapo Eso, Zhigang Zak Fang, and Anthony Griffo, "Kinetics of cobalt gradient formation during the liquid phase sintering of functionally graded WC-Co", *Int. J. Refract. Met. Hard Mater.,* **2007,** *25(4)*, 286-292.

17) Brady G. Butler, Jun Lu, Zhigang Zak Fang, and Raj K. Rajamani, "Production and Characteristics of Nanocrystalline Tungsten Carbide Powder Using a High Energy Dual-Drive Planetary Mill", *Int. J. Powder Metall.*, **2007**, *43(1),*35-44.

18) Vineet Kumar, Zhigang Zak Fang, Stuart I. Wright, and M. M. Nowell, "An Analysis of Grain Boundary and Grain Growth During Sintering of WC-Co using OIM", *Metall. Mater. Trans. A,* **2006**, *37A*, 599-607.

19) Zhigang Zak Fang, Praveen Maheshwari, Xu Wang, H. Y. Sohn, A. Griffo, and R. Riley, "An Experimental Study of the Sintering of Nanocrystalline WC-Co Powders", *Int. J. Refract. Met. Hard Mater.,* **2005**, *23(4-6)*, 249-257.

20) O. Eso, Zhigang Zak Fang, and A. Griffo, "Liquid Phase Sintering of Functionally Graded WC-Co Composites", *Int. J. Refract. Met. Hard Mater.,* **2005**, *23(4-6)*, 233-241.

21) Zhigang Zak Fang and Oladapo Eso, "Liquid Phase Sintering of Functionally Graded WC-Co composites". *Scripta Mater.*, **2005**, *52(8)*, 785-791.

Conference Proceedings:

1) Taegong Ryu, H. Y. Sohn, Kyu Sup Hwang, and Z. Z. Fang, "Plasma-assisted chemical vapor synthesis of tungsten carbide and cobalt nanocomposite powder," Materials Processing Fundamentals, TMS, Warrendale, PA, **2009**.

2) H.Y. Sohn, Taegong Ryu, Kyu Sup Hwang, and Zhigang Z. Fang, "Plasma-assisted chemical vapor synthesis of nanopowders," Proceedings of 2nd International Conference on New Trends in Chemistry and Their Applications, NTCA 2, Hurghada, Egypt, pp. 172-178, **2008**.

3) Taegong Ryu, Kyu Sup Hwang, H.Y. Sohn, and Zhigang Z. Fang, "Synthesis of Nanosized Tungsten Carbide by a Thermal Plasma Process," EPD Congress 2008, Materials Processing Fundamentals, ed. by P. N. Anyalebechi, TMS (The Minerals, Metals & Materials Society), Warrendale, PA, pp. 385-391, **2008**.

4) Xu Wang, Zhigang Z. Fang and H.Y. Sohn. "Sintering and Properties of Nanocrystalline WC/Co", in Proceedings of the 2008 Proceedings of the Seventh International Conference on Tungsten, Refractory & Hardmaterials, edited by A. Bose, R. J. Dowding, MA, MPIF, P. 05-03, **2008**.

5) Wang X, Fang ZZ and Sohn HY. "Nanocrystalline cemented tungsten carbide sintered by an ultra-high-pressure rapid hot consolidation process", in "Proceedings of the 2007 International Conference on Powder Metallurgy & Particulate Materials", edited by John Engquist and Thomas F. Murphy ,Denver, MPIF, P. 08-01., **2007**.

6) T. Ryu, M. Mena, H. Y. Sohn, G. Han, and Z. Z. Fang, "Nano-Grained WC-Co Composite Powders by the Chemical Vapor Synthesis," Advanced Metallic Composites and Alloys for High Performance Applications, ed. by A. Pandey, K. L. Kendig and J. Lewandowsky, pp. 73-82, Collected Proceedings: Emerging Materials, TMS (The Minerals, Metals & Materials Society), **2007**.

7) Wang X, Fang ZZ and Sohn HY. "Grain growth during the early stage of sintering of nanosized WC–Co powder". Proceedings of the Conference Euro PM 2006, Ghent, Belgium, **2006**.

8) Peng Fan, Oladapo O. Eso, Z. Z. Fang, and H. Y. Sohn, "Liquid Phase Migration during the Sintering of Functionally Graded WC-Co," Sohn International Symposium Advanced Processing of Metals and Materials Vol. 3 – Thermo and Physicochemical Principles: Special Materials and Aqueous and Electrochemical Processing, ed. by F. Kongoli and R.G. Reddy, TMS (The Minerals, Metals & Materials Society), pp. 111-119, **2006**.

9) M. Mena, T. Ryu, H. Y. Sohn, G. Han, Y.-U. Kim, and Z. Z. Fang, "Chemical Vapor Synthesis of WC-Co Nnanocomposite Powders," Sohn International Symposium Advanced Processing of Metals and Materials Vol. 3 – Thermo and Physicochemical Principles: Special Materials and Aqueous and Electrochemical Processing, ed. by F. Kongoli and R.G. Reddy, TMS (The Minerals, Metals & Materials Society), pp. 195-202, **2006**.

10) Oladapo Eso, Peng Fang and Z. Zak Fang, "Kinetics of the formation of cobalt gradient in WC-Co during liquid phase sintering", 2006 MPIF/APMI International Conference on Powder Metallurgy & Particulate Materials, June 18-21, San Diego, California, **2006**.

11) Praveen Maheshwari, Zhigang Zak Fang, and H.Y. Sohn, "Early Stage Densification and Grain Growth of Nanocrystalline WC-Co during Sintering", Int. Conf. Tungsten, Refractory and Hardmetals, February 6-8, 2006, Orlando, Florida, USA, **2006**.

12) Praveen Maheshwari, Xu Wang, Z. Zak Fang and H. Y. Sohn, "Effect of Particle Size on Sintering of WC-Co Powders", in Science and Technology of Powder Materials: Synthesis, consolidation and Properties, Proc. of MS&T 2005, September, 26-28, Pittsburgh, PA. Materials Science and Technology, v 4, Materials Science and Technology 2005 - Proceedings of the Conference, 2005, p 71-78, **2005**.

13) Vineet Kumar, Z. Zak Fang, S. Wright and M. Nowell, "Evolution of Faceted and Low Angle Like Boundaries during Sintering of Cemented Tungsten Carbide", in TMS Letters, Proc. of MS&T 2005, September, 26-28, Pittsburgh, PA, **2005**.

14) Xu Wang, Z. Zak Fang and H. Y. Shon, "A Study of Grain Growth during Sintering of Monolithic Nanosized tungsten Carbide", in TMS Letters, Proc. of MS&T 2005, September, 26-28, Pittsburgh, PA. Materials Science and Technology, v 3, Materials Science and Technology 2005 - Proceedings of the Conference, 2005, p 23-29, **2005**.

15) Brady G. Butler, Jun Lu, Z. Zak Fang, and Raj K. Rajamani, "Production of Nanocrystalline WC/Co Composite Powder Using a High Energy Dual-Drive Planetary Mill", Advances in Powder Metallurgy & Particulate Materials – **2005**, Proc. of the 2005 Int. Conference on Powder Metallurgy & Particulate Materials, Montreal, Canada, June, **2005**.

16) O. Eso and Z. Zak Fang, "A New Method for Making Functionally Graded WC-Co Composites via Liquid Phase Sintering", Advances in Powder Metallurgy &

Particulate Materials – 2004, Proc. of the 2004 Int. Conference on Powder Metallurgy & Particulate Materials, Chicago, June, **2004**.

2. Inventions and patents

1) Sohn HY, Fang ZZ, Ryu T, Han G, Mena M. A Method of synthesizing tungsten carbide-cobalt composite powder with uniform composition. U.S. Patent. patent applied for, June 20, **2007**.

3. Thesis:

1) X. Wang, "Grain growth, densification and mechanical properties of nanocrystalline WC/Co," Ph.D. Dissertation, University of Utah, July, **2008**.
2) T. Ryu, "Chemical Vapor Synthesis (CVS) and Characterization of Tungsten Carbide-Cobalt Nanocomposite Powder," Ph.D. Dissertation, University of Utah, June, **2008**.
3) M. M. Mena, "Chemical Vapor Synthesis of WC-Co Nanoparticles," MS Thesis, University of Utah, August **2006**.
4) P. Maheshwari, "Sintering Studes of WC-Co Powders," MS Thesis, University of Utah, August **2005**.

References

[1] North B. Invited Presentation. Annual Conference of European Powder Metallurgy Association 2005;Kennametal, Inc.

[2] McCandlish LE, Kear BH, Kim BK, Wu LW. Metastable Nanocrystalline Carbide in Chemically Synthesized W-Co-C Ternary Alloys, in Multi-component Ultrafine Microstructure. In: McCandlish LE, Polk DE, Siegel RW, Kear BH, editors. MRS Symposium Proceedings, V, vol. 132. 1989. p.67.

[3] Yao Z, Stiglich JJ, Sudarshan TS. Nanosized WC-Co holds promise for the future. Metal Powder Report 1998;53(3):26-33.

[4] Siegel RW. Synthesis, Structure and Properties of Nanocrystalline Materials. In: Fiorani D, Sberveglieri G, editors. Fundamental Properties of Nanocrystalline Materials. Rimini, Italy, 1993. p.3-19.

[5] Gleiter H. Materials with ultrafine microstructures: retrospectives and perspectives. Nanostruct Mater 1992;1(1):1-19.

[6] Swihart MT. Vapor-phase synthesis of nanoparticles. Curr Opin Colloid In 2003;8(1):127-33.

[7] Kruis FE, Fissan H. Nano-Process Technology for Synthesis and Handling of Nanoparticles. Kona 1999;17:130-9.

[8] Sohn HY, Paldey S. Synthesis of ultrafine particles and thin films of Ni_4Mo by the vapor-phase hydrogen coreduction of the constituent metal chlorides. Mater Sci A 1998;247(1-2):165-72.

[9] Sohn HY, Pal_Dey S. Synthesis of ultrafine nickel aluminide particles by the hydrogen reduction of vapor-phase mixtures of $NiCl_2$ and $AlCl_3$. J Mater Res 1998;13(11):3060-9.

[10] Sohn HY, Paldey S. Synthesis of ultrafine particles of intermetallic compounds by the vapor-phase magnesium reduction of chloride mixtures: Part II. Nickel aluminides. Metall Mater Trans B 1998;29(2):465-9.

[11] Hojo J, Oku T, Kato A. Tungsten carbide powders produced by the vapor phase reaction of the WCl_6-CH_4-H_2 system. J Less-Common Met 1978;59(1):85-95.

[12] Tang X, Haubner R, Lux B, Kieffer B. Preparation of ultrafine CVD WC powders deposited from WCl6 gas mixtures. J Phys IV Colloq 1995;51013-20.

[13] Won C-W, Chun B-S, Sohn HY. Preparation of ultrafine tungsten carbide powder by CVD method from WCl_6-C_2H_2-H_2 mixtures. J Mater Res 1993;8(10):2702-8.

[14] Kim JC, Kim BK. Synthesis of nanosized tungsten carbide powder by the chemical vapor condensation process. Scripta Mater 2004;50(7):969-72.

[15] Bartha L, Atato P, Toth AL, Porat R, Berger S, Rosen A. Investigation of hip-sintering of nanocrystalline WC/Co powder. J Adv Mater 2000;32(3):23-6.

[16] Carroll DF. Sintering and microstructural development in WC/Co-based alloys made with superfine WC powder. Int J Refractory Met Hard Mater 1999;17(1-3):123-32.

[17] Fang ZZ. Powder processing sintering and fracture toughness of sintered WC-Co Using Nanocarb powder by Nanodyne Unpublished data 1994.

[18] Fang ZZ, Eason JW. Study of nanostructured WC-Co composites. Int J Refractory Met Hard Mater 1995;13(5):297-303.

[19] McCandlish LE, Kear BH, Kim BK. Processing and properties of nanostructured WC-Co. Nanostruct Mater 1992;1(2):119.

[20] McCandlish LE, Seegopaul P, Sadangi RK. Inhibition of WC grain growth during sintering of nanostructured WC-Co powder compacts. Adv Powder Metall Particulate Mater 1995;313-7.
[21] Porat R, Berger S, Rosen A. Dilatometric study of the sintering mechanism of nanocrystalline cemented carbides. Nanostruct Mater 1996;7(4):429-36.
[22] WU L, etal. Grain growth inhibition in sintering of nanostructured WC-Co alloys. Pro 13th Int Plansee Seminar, , vol. 3. Reutte, 1993. p.667-9.
[23] Zhang L, Madey TE. Initial stages of sintering of nanostructured WC-7wt.%Co. Nanostruct Mater 1993;2(5):487-93.
[24] Azcona I, Ordonez A, Sanchez JM, Castro F. Hot isostatic pressing of ultrafine tungsten carbide-cobalt hardmetals. J Mater Sci 2002;37(19):4189-95.
[25] Agrawal D, Cheng J, Seegopaul P, Gao L. Grain growth control in microwave sintering of ultrafine WC-Co composite powder compacts. Powder Metall 2000;43(1):15-6.
[26] Breval E, Cheng JP, Agrawal DK, Gigl P, Dennis M, Roy R, et al. Comparison between microwave and conventional sintering of WC/Co composites. Mater Sci A 2005;391(1-2):285-95.
[27] Liu XQ, Lin T, Guo ZM, Cui FE, Luo J. Consolidation of ultrarine binderless cemented carbide by spark plasma sintering. J Iron Steel Res Int 2007;1482-4.
[28] Zhang F, Shen J, Sun J. The effect of phosphorus additions on densification, grain growth and properties of nanocrystalline WC-Co composites. J Alloys Comp 2004;385(1-2):96-103.
[29] Zhao SX, Song XY, Zhang JX, Liu XM. Effects of scale combination and contact condition of raw powders on SPS sintered near-nanocrystalline WC-Co alloy. Mater Sci A 2008;473(1-2):323-9.
[30] Sivaprahasam D, Chandrasekar SB, Sundaresan R. Microstructure and mechanical properties of nanocrystalline WC-12Co consolidated by spark plasma sintering. Int J Refractory Met Hard Mater 2007;25(2):144-52.
[31] Zhao HF, Zhu LH, Huang QW. Nanocrystalline WC-10%Co-0.8%VC cemented carbides prepared by spark plasma sintering. Rare Met Mat Eng 2005;34(1):82-5.
[32] Xie YF, Wang YQ, Chen LD, Li YD, Guo HL. Preparation of superfine-cemented carbide by spark plasma sintering. J Wu Han Univer Technol 2006;21(1):42-5.
[33] Maizza G, Grasso S, Sakka Y, Noda T, Ohashi O. Relation between microstructure, properties and spark plasma sintering (SPS) parameters of pure ultrafine WC powder. Sci Tech Adv Mater 2007;8(7-8):644-54.
[34] Wang XQ, Xie YG, Guo HL, Van der Biest O, Vleuge J. Sintering of WC-Co powder with nanocrystalline WC by spark plasma sintering. Rare Met 2006;25(3):246-52.
[35] Cha SI, Hong SH, Kim BK. Spark plasma sintering behavior of nanocrystalline WC-10Co cemented carbide powders. Mater Sci A 2003;351(1-2):31-8.
[36] Jia CC, Tang H, Mei XZ, Yin FZ, Qu XH. Spark plasma sintering on nanometer scale WC-Co powder. Mater Lett 2005;59(19-20):2566-9.
[37] Sun L, Jia CC, Lin CG, Cao RJ. VC addition prepared ultrarine WC-11Co composites by spark plasma sintering. J Iron Steel Res Int 2007;1485-9.
[38] Huang SG, Li L, Vanmeensel K, Van der Biest O, Vleuges J. VC, Cr3C2 and NbC doped WC-Co cemented carbides prepared by pulsed electric current sintering. Int J Refractory Met Hard Mater 2007;25(5-6):417-22.
[39] Kim HC, Jeong IK, Shon IJ, Ko IY, Doh JM. Fabrication of WC-8 wt.%Co hard

materials by two rapid sintering processes. Int J Refractory Met Hard Mater 2007;25(4):336-40.
[40] Kim HC, Oh DY, Shon IJ. Sintering of nanophase WC-15vol.%Co hard metals by rapid sintering process. Int J Refractory Met Hard Mater 2004;22(4-5):197-203.
[41] Kim HC, Shon IJ, Jeong IK, Ko IY, Yoon JK, Doh JM. Rapid sintering of ultra fine WC and WC-Co hard materials by high-frequency induction heated sintering and their mechanical properties. Mat Mater Int 2007;13(1):39-45.
[42] Dubensky EM, Nilsson RT. Dense fine grained monotungsten carbide-transition metal cemented carbide body and preparation thereof. US patent 5773735 1996.
[43] Michalski A, Siemiaszko D. Nanocrystalline cemented carbides sintered by the pulse plasma method. Int J Refractory Met Hard Mater 2007;25(2):153-8.
[44] Densley JM, Hirth JP. Fracture toughness of a nanoscale WC-Co tool steel. Scripta Materialia 1997;38(2):239-44.
[45] Jia K, Fischer TE, Gallois B. Microstructure, hardness and toughness of nanostructured and conventional WC-Co composites. Nanostruct Mater 1998;10(5):875-91.
[46] Schubert WD. 2000 Int Conf On Tungsten Hard Metals and Refractory Alloys Annapolis, MD, US, 2000.
[47] Petersson A, Agren J. Rearrangement and pore size evolution during WC-Co sintering below the eutectic temperature. Acta Mater 2005;53(6):1673-83.
[48] Goren-Muginstein GR, Berger S, Rosen A. Sintering study of nanocrystalline tungsten carbide powders. Nanostruct Mater 1998;10(5):795-804.
[49] Gille G, Szesny B, Dreyer K, van den Berg H, Schmidt J, Gestrich T, et al. Submicron and ultrafine grained hardmetals for microdrills and metal cutting inserts. Int J Refractory Met Hard Mater 2002;20(1):3-22.
[50] Wang X, Fang ZZ, Sohn HY. Grain growth during the early stage of sintering of nanosized WC-Co powder. Int J Refractory Met Hard Mater 2008;26(3):232-41.
[51] Bock A, Schubert WD, Lux B. Inhibition of grain growth on submicron cemented carbides. Power metall Int 1992;24(1):20-6.
[52] Lay S, Thibault J, Hamar-Thibault S. Structure and role of the interfacial layers in VC-rich WC-Co cermets. Philos Mag 2003;83(10):1175-90.
[53] Adorjan A, Schubert WD, Schon A, Bock A, Zeiler B. WC grain growth during the early stages of sintering. Int J Refractory Met Hard Mater 2006;24(5):365-73.
[54] Cha SI, Hong SH. Hardness and fracture toughness of ultra-rine WG-10Co-X cemented carbides prepared from nanocrystalline powders. Z MetaIlkd 2005;96(2):172-6.
[55] Kim BK, Ha GH, Lee GG, Lee DW. Structure and properties of nanophase WC/Co/VC/TaC hardmetal. Nanostruct Mater 1997;9(1-8):233-6.
[56] Li N, Qiu YX, Zhang W, Wen YH, Zhang Y, Zhou YG. Influence and function of inhibitor VC/Cr3C2 on the grain growth in super fine WC-Co cermets. Rare Met Mat Eng 2007;36(10):1763-6.
[57] Lin CG, Kny E, Yuan GS, Djuricic B. Microstructure and properties of ultrafine WC-0.6VC-10Co hardmetals densified by pressure-assisted critical liquid phase sintering. J Alloys Comp 2004;383(1-2):98-102.
[58] Sadangi RK, McCandlish LE, Kear BH, Seegopaul P. Grain growth inhibition in liquid phase sintered nanophase WC/Co alloys. Int J Powder Metall 1999;35(1):27-33.
[59] Johansson SAE, Wahnström G. The structure and formation of thin films at WC/Co interfaces. 9th Int conf on Science of Hard Materials. Jamaica, 2008.

[60] Gonzalez EJ, Piermarini GJ. Low-temperature compaction of nanosize powders.
[61] Prummer R, Weimar P. Explosive consolidation of nanopowders. InterCeram 2002;46(6):394-8.
[62] Yavari AR, Botta Filho WJ, Rodrigues CAD, Cardoso C, Valiev RZ. Nanostructured bulk Al90Fe5Nd5 prepared by cold consolidation of gas atomised powder using severe plastic deformation. Scripta Mater 2002;46(10):711-6.
[63] Sun L, Ha CC, Xian M. A research on the grain growth of WC-Co cemented carbide. Int J Refractory Met Hard Mater 2007;25(2):121-4.
[64] El-Eskandarany MS, Mahday AA, Ahmed HA, Amer AH. Synthesis and characterizations of ball-milled nanocrystalline WC and nanocomposite WC-Co powders and subsequent consolidations. J Alloys Comp 2000;312(1-2):315-25.
[65] Zhu LH, Huang QW, Zhao HF. Preparation of nanocrystalline WC-10Co-0.8VC by spark plasma sintering. J Mater Sci Lett 2003;22(22):1631-3.
[66] Munir ZA, Anselmi-Tamburini U, Ohyanagi M. The effect of electric field and pressure on the synthesis and consolidation of materials: A review of the spark plasma sintering method. J Mater Sci 2006;41(3):763-77.
[67] Groza JR, Zavaliangos A. Nanostructured bulk solids by field activated sintering. Rev Adv Mater Sci 2003;5(1):24-33.
[68] Siegel RW. Synthesis structure and properties of nanostructured materials: World Scientific 1993.
[69] Porat R, Berger S, Rosen A. Sintering behavior and mechanical properties of nanocrystalline WC/Co. Materials Science Forum 1996;225-227(Pt 1):629-34.
[70] Richter V, Ruthendorf MV. On hardness and toughness of ultrafine and nanocrystalline hard materials. vol. 17. Lanzarote, Spain: Elsevier, 1999. p.141-52.
[71] Fang ZZ. Wear Resistance of Powder Metallurgy Alloys. ASM Handbook 1998;7(Powder Metallurgy):965-77.
[72] Sigl LS, Exner HE. Experimental study of the mechanics of fracture in WC-Co alloys. Metall Mater Trans A 1987;18A(7):1299-308.
[73] Gleiter H. Materials with ultrafine microstructures. Retrospectives and perspectives. Nanostructured Materials 1992;1(1):1.
[74] Jia K, Fischer TE. Sliding wear of conventional and nanostructured cemented carbides. Wear 1997;203-204310-18.
[75] Outokumpu Research Oy. HSC Chemistry. Finland, 2002.
[76] Cullity BD, editor Elements of X-ray diffraction. Reading, MA: Addison-Wesley Pub. Co, 1978.
[77] Butler BG, Lu J, Fang ZGZ, Rajamani RK. Production of nanometric tungsten carbide powders by planetary milling. Int J Powder Metall 2007;43(1):35-43.
[78] Williamson GK, Hall WH. X-ray line broadening from filled aluminum and wolfram. Acta Metall 1953;1:22-31.
[79] Image Tool Software. http://ddsdx.uthscsa.edu/dig/itdesc.html.
[80] Shetty DK, Wright IG, Mincer PN, Clauer AH. Indentation fracture of WC-Co cermets. J Mater Sci 1985;20(5):1873-82.
[81] Sohn HY, Fang ZZ, Ryu T, Han G, Mena M. A Method of synthesizing tungsten carbide-cobalt composite powder with uniform composition. U.S. Patent. patent applied for, June 20, 2007.
[82] Fu L, Cao LH, Fan YS. Two-step synthesis of nanostructured tungsten carbide-cobalt

powders. Scripta Mater 2001;44(7):1061-8.
[83] Sara RV. Phase Equilibria in the System Tungsten-Carbon. J Amer Ceram Soc 1965;48(5):251-7.
[84] Malow TR, Koch CC. Grain growth in nanocrystalline iron prepared by mechanical attrition. Acta Mater 1997;45(5):2177-86.
[85] Krill CE, Helfen L, Michels D, Natter H, Fitch A, Masson O, et al. Size-dependent grain-growth kinetics observed in nanocrystalline Fe. Phys Rev Lett 2001;86(5):842-5.
[86] Chen IW, Wang XH. Sintering dense nanocrystalline ceramics without final-stage grain growth. Nature 2000;404(6774):168-71.
[87] Lee YI, Kim YW, Mitomo M, Kim DY. Fabrication of dense nanostructured silicon carbide ceramics through two-step sintering. J Amer Ceram Soc 2003;86(10):1803-5.
[88] Gothelid M, Haglund S, Agren J. Influence of O and Co on the early stages of sintering of Wc-Co: A surface study by AES and STM. Acta Mater 2000;48(17):4357-62.
[89] P Da Silva AG, Schubert WD, Lux B. The role of the binder phase in the WC-Co sintering. Mater Res 2001;4(2):59-62.
[90] German RM. Quantitative theory of diffusional activated sintering. Sci of sintering;15(1):27-42.